Issue 1 2017 | Volume 13

The Journal on Advanced Studies in Theoretical and Experimental Physics, including Related Themes from Mathematics

PROGRESS IN PHYSICS

"All scientists shall have the right to present their scientific research results, in whole or in part, at relevant scientific conferences, and to publish the same in printed scientific journals, electronic archives, and any other media." — Declaration of Academic Freedom, Article 8

ISSN 1555-5534

The Journal on Advanced Studies in Theoretical and Experimental Physics, including Related Themes from Mathematics

PROGRESS IN PHYSICS

A quarterly issue scientific journal, registered with the Library of Congress (DC, USA). This journal is peer reviewed and included in the abstracting and indexing coverage of: Mathematical Reviews and MathSciNet (AMS, USA), DOAJ of Lund University (Sweden), Scientific Commons of the University of St. Gallen (Switzerland), Open-J-Gate (India), Referativnyi Zhurnal VINITI (Russia), etc.

Electronic version of this journal:
http://www.ptep-online.com

Postal Address

Department of Mathematics and Science,
University of New Mexico,
705 Gurley Ave., Gallup, NM 87301, USA

ISSN: 1555-5534 (print)
ISSN: 1555-5615 (online)

Standard Address Number: 297-5092
Printed in the United States of America

January 2017 **Vol. 13, Issue 1**

CONTENTS

Information for Authors

Progress in Physics has been created for rapid publications on advanced studies in theoretical and experimental physics, including related themes from mathematics and astronomy. All submitted papers should be professional, in good English, containing a brief review of a problem and obtained results.

All submissions should be designed in LaTeX format using *Progress in Physics* template. This template can be downloaded from *Progress in Physics* home page http://www.ptep-online.com

Preliminary, authors may submit papers in PDF format. If the paper is accepted, authors can manage LaTeXtyping. Do not send MS Word documents, please: we do not use this software, so unable to read this file format. Incorrectly formatted papers (i.e. not LaTeXwith the template) will not be accepted for publication. Those authors who are unable to prepare their submissions in LaTeXformat can apply to a third-party payable service for LaTeX typing. Our personnel work voluntarily. Authors must assist by conforming to this policy, to make the publication process as easy and fast as possible.

Abstract and the necessary information about author(s) should be included into the papers. To submit a paper, mail the file(s) to the Editor-in-Chief.

All submitted papers should be as brief as possible. Short articles are preferable. Large papers can also be considered. Letters related to the publications in the journal or to the events among the science community can be applied to the section *Letters to Progress in Physics*.

All that has been accepted for the online issue of *Progress in Physics* is printed in the paper version of the journal. To order printed issues, contact the Editors.

Authors retain their rights to use their papers published in *Progress in Physics* as a whole or any part of it in any other publications and in any way they see fit. This copyright agreement shall remain valid even if the authors transfer copyright of their published papers to another party.

Electronic copies of all papers published in *Progress in Physics* are available for free download, copying, and re-distribution, according to the copyright agreement printed on the titlepage of each issue of the journal. This copyright agreement follows the *Budapest Open Initiative* and the *Creative Commons Attribution-Noncommercial-No Derivative Works 2.5 License* declaring that electronic copies of such books and journals should always be accessed for reading, download, and copying for any person, and free of charge.

Consideration and review process does not require any payment from the side of the submitters. Nevertheless the authors of accepted papers are requested to pay the page charges. *Progress in Physics* is a non-profit/academic journal: money collected from the authors cover the cost of printing and distribution of the annual volumes of the journal along the major academic/university libraries of the world. (Look for the current author fee in the online version of *Progress in Physics*.)

An Explanation of De Broglie Matter Waves in Terms of the Electron Coupling to the Vacuum State

William C. Daywitt

National Institute for Standards and Technology (retired), Boulder, Colorado. E-mail: wcdaywitt@me.com

This paper examines the de Broglie wave theory derived by Synge who assumed that Hamilton's variational principle in three dimensions applies also to the four-dimensional Minkowski spacetime. Based on the Planck vacuum (PV) view of the electron coupling to the vacuum state, calculations here suggest that the Synge de Broglie waves exist and travel within the PV state.

1 Introduction

In the early part of the twentieth century when it was realized that the massless photon had *particle-like* properties, de Broglie figured therefor that the massive electron must have *wave-like* properties — and the de Broglie matter wave was born [1, p.55].

In circa 1954 Synge [2] published a study on the idea of 3-waves propagating in the 4-dimensional Minkowski spacetime. The study was based on the properties of a *medium-function* which the present author interprets as a vacuum medium. In the PV theory, the occurrence of 3-waves in a 4-dimensional spacetime is symptomatic of an invisible vacuum continuum interacting with a free-space particle.

What follows compares the Compton-(de Broglie) relations derived in the PV theory with the Synge ray-wave diagram in spacetime, and concludes that his de Broglie waves propagate within the vacuum state rather than free space.

2 Compton-(de Broglie) relations

In the PV theory the interaction of the electron with the vacuum state leads to the Compton-(de Broglie) relations [3]

$$r_c \cdot mc^2 = r_d \cdot cp = r_L \cdot E = r_* \cdot m_* c^2 = e_*^2 \ (= c\hbar) \qquad (1)$$

where e_* is the massless bare charge that is related to the electronic charge via $e = \alpha^{1/2} e_*$, and α and m_* are the fine structure constant and the Planck particle mass. The radii $r_c\,(= e_*^2/mc^2)$ and $r_*\,(= e_*^2/m_* c^2)$ are the electron and Planck-particle Compton radii respectively and m is the electron mass. The magnitudes of r_* and m_* are equal to the Planck length and mass respectively [4, p. 1234]. It is because $r_* \neq 0$ that the PV state is a quasi-continuum.

The de Broglie radii, r_L and r_d, are derived from r_c and the Lorentz invariance of the vanishing electron/PV coupling force (A1) at $r = r_c$

$$i\left(\frac{e_*^2}{r_c^2} - \frac{mc^2}{r_c}\right) = 0 \qquad (2)$$

and result in

$$r_L = \frac{r_c}{\gamma} \qquad \text{and} \qquad r_d = \frac{r_c}{\beta\gamma} \qquad (3)$$

where $\beta = v/c$ and $\gamma = 1/\sqrt{1-\beta^2}$. From (3) $\beta = r_L/r_d$ yields the relative velocity of the electron in the coupled electron/PV system. The relations in (1) also lead to the relativistic electron energy $E = \sqrt{m^2c^4 + c^2p^2}$.

The relativistic scaler wave equation is [5, p. 319]

$$\left(\frac{\hbar}{mc}\right)^2 \left(\nabla^2 - \frac{\partial^2}{c^2\partial t^2}\right)\psi = r_c^2 \left(\nabla^2 - \frac{\partial^2}{c^2\partial t^2}\right)\psi = \psi \qquad (4)$$

while its nonrelativistic counterpart reads

$$\left(\nabla^2 - \frac{\partial^2}{v^2\partial t^2}\right)\psi = 0 \qquad (5)$$

where $v \ll c$; so the electron radii in (1) and (4) are relativistic parameters.

The planewave solution ($\psi \propto \exp i\phi$) to (4) in the z-direction involves the phase

$$\phi = \frac{Et - pz}{\hbar} = \frac{Ect - cpz}{c\hbar} = \frac{Ect - cpz}{e_*^2}$$

$$\phi = \frac{ct}{r_L} - \frac{z}{r_d} \qquad (6)$$

where the relativistic energies $E\,(= m\gamma c^2)$ and $cp\,(= cm\gamma v)$ from (1) are used in the final expression. The normalization of ct and z by the de Broglie radii r_L and r_d is a characteristic of the PV model of the vacuum state, and is related to the Synge primitive (planewave) quantization of spacetime to be discussed below.

3 De Broglie waves

The Ray/3-Wave diagram that represents the Synge de Broglie wave propagation in spacetime [2, p. 106] is shown in Fig. 1, where the electron propagates upward at a uniform velocity v along the Ray. The vertical axis is ict and the horizontal axes are represented by (x, y, z). The need for quantizing the Synge vacuum waves (adding the parameters r_c, r_L, and r_d to Fig. 1) is explained in the following quote. "So far the [variational-principle] theory has been confined to the domain of geometrical mechanics. The de Broglie waves have no phase, no frequency, no wave-length. It is by *quantization*

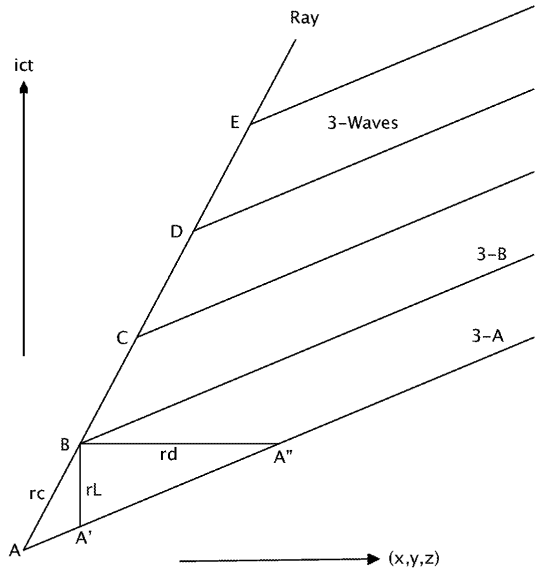

Fig. 1: Planewave quantization of de Broglie Waves in Spacetime. The figure consists of a single Ray and a partial picture of the corresponding 3-Waves propagating toward the upper left. The Ray and their 3-Waves are orthogonal in the 4-dimensional spacetime sense. The quantization consists of the normalization constants r_c, r_L, and r_d.

that these things are introduced, in much the same way as they are introduced in the transition from geometrical optics to physical optics" [2, p. 105].

The parameters in the figure correspond to rc = r_c, rL = r_L, and rd = r_d; the Compton and de Broglie radii from (1). In the quantization, the Synge theory utilizes the wavelengths $2\pi r_c$, $2\pi r_L$ and $2\pi r_d$. Thus there is a one-to-one correspondence between the electron/PV coupling radii from (1) and the Synge wave theory regarding Fig. 1. In the PV theory the electron radii (r_c, r_L, r_d) are parameters generated by the electron/PV interaction — thus it is reasonable to conclude that the de Broglie waves travel within the vacuum state.

Appendix A: Coupling force

In its rest frame, the coupling force the electron core $(-e_*, m)$ exerts on the PV quasi-continuum is [3]

$$i\left(\frac{e_*^2}{r^2} - \frac{mc^2}{r}\right) \tag{A1}$$

where the radius r begins at the electron core. The spacetime coordinates are denoted by

$$x_\mu = (x_0, x_1, x_2, x_2) = (ict, x, y, z) \tag{A2}$$

where $\mu = (0, 1, 2, 3)$ and $r = (x^2 + y^2 + z^2)^{1/2}$.

The force (A1) vanishes at the electron Compton radius r_c and leads to:

$$\frac{i}{r_c}\left(\frac{e_*^2}{r_c} - mc^2\right) = 0 \tag{A3}$$

in the electron rest frame; and when (A3) is Lorentz transformed it results in the two coupling forces

$$\frac{i}{r_L}\left(\frac{e_*^2}{r_c} - mc^2\right) = 0 \tag{A4}$$

and

$$\frac{1}{r_d}\left(\frac{e_*^2}{r_c} - mc^2\right) = 0 \tag{A5}$$

in the uniformly moving frame.

To complete the PV perspective, the space and time derivatives in the scaler wave equation

$$r_c^2\left(\nabla^2 - \frac{\partial^2}{c^2\partial t^2}\right)\psi = \psi \tag{A6}$$

and the Dirac electron equation [6, p. 74]

$$ic\hbar\left(\boldsymbol{\alpha}\cdot\nabla + \frac{\partial}{c\partial t}\right)\psi = mc^2\beta\psi$$

or

$$ir_c\left(\boldsymbol{\alpha}\cdot\nabla + \frac{\partial}{c\partial t}\right)\psi = \beta\psi \tag{A7}$$

are quantized (normalized, scaled) by the same constant r_c, where the 4×4 vector matrix $\boldsymbol{\alpha}$ accounts for electron spin. [The β in (A7) is a 4×4 matrix, not a relative velocity.]

Submitted on September 28, 2016 / Accepted on October 8, 2016

References

1. De Broglie L., Brillouin L. Selected Papers on Wave Mechanics. 1928, London and Glasgow, Blackie.
2. Synge J.L. Geometrical Mechanics and de Broglie Waves. 1954, Cambridge University Press.
3. Daywitt W.C. The de Broglie relations derived from the electron and proton coupling to the Planck vacuum state. *Progress in Physics*, 2015, v. 11, Issue 2 (April), 189. See also www.planckvacuum.com.
4. Carroll B.W. Ostlie D.A. An Introduction to Modern Astrophysics. 2007, Addison-Wesley, San Francisco—Toronto.
5. Schiff L.I. Quantum Mechanics. 1955, McGraw-Hill Book Co., Inc., Second Edition, New York.
6. Gingrich D.M. Practical Quantum Electrodynamics. 2006, CRC, The Taylor & Francis Group, Boca Raton, London, New York.

Beyond the Hubble's Law

Nilton Penha Silva
Departmento de Física (Retired Professor), Universidade Federal de Minas Gerais, Belo Horizonte, MG, Brazil.
Email: nilton.penha@gmail.com

Based on the Universe's scale factor introduced by Silva [1], we derive an expression for the receding velocities of arbitrary astronomical objects, which increase linearly up to the lookback distance of 2.1×10^3 Mpc and after that they increase in a positively accelerated way. The linear part corresponds to the Hubble'law.

1 Introduction

In a 2014 paper, Silva [1] introduced an expression for Universe's scale factor to describe the Universe's expansion,

$$a(t) = \exp\left(\frac{H_0 T_0}{\beta}\left(\left(\frac{t}{T_0}\right)^{\beta} - 1\right)\right), \tag{1}$$

where

$$\beta = 1 + H_0 T_0\left(-\frac{1}{2}\Omega_m(T_0) + \Omega_\Lambda(T_0) - 1\right), \tag{2}$$

H_0 is the Hubble constant, T_0 is the Universe current age, $\Omega_m(T_0)$ is the cosmic matter density parameter (baryonic + non-baryonic matter), $\Omega_\Lambda(T_0)$ is the cosmic dark energy density parameter [2].

In reference [1] matter and dark energy are treated as perfect fluids and it is shown that it very difficult to distinguish between closed ($k = 1$), flat ($k = 0$) and open ($k = -1$) universes. In this paper we intuitively adopt $k = 1$ and explore the Universe as being closed.

The spacetime metric for $k = 1$ according to Friedmann-Lemaitre-Robertson-Walker (FLRW) is [1, 3]

$$ds^2 = \mathfrak{R}^2(T_0)a^2(t)\left(d\psi^2 + \sin^2\psi\left(d\theta^2 + \sin^2\theta d\phi^2\right)\right) - c^2dt^2 \tag{3}$$

where ψ, θ and ϕ are the the comoving space coordinates ($0 \leqslant \psi \leqslant \pi$, $0 \leqslant \theta$ and $0 \leqslant \phi \leqslant 2\pi$); $\mathfrak{R}(T_0)$ is the current Universe's radius of curvature. This proper time t is the cosmic time.

It is known that at $t = 380,000$ yr $\simeq 10^{-4}$ Gyr, after the Big Bang, the Universe became transparent and the first microwave photons started traveling freely through it. They constitute what is called the Cosmic Microwave Background (CMB).

The observer (Earth) is assumed to occupy position $\psi = 0$ for any time t in the comoving reference system. To reach the observer at the Universe age T the CMB photons leave a specific position ψ_T ($t \simeq 10^{-4}$ Gyr). They follow a null geodesic.

It's time to make the following observation: since we will be dealing with large times values (some *giga* years) we have no loss if we treat $t \simeq 10^{-4}$ Gyr as $t \simeq 0$ Gyr for practical purposes.

For a null geodesic we have:

$$-\frac{c\,dt}{\mathfrak{R}(0)} = d\psi, \tag{4}$$

$$\psi_T = \frac{c}{\mathfrak{R}(0)}\int_0^T \frac{1}{a(t)}\,dt. \tag{5}$$

We have seen then that CMB photons emitted at ψ_{T_0} and $t = 0$ should arrive at the observer, $\psi = 0$ and T_0. Along their trajectory, other emitted photons, at later times, by astronomical objects that lie on the way, join the the photons troop and eventually reach the observer. They form the picture of the sky that the observer "sees". Certainly CMB photons emitted at $\psi > \psi_{T_0}$ will reach the observer at times latter than T_0.

2 The receding velocity

As the Universe expands, the streching distance between the observer and any astronomical object at time t is given by

$$\begin{aligned} d(t) &= \mathfrak{R}(0)\,a(t)\,(\psi_{T_0} - \psi_t) + ct \\ &= c\,a(t)\left(\int_0^{T_0}\frac{1}{a(t')}\,dt' - \int_0^{t}\frac{1}{a(t')}\,dt'\right) + ct \\ &= c\,a(t)\int_t^{T_0}\frac{1}{a(t')}\,dt + ct. \end{aligned} \tag{6}$$

The receding velocity of any astronomical object with respect to the observer is

$$\begin{aligned} v_{rec}(t) &= \dot{a}(t)\,c\int_t^{T_0}\frac{1}{a(t')}\,dt' \\ &= a(t)H(t)\,c\int_t^{T_0}\frac{1}{a(t')}\,dt', \end{aligned} \tag{7}$$

where we have used the fact that

$$\dot{a}(t) = a(t)H(t). \tag{8}$$

According to reference [1],

$$H(t) = H_0\left(\frac{t}{T_0}\right)^{\beta-1} \tag{9}$$

By performing the integration in equation (8) we have

$$v_{\mathrm{rec}}(t) = c\left(\frac{H_0T_0}{\beta}\right)^{1-\frac{1}{\beta}}\left(\frac{t}{T_0}\right)^{-1+\beta}\exp\left(\frac{H_0T_0}{\beta}\left(\frac{t}{T_0}\right)^{\beta}\right) \times\left(\Gamma\left(\frac{1}{\beta},\frac{H_0T_0}{\beta}\left(\frac{t}{T_0}\right)^{\beta}\right)-\Gamma\left(\frac{1}{\beta},\frac{H_0T_0}{\beta}\right)\right) \tag{10}$$

where $\Gamma(A,B)$ and $\Gamma(A,C)$ are incomplete Gamma Functions [4].

Taking into account that

$$\Gamma(A,B)-\Gamma(A,C)=\Gamma(A,B,C), \tag{11}$$

where $\Gamma(A,B,C)$ are generalized incomplete Gamma Functions [4], we have

$$v_{\mathrm{rec}}(t) = c\left(\frac{H_0T_0}{\beta}\right)^{1-\frac{1}{\beta}}\left(\frac{t}{T_0}\right)^{-1+\beta}\exp\left(\frac{H_0T_0}{\beta}\left(\frac{t}{T_0}\right)^{\beta}\right) \times\Gamma\left(\frac{1}{\beta},\frac{H_0T_0}{\beta}\left(\frac{t}{T_0}\right)^{\beta},\frac{H_0T_0}{\beta}\right). \tag{12}$$

3 Comparison to Hubble's law

By replacing t by $T_0 - d_{lb}/c$, where $d_{lb} = ct_{lb}$ is the so called lookback distance, t_{lb} being the lookback time:

$$v_{\mathrm{rec}}(d_{lb}) = c\left(\frac{H_0T_0}{\beta}\right)^{1-\frac{1}{\beta}}\left(1-\frac{d_{lb}}{cT_0}\right)^{-1+\beta} \times\exp\left(\frac{H_0T_0}{\beta}\left(1-\frac{d_{lb}}{cT_0}\right)^{\beta}\right) \times\Gamma\left(\frac{1}{\beta},\frac{H_0T_0}{\beta}\left(1-\frac{d_{lb}}{cT_0}\right)^{\beta},\frac{H_0T_0}{\beta}\right). \tag{13}$$

Figure 1 shows that the receding velocities increase as the lookback distance increases, initially in a linear way. Distant astronomical objects are seen to recede at much faster velocities than the nearest ones.

By expanding expression (13) in power series of d_{lb}, and retaining the lowest order term we get

$$v_{\mathrm{rec}}(d_{lb}) = H_0 v_{\mathrm{rec}}(d_{lb}) + \text{higher order terms}. \tag{14}$$

The Hubble's law,

$$v_{\mathrm{rec}}(d_{lb}) = H_0 v_{\mathrm{rec}}(d_{lb}), \tag{15}$$

is an approximation to our just obtained expression. According to the present work, Hubble's law holds up to ~ 7 Gly or, equivalently $\sim 2.1\times10^3$ Megaparsecs.

For this work, we have used the following experimental data [5]:

$$H_0 = 69.32\ \mathrm{kms^{-1}Mpc^{-1}} = 0.0709\ \mathrm{Gyr^{-1}},\quad T_0 = 13.772\ Gyr. \tag{16}$$

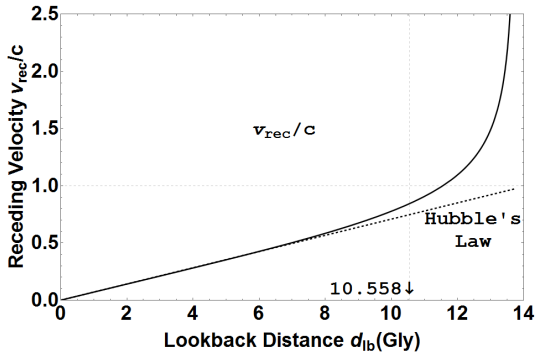

Fig. 1: Receding velocities as function of d_{lb}, the lookback distances from astronomical objects to the observer, on Earth.

As indicated by references [1, 6] the present scale factor predicts that the Universe goes from a matter era to a dark energy era at the age of $T_\star = 3.214$ Gyr. Before that matter dominated, and after that dark energy era dominates.

4 Conclusion

The Universe's scale factor $a(t) = \exp\left(\frac{H_0T_0}{\beta}\left(\left(\frac{t}{T_0}\right)^{\beta}-1\right)\right)$, with $\beta = 1 + H_0T_0\left(-\frac{1}{2}\Omega_m(T_0)+\Omega_\Lambda(T_0)-1\right)$ introduced by Silva [1] has been used to find an expression for the receding velocities of astronomical objects caused by the expansion of the Universe. The expression found, equation (13), is a generalization of Hubble's law. This later one should be valid up to $\sim 2.1\times10^3$ Megaparsecs.

After such very good results we feel very stimulated with the idea that expression (1) is a very good candidate for describing the geometrical evolution of our Universe.

Submitted on October 16, 2016 / Accepted on October 21, 2016

References

1. Silva N.P. A Model for the Expansion of the Universe. *Progress in Physics*, 2014, v. 10 (2), 93–97.
2. Silva N.P. The Universe's Expansion Factor and the Hubble's Law. *ResearchGate*, 2016, https://www.researchgate.net/publication/296060533.
3. Peebles P.J.E. The Large-scale Structure of the Universe. Princeton University Press, 1980.
4. Wolfram Research, Inc., Mathematica, Version 10, Champaign, IL, 2014.
5. Bennet C.L. et al. Nine-Year Wilkinson Microwave Anisotropy Probe (WMAP) Observations: Final Maps and Results. arXiv: astro-ph.CO. 2013.
6. Silva N.P. The Universe's Scale Factor: From Negative to Positive Acceleration of the Expansion. *ResearchGate*, 2016, https://doi.org/10.13140/RG.2.1.1540.3608.

Are Quazars White Holes?

Anatoly V. Belyakov

E-mail: belyakov.lih@gmail.com

Based on the mechanistic interpretation of J. Wheeler's geometrodynamic concept, which allows for transitions between distant regions of space, it was suggested that a quasar is a cosmological object, i.e. a white hole, where gravitational forces are replaced with dynamic ones with together the balance of electric and magnetic forces. Thus, a schematic model of a typical quasar was proposed. Its parameters (calculated on the basis of this model) are consistent with the observational data on quasars.

1 Quazars according to Wheeler's geometrodynamics

Quasars are still the most striking mystery of modern astrophysics. According to the most common hypothesis, a quasar is a distant active galaxy with a supermassive *black hole* in the centre. An alternative hypothesis belongs to V. Ambartsumyan. According to the latter, quasar nuclei are the place of matter transition from prestellar existence in the form of super-dense bodies to existence in the form of stars and rarefied interstellar medium, which are more common for astronomy. The transition can occur in the following sequence: super-dense state — kinetic energy — synchrotronic radiation. This process may be connected with formation of a *white hole*. Possibility of existence of white holes is also admitted by some other researchers [1, 2].

This approach is the closest to J. Wheeler's geometrodynamic concept allowing for drain-source transitions between distant regions of space ("wormholes"), thus ensuring circulation of matter along the *vortex tubes* (power lines) along some closed *contour*. The mechanistic interpretation of Wheeler's idea that only uses balances of main forces (electric, magnetic, gravitational and dynamic ones) makes it possible to build schematic models of cosmological objects and successfully determine some of their important parameters [3, 4]. In this case, there is no need to delve into the complex dynamics of phenomena and their mechanisms, which are the research subjects of specialised scientific disciplines. The same approach was used here to construct a schematic model of a quasar, assuming that it is a white hole.

Indeed, the most dramatic transition in the general circulation of matter is the transition, when the gravitational forces are replaced with dynamic ones (centrifugal forces in our case). In other words, it is the transition when interactions change their polarity. Probably, such a phase transition (inversion) occurs in quasars, where the super-dense state of matter transforms into radiation and diffused matter followed by its condensation. Under such a phase transition, the initially closed contour, which are based on the balance of gravitational and magnetic forces, break leaving unclosed vortex tubes with contradirectional currents. These currents carry charges of different polarity at the circuit break point. The charges are gradually destructing each other (not necessarily through annihilation). The reverse process occurs in black holes, respectively.

At the same time, the characteristic value of R_c (determined by the balance of electric and magnetic forces [3]) is preserved, since the same result is obtained from the balance of gravitational and magnetic forces, when the *evolutionary parameter* ε (characterises the difference of the material medium from vacuum) becomes numerically equal to the ratio of electric forces to gravitational ones. The R_c value is the geometric mean of linear values. They are the distance between the charges r and length l of the conductor (force line, current line or contour):

$$R_c = \sqrt{l\,r} = 7.52 \times 10^8 \text{ m}. \tag{1}$$

Assuming that the energy release in the quasar is due to mutual destruction of the charges with opposite polarity, the quasar may be schematically represented as a number of z charge unit contours or vortex thread concentrated to the maximum extent in the region with the radius R_c typical of the transition. Let us determine their number as follows:

$$z = \left(\frac{R_c}{r}\right)^3. \tag{2}$$

As the central mass, the quasar mass is determined by the following virial:

$$M = \frac{v^2 l}{\gamma}, \tag{3}$$

where v is the velocity of matter circulation in the contour, also known as peripheral speed and γ is the gravitational constant.

As the total mass of all the contours, the same mass is determined as follows:

$$M = z\varepsilon_0 l, \tag{4}$$

where ε_0 is linear density of the unit contour, which is equal to $m_e/r_e = 3.23 \times 10^{-16}$ kg/m^3.

It is clear that the evolutionary parameter of the general contour is increased proportionally to the number of unit counters, so $\varepsilon = z$.

Solving equations (1) to (4), we find the number of unit contours, distance between the charges, length of the contour

and quasar mass:

$$z = \frac{v^2}{\varepsilon_0 \gamma}, \tag{5}$$

$$r = \frac{R_c}{z^{1/3}}, \tag{6}$$

$$l = z^{1/3} R_c, \tag{7}$$

$$M = z^{4/3} \varepsilon_0 R_c. \tag{8}$$

Let us assume that the process of mutual destruction of charges occurs at the velocity of matter motion in the contour in all the individual contours simultaneously. Then the quasar's life time is:

$$\tau = \frac{l}{v}, \tag{9}$$

the average energy released by the quasar "burnout" is:

$$N = \frac{Mv^2}{\tau} = z\varepsilon_0 v^3, \tag{10}$$

and minimum radiation wavelength, referring to [3], is:

$$\lambda = \frac{\lambda_k c}{v}, \tag{11}$$

where λ_k is the Compton electron wavelength equal to 2.426 $\times 10^{-12}$ m.

Each contour has minimum reference length:

$$l_{min} = \frac{l}{z^{1/3}} = R_c, \tag{12}$$

then the minimum characteristic time interval for the quasar "burnout" or radiation will be:

$$\tau_{min} = \frac{R_c}{v}, \tag{13}$$

thus, the characteristic or standard mass converted into radiation during this time interval is:

$$M_{st} = \frac{M\tau_{min}}{\tau} = \frac{M}{z^{1/3}}, \tag{14}$$

and the number of standard masses in the mass of the quasar is:

$$n_{st} = \frac{M}{M_{st}} = z^{1/3}. \tag{15}$$

To some extent, the quasar inherits some super-dense state (microcosm) features, so the visible size of the quasar — its core l_0 — is determined by analogy with the Bohr atom, assuming that the core is $(an)^2$ times smaller than the contour size. Therefore:

$$l_0 = \frac{l}{(an)^2}, \tag{16}$$

where a is the reverse fine structure constant.

To determine the quasar's parameters, we need to know the velocity of matter circulation in the contour, i.e. the quantum number n. The main quantum number for a standard electronic contour [5] is:

$$n_s = \frac{c_0^{1/3}}{a} = 4.884, \tag{17}$$

and velocity is

$$v = \frac{c c_0^{1/3}}{(an_s)^2} = 4.48 \times 10^5 \text{ m/sec}, \tag{18}$$

with indication of $c_0 = c/[\text{m/sec}]$.

As shown by (4), (5), (17) and (18), the ratio of the quasar core linear density M/l_0 to the same of the electron m_e/r_e for such a standard quasar becomes the maximum possible and equal to the ratio of electric to the gravitational forces $f = c^2/\varepsilon_0\gamma = 4.17 \times 10^{42}$, i.e. $\varepsilon = f$. Moreover, as we see from the dependencies above, kinetic energy Mv^2 for a quasar contour is equal to electrostatic energy, provided that the number of individual charges placed along the length of the unit contour equals to l/r_e, and the distance between them is equal to the size of a standard contour. For a unit contour, this energy is equal to the following:

$$E_i = \frac{\varepsilon_0^{2/3} v^{8/3} R_c}{\gamma^{1/3}} = 1.03 \times 10^{17} \text{ J}. \tag{19}$$

2 The balance of electric and magnetic forces requires "stretching" charge contours of quasars to cosmic distances

Thus, the quasar model includes linear objects (force lines or vortex tubes) with the length of hundreds of light-years. This indicates the need for a mechanism of energy transfer from the quasar core to remote distances. Apparently, such extended formations are double radio sources. They often have a compact radio source between them, coinciding by its coordinates with the optical object — a quasar or a galaxy [6]. Notably, the outer edges of these structures are the brightest parts of the radio components. It is clear that in our model they are associated with the ends of quasar vortex tubes. The latter may be considered as super-charges, which are gradually destroying each other. Radiation comes from the peripheral part of the contours as charged particles move in the areas of the magnetic field's force lines with the greatest curvature, which are sources of synchrotron radiation.

Let us estimate the nature of the radiation emitted by such a contour. Continuing the analogy with the Bohr atom, we shall consider this contour as a super-atom. For a proton-electron contour, the wave range is within the range from 3.7×10^{-6} to 0.95×10^{-7} m under transitions within quantum numbers from n_s to 1. We suppose that, for the super-atom quasar, the wavelength increases in proportion to the ratio $r/(n_s^2 R_B)$. Then their range changes up to the range 1.05 m to 0.027 m (290 MHz to 11,000 MHz), which exactly covers most of the radio emission spectrum of typical galaxies and quasars.

Parameters	Values
Number of individual contours, z	9.33×10^{36}
Quasar mass M, kg	4.76×10^{42}
Total energy of the quasar E, J	9.61×10^{53}
Average radiation power N, W	2.72×10^{38}
Contour length or the maximum size of the quasar l, m	1.58×10^{21} (1.67×10^{5} light years)
Observed size of the quasar core l_0, m	$3.53 \times 10^{15} \ldots 1.26 \times 10^{11}$
Distance between charges r, m	3.57×10^{-4}
Minimum radiation wavelength λ, m	1.62×10^{-9}
Core pulsation period (minimum) τ_0, sec	70,400 (19.6 hours)
Periphery pulsation period (maximum) τ_{0_m}, sec	1.98×10^{9} (62.6 years)
Generalised pulse duration of the vortex tube τ_i, sec	117…5,440
Minimum light period τ_{min}, sec	1,675
Quasar life time τ, years	1.12×10^{8}
Standard "burnable" mass M_{st}, kg	2.26×10^{30}
Number of standard masses in the quasar n_{st}	2.10×10^{12}

Table 1.

Dual radio sources are relatively rare (it is possible due to that reason that we observe not the true size of a radio-source but its projection into the celestial sphere [8]) This implies that most of the long contours of the quasar are completely or partially spirally twisted forming a vortex structure or a tube immersed in the Y area (an extra dimension or a degree of freedom in relation to our world [8]). We can say that this vortex tube "is beaded" with future standard stellar masses convertible into radiation in respective portions (a sort of quanta).

Thus, the quasar as a phenomenon — on the much greater scale though — resembles the process of neutronisation [3], but occurs reversely, when the nominal one-dimensional vortex tube of the quasar is eventually transformed into a nominal two-dimensional disk spiral structure and further into a galaxy.

Some parameters of the quasar can be estimated using the most general equations obtained for stellar objects in the paper [3]. Thus, the core diameter is:

$$l_0 = M^j R_s \,, \tag{20}$$

where $j = 1 \ldots \frac{1}{3}$, the factor considering packing (the shape) of the object with the greatest value at $j = 1$ (a sphere) coinciding with the result of formula (16), and the lowest value at $j = \frac{1}{3}$ (a vortex tube) being close to the size of the Earth's orbit.

It is logical to assume that the quasar pulses relative to the symmetry axis, as do stellar objects, which is manifested in changing luminosity of the quasar. Thus, duration of the generalized momentum τ_i of a pulsar with the mass of a quasar as a vortex tube is:

$$\tau_i = 2.51\, M^{1/2 \ldots 1/4} \text{ sec}, \tag{21}$$

and pulsation periods of the core τ_0 and periphery τ_{0_m} of a stellar object with the mass of a quasar as a two-dimensional spiral object are:

$$\tau_0 = 2.51\, \frac{f}{\varepsilon} \left(\frac{M}{M_m} \right)^{2/3} \text{ sec}, \tag{22}$$

$$\tau_{0_m} = 2.51 \left(\frac{f}{\varepsilon} \right)^{3} \left(\frac{M}{M_m} \right)^{4/3} \text{ sec}, \tag{23}$$

where $M_m = 1.013 \times 10^{36}$ kg is the characteristic mass, determined by the formula (3) with $r = R_c$ and $v = c$. We may take $\varepsilon = f$ for the initial period of the quasar's life (the super-dense state). Then the periods determined by (22) and (23) are only dependent on the mass of the object.

Since the quasar pulsation periods vary depending on its form, the quasar emits at different frequencies. In addition, variability of radiation within different frequency ranges is asynchronous [9]. In particular, Seyfert galaxies — with a quasar presumably located in the centre of each — have a rapid high-amplitude radiation component (which are weeks and months) along with the slow low-amplitude radiation component (years), and the variability of radiation within different ranges is shifted in time. Thus, radio bursts can lag behind optical flares by years.

The state of a quasar in the form of a vortex tube may be observed as a *blazar*, which is believed to be an extremely compact quasar. It is characterised by rapid and considerable changes in luminance in all the spectrum ranges over a period of several days or even several hours [10].

It is understood that the quasar's parameters and its external appearance seen by the viewer will depend on the quantum number, density of packing of the charge pairs in the quasar volume, as well as on the quasar's age, pulsation phase, possible shape and orientation relative to the viewer. In general, the model estimates are consistent with the available data on quasars.

Calculated parameters of a standard quasar with $n_s = 4.884$ are shown in Table 1.

Indeed, the quasar mass estimated by the mass-luminance ratio should be about 10^{12} or more masses of the Sun; cumulative luminance throughout the spectrum may reach 10^{39} W to 10^{40} W; and energy contained in radio components alone may reach 10^{52} J. As for the quasar's life time, the analysis of the radio source observation data shows that energy emitted by the core as a result of a continuous (non-explosive) process may be emitted for 10^7 to 10^9 years [11–13].

The quasar's radiation is variable in all the wavelength ranges up to the X-ray and gamma radiation. The variability periods characteristic of quasars — months or even days — indicate that the generating area of the quasar radiation is not large, i.e. the linear dimensions of the emitting area (the quasar's core or active part) are fairly small — from one light year to the Solar System size [2, 10]. The shortest variation observed had a period of about one hour, which is within the range of the generalized pulse duration. This is consistent with the "burnout" time of the standard mass that corresponds to a typical stellar mass.

At the same time, the areas emitting within the radio range (double radio sources) are dozens and hundreds or more light-years away from the central optical object — a quasar or a galaxy [6, 7] — which is consistent with the length of the open contour. Their variability (months or years) may depend on the period of the quasar's outer cycle time (the periphery). As the quasar evolves, its evolutionary parameter ε decreases, but pulsation periods increase. We may assume that the initial configuration of the quasar is inherited in future, as matter condensates and stars form, and somehow "freezing" with a sharp decrease in the periphery spin velocity, it manifests itself in various forms of galaxies (elliptical or spiral).

3 Conclusion

It has been established by now that there were a lot more quasars at the earlier stages of the Universe evolution than there are now. Obviously, the quasar is the ancestor of other subsequent cosmological objects. In particular, this may explain the oddity of closeness of their energies of various origins, noted by astrophysics. Thus, we can conclude that quasars, their varieties and different types of galaxies (with quasars or black holes in the centre) are cosmological objects, gradually and naturally evolving from the white hole singularity to the black hole singularity.

Submitted on October 3, 2016 / Accepted on October 25, 2016

References

1. Retter A., Heller S. The revival of white holes as small bangs. arXiv: 1105.2776.:1105.2776
2. Narlikar J. Violent Phenomena in the Universe. Oxford University Press, 1984.
3. Belyakov A.V. Evolution of stellar objects according to J. Wheeler's geometrodynamic concept. *Progress in Physics*, 2013, v.1, 25–40.
4. Belyakov A.V. On some general regularities of formation of the planetary systems. *Progress in Physics*, 2014, v.10, 28–35.
5. Belyakov A.V. Charge of the electron, and the constants of radiation according to J. A. Wheeler's geometrodynamic model. *Progress in Physics*, 2010, v.4, 90–94.
6. Verkhanov O.V., Pariysky Yu.N. Radio Galaxies and Cosmology. Fizmatlit, Moscow, 2009.
7. Amirkhanyan V. R. Angular size — redshift: experiment and calculation. *Astrophysical Bulletin*, 2014, v. 69, no. 4, 383–389.
8. Belyakov A.V. Macro-analogies and gravitation in the micro-world: further elaboration of Wheeler's model of geometrodynamics. *Progress in Physics*, 2012, v.2, 47–57. *Nature*, v.379, issue 6563 (25 January 1996), 304.
9. Serjeant S., Rawlings S. Hidden quasars reddened by dust? Nature, v.379, issue 6563 (25 January 1996), 304.
10. Kantharia N. G. Decoding quasars: gravitationally redshifted spectral lines! arXiv: 1609.01593 [astro-ph.GA].
11. Shklovsky I.S. Radiogalaxies. *Soviet Uspekhi-Physics*, 1962, v.77, no. 5, 365–400.
12. Vorontsov-Velyaminov B.A. Extragalactic Astronomy. Revised and Exp. edition, Harwood Academic Publishers, 1987.
13. Pacholczyk A.G. Radiogalaxies. Pergamon Press, 1977.

Atom of Long-Range Action Instead of Counter-Productive Tachyon Phenomenology. Decisive Experiment of the New (Additional) Phenomenology Outside of the Light Cone

Boris M. Levin

Semenov Institute of Chemical Physics, Russ. Acad. Sci, Moscow (1964–1987)
In cooperation with Konstantinov Institute of Nuclear Physics, Russ. Acad. Sci., Gatchina (St. Petersburg) (1984–1987)
Ioffe Physical-Technical Institute, Russ. Acad. Sci., St. Petersburg (2005–2007)
E-mail: bormikhlev@yandex.ru

Limited, ultramicroscopic action radii of weak ($\sim 10^{-16}$ cm) and baryon ($\sim 10^{-13}$ cm) charges (interactions) against unlimited action radii of electrical and gravitational ones are the basis of phenomenology explaining the anomalies of positron annihilation in the "positron beta-decay Na-22 — neon (~9% Ne-22)" system established experimentally (1956–2003). A priori, it was impossible to imagine that the study of positron beta-decay positron annihilation (Na-22, Cu-64, and Ga-68) in noble gases would rise the issue of overcoming stagnation of fundamental physics (from mid-1970's) on the way to the expansion of the Standard Model and unification of physical interactions.

In noble (and any monoatomic) gases, slowing of positrons (e^+) under the positronium formation threshold (Ps; $E_{e^+} < E_0 = I - 6.8$ eV, where I is the atom ionization potential and 6.8 eV is the binding energy of Ps) is only possible through elastic collisions with atoms and may be observed, since: first, it is relatively long process (small parameter $\zeta = 2m_e/M$, where m_e is the positron mass and M is the atomic mass); and secondly, when the positron slows down to certain energy E_1 (determined by the inequalities $E_0 \gg E_1 \gg kT \cong 0.025$ eV) the positron annihilation rate rises more or less sharply, depending on the atomic number Z, as the positron polarize outermost electron shell of the atom. The combined effect of these two factors creates a non-exponential feature, the so-called *shoulder* in the time spectra of positron annihilation in inert gases (delayed $\gamma_n - \gamma_a$-coincidences; where γ_n is the nuclear gamma-quantum of the daughter nucleus after the β^+-decay of $^{22}\mathrm{Na} \xrightarrow{e^+_\beta + \nu} {}^{22*}\mathrm{Ne} \xrightarrow{E_{\gamma n} \cong 1.28\mathrm{MeV}} {}^{22}\mathrm{Ne}$)/"start", γ_a is one of the annihilation gamma-quanta/"stop"). The simplified theory of elastic slowing down says that the product of the shoulder length t_s and gas density (pressure, p) is the constant $t_s \times p$ for inert gas. In approximation of ideas gas, the constant is dependent on its parameters according to the following formula

$$(t_s \times p)_Z \cong \frac{\sqrt{2m_e}}{2.7 \times 10^{19}\, \sigma_e \zeta} \left(\frac{1}{\sqrt{E_1}} - \frac{1}{\sqrt{E_0}} \right),$$

where σ_e is the averaged cross section of elastic scattering of positrons [1].

When comparing lifetime charts of positrons of β^+-decay ^{22}Na for the entire range of noble gases, we cannot but notice the absence (or blurring) of the shoulder in neon [2]. Annihilation of *quasi-free positrons* after the shoulder with rate Λ depends on the number of electrons in the outermost shell of atom (Z_V). Value of Λ are shown in Table 1 [2]:

Table 1:

Noble gas	Λ, $\mu\mathrm{sec}^{-1} \times \mathrm{atm}^{-1}$	Z_V
Xenon (Xe)	26.3	8
Kripton (Kr)	5.78	8
Argon (Ar)	2.78	8
Neon (Ne)	0.661	8
Helium (He)	0.453	2

The chart $\Lambda/Z_V(Z)$ shown that neon falls out of the general monotonic dependence (Fig.1).

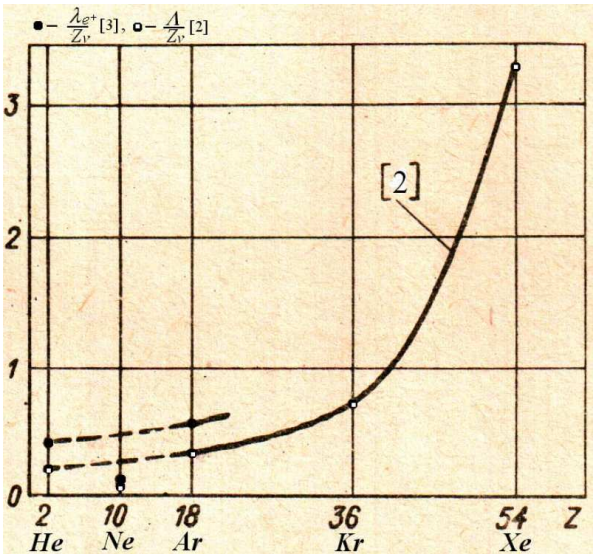

Fig. 1: Dependence of λ_{e^+}/Z_V [3] and Λ/Z_V [2] on Z (the atomic number of inert gas), where Z_V is the number of electrons in the outermost atomic shell.

Blurring of the shoulder in neon has been confirmed in other laboratories [3–7]. All these experiments showed different degrees of blurring. It should be noted in this regard that the shape of the shoulder is influenced by the orthopositronium ($o-$Ps, ^{T}Ps) component of the lifetime spectrum (I_2), following the component of annihilation of quasi-free positrons (e^+_β) on the time axis. Special features of neon individuating it in terms of measurements in the range of inert gases also include the following:

1. There is a big difference (twofold) in the data on the portion of positrons forming Ps in neon, obtained by the lifetime method with ^{22}Na as the source of positrons ($f = (28 \pm 3)\%$ [3] and $f = 26\%$ [8]) and by another method, i.e. according the energy spectrum of annihilation γ_a-quanta with ^{64}Cu as the source of positrons ($f = (55 \pm 6)\%$ [9]). This discrepancy between the results of independent experiments was noted in [7]. However, it was not discussed because of the lack of any basis for its explanation.
   In note [10], we have drawn attention to the fact that the start in the lifetime method is marked by the detection of the nuclear γ_n-quantum from transition of the excited daughter nucleus of ^{22*}Ne to the ground state of ^{22}Ne ($E_{\gamma_n} \cong 1.28$ MeV). This method usually provides high-precision measurements of the time spectra, since the lifetime of the excited state $^{22*}\mathrm{Ne}(E2)$ $\tau^* \cong 4 \times 10^{-12}$ s is considerably less than the resolving time of a spectrometer $\tau \sim 10^{-9}$ s.
   Hence, the question suggested itself in respect of the measurements in neon – whether the destiny of marker γ_n-quantum accompanying β^+-decay of ^{22}Na could be affected to some extent by high concentration of atoms with non-excited identical nuclei ($\sim 9\%$ ^{22}Ne)? In argon, where such a question is impossible, these different measurement methods provide consistent ($f = (30 \pm 3)\%$ [3] and $f = (36 \pm 6)\%$ [9]).
2. In contrast to helium and argon [7], there is large difference between experimental values of the constant characterizing the shoulder in neon $t_s \times p = 500 \div 900$ ns×atm [3] (see also [4,7]), $t_s \times p = 2200 \pm 6\%$ ns×atm [5] and $t_s \times p = 1700 \pm 200$ ns×atm [6]. The discrepancy between shoulder lengths may be an indication of the difference between neon samples in impurities of polyatomic gases. Nevertheless, authors characterized neon as *high purity* gas in all measurements. On the other hand, almost double the difference in shoulder length in measurements with the same sample of neon [3] (see also [4, 7]) also shows another uncontrollable cause of such a big difference in $t_s \times p$ neon in all measurements with ^{22}Na as the source of positrons [2–6].
3. There is also a strong discrepancy between the data on the cross section of elastic scattering of positrons under the threshold of formation of Ps obtained with beams of slow positrons using the lifetime method (with ^{22}Na as the positron source). Even the greatest of the values of the constant $t_s \times p$ in neon, obtained in work [5], is almost three times less than the estimated one, if we use the cross section of elastic scattering of positrons in neon are in full compliance with the theory and with results of beam experiments [11, 12].

All the experimental results of special manifestations of annihilation in the "β^+-decay ^{22}Na – neon ($\sim 9\%$ ^{22}Ne)" system were presented at the 7th Conference of Positron Annihilation (ICPA-7) [13].

A critical experiment (*falsification* by Karl Popper) was performed a decade after the publication of a proposal for experimental verification of the paradoxical idea of nuclear gamma-resonance in *gaseous* neon of natural isotopic compositions [10]. The successful experiment [14], which confirmed the paradoxical implementation of the Mössbauer Effect in gas in final state of β^+-decay $^{22}\mathrm{Na}(3^+) \xrightarrow{e^+_\beta+\nu} {}^{22*}\mathrm{Ne}(2^+)$ opened the prospect of building a phenomenology of extension of the Standard Model [15] in the suggestion that the limited four-dimensional space-time of the final state of β^+-decay of this type ($\Delta J^\pi = 1^\pi$) is topologically non-equivalent to the initial state (the *topological quantum transition*). With this in mind, let us denote the orthopositronium formed in the gas by the β^+-decay positron as β^+-orthopositronium: $^3(e^+_\beta e^-)_1$.

Since there is an *isolated virtual photon* $\widetilde{\gamma}$ in $o-$Ps dynamics, there is a possibility that the β^+-orthopositronium may overcome the *light barrier* due to quantum-mechanical oscillations. Hence we have sensing of four-dimensional space-time "on the outside" of the light cone and, consequently, an additional (single quantum) mode of annihilation involving a double-valued ($\pm$) space-like structure. The existence of the Planck mass $\pm M_{Pl} = \pm(\hbar c/G)^{1/2}$ opens a unique opportunity to represent a macroscopic space-like structure.

The phenomenology of physical nature of "resonance conditions" in the "β^+-decay ^{22}Na — neon ($\sim 9\%$ ^{22}Ne)" system formulated in [15]* leads to the conclusion that the uncontrollable factor in all neon measurements is the gas temperature (laboratory temperature). This means that deciding experiment aiming to confirm double resonance I_2 within the range ± 30°C (see below) is out of the question in Standard Model.

Theorists have been independently (for their own reasons) probing the possibility of going beyond the Standard Model:

*The Michigan group have renounced their results in the β^+-o-Ps self-annihilation rate by $(0.19 \pm 0.02 \div 0.14 \pm 0.023)$ percent over the theoretical value (*QED*) [16]. The findings of this work are most likely to be erroneous, since they were obtained by introducing an auxiliary electric field into the space of the measuring chamber. The field might "obscure" the effect. Fairly speaking, the work-2003 by the Michigan group has also played a constructive role. It destructive conclusions made it possible to detect and substantiate the fundamental link between gravity and electricity [17] — the cause of the erroneous nature of the conclusion made by the Michigan group, who did not have all the experimental data available by the time [14]. *A decisive experiment is needed.*

1. **Lev Landau** at the International Conference on High Energy Physics (Kiev, 1959) spoke about the limited perspective of the *Hamiltonian method* for strong interactions (the text of the presentation was included in the collection of articles in memory of **Wolfgang Pauli**, 1962) [18].
   Although quantum chromodynamics (QCD) was formulated in the framework of the *Hamiltonian method* in the 1960s–1970s, it did not solve the problem of strong interactions (the absence of fundamental justification of *confinement*), and the problem of the fundamental interactions unification (*Theory of Everything*) was complicated by mysterious nature of *dark matter* and *dark energy* (~ 95% of the Universe);

2. **R. F. Feynman [19]:** "At the suggestion of Gell-Mann I looked at the theory Yang-Mills with zero mass [...] it should been noticed by meson physicists who had been fooling around the Yang-Mills theory. They had not noticed it because they're practical, and the Yang-Mills theory with zero mass obviously does not exist, because a zero mass field would be obvious; it would come out of nuclei right away. So they didn't take the case of zero mass and no investigate it carefully";

3. **F. Hoyle and J. V. Narlikar** considered discrete scalar C-field with negative mass density [20]. This allowed presenting the final state of the topological quantum transition in β^+-decay of ^{22}Na (and the like) as a vacuum structure $U^{\pm}$, in which the space-like negative mass is balanced by the vacuum-like state of matter (an *atom of long-range action with a nucleus*). That is β^+-decay of $^{22}\mathrm{Na}(3^+) \xrightarrow{e^+_\beta+\nu} {}^{22}\mathrm{Ne}(2^+)$ under expansion of the Standard Model will be $^{22}\mathrm{Na}(3^+) \xrightarrow{e^+_\beta+\nu+U^{\pm}} {}^{22*}\mathrm{Ne}(2^+)$;

4. **E. B. Gliner [21]:** "The physical interpretation of some algebraic structures of the energy-momentum tensor allows us to suppose that there is a possible form of matter, called the μ-vacuum, which macroscopically possesses the properties of vacuum. [...] Because of the multiplicity of the comoving reference systems we cannot introduce the concept of localization of an element of μ-vacuum matter, and consequently cannot introduce the concepts of particle and of the number of particles of the μ-vacuum in a given volume, if we understand by a particle an object singled out in a classical sense relative to the remaining "part" of the matter. Similarly, one cannot introduce the classical concept of a photon".
   Views on β^+-decay of the type $\Delta J^{\pi} = 1^{\pi}$, $^{22}\mathrm{Na}(3^+) \rightarrow {}^{22}\mathrm{Ne}(2^+)$, $^{64}\mathrm{Cu}(1^+) \rightarrow {}^{64}\mathrm{Ni}(0^+)$, $^{64}\mathrm{Ga}(1^+) \rightarrow {}^{68}\mathrm{Zn}(0^+)$ in the Standard Model's expansion $^{22}\mathrm{Na}(3^+) \xrightarrow{e^+_\beta+\nu+U^{\pm}} {}^{22*}\mathrm{Ne}(2^+)$ (see item 3 above) was based on Gliner's cosmological ideas;

5. **V. I. Ogievetskii and I. V. Polubarinov** discussed the *notoph* in [22]: "...a massless particle with zero helicity, additional on the properties to photon. In interactions notoph, as well as photon, transfers spin 1".
   This makes possible to postulate an additional mode of annihilation of β^+-*o*-Ps by one notoph (γ°) $\beta^+ - {}^{\mathrm{T}}\mathrm{Ps} \rightarrow \gamma^{\circ} U^{\pm}$ (see items 3 and 4 above). Annihilation of *o*-Ps by one photon is prohibited in *QED* by the law of conservation of momentum;

6. **G. J. Iverson and G. Mack [23]** on the possibility of the space-like nature of some types of neutrinos;

7. **V. L. Lyuboshits and M. I. Podgoretskii** about the identity of elementary particles; the mirror world outside context of the P and CP violation [24].
   This opened the possibility of consideration of β^+-*o*-Ps oscillations in the mirror world, as Ps *initially is object of quantum electrodynamics* (electromagnetic interactions) preserving the P and CP symmetries, while the mirror was considered in the context of their violation under weak interactions;

8. **Yu. A. Golfand and E. P. Likhtman** discovered the mathematical structure of supersymmetry [25].
   Since the mid-1970s no common physical realization of supersymmetry has been found;

9. **S. W. Hawking and C. F. R. Ellis [26]:** "...the simultaneous creation of quanta of positive energy fields and of the negative energy C-field".
   This justifies the postulation of $U^{\pm}$ on an experimental basis [2–6, 9, 14, 15] (see item 3 above);

10. **J. L. Synge [27]:** "Anti-Compton scattering" — the idea that was not seen by the author as a physical concept — was developed in [28] to justify additional realization of supersymmetry (*superantipodal symmetry*) manifested in lifetime anomalies of β^+(^{22}Na)-*o*-Ps in neon;

11. **A. F. Andreev:** "Gravitational Interaction of Zero-Mass Particles", "Macroscopic Bodies with Zero Rest Mass" [29]; complete relativity, i.e. equivalence of "...all speeds (but speed of light)" [30].
   This was the first quantum-field justification of space-like fundamental structures previously postulated on the basis of general theory of relativity (the μ-vacuum concept, see item 4 above);

12. **P. Fayet and M. Mezard [31]:** Calculation of the probability of *o*-Ps annihilation by a single γ_a-quantum and a neutral supersymmetric gauge boson U with spin 1: $B(^{\mathrm{T}}\mathrm{Ps}) \rightarrow \gamma_a U = 3.5 \times 10^{-8}(1 - x^4)$, where $x = m_U/m_e \rightarrow 0$, m_e standing for the electron (positron) mass;

13. **P. Di Vecchia and V. Schuchhardt [32]:** complete degeneration of $N = 2$ para- and orthosuperpositronium.
   This has set a precedent of complete degeneration of para- and orthopositronium while maintaining superantipodal symmetry in the final state of β^+-decay ^{22}Na

and others. We know that conservation of full spin Ps is unequivocal law, not related to approximation. It follows from the CP-invariance of electromagnetic interactions, while the annihilation modes (the even number of γ_a-quanta for parapositronium ^{S}Ps and the odd number for ^{T}Ps) are determined by conservation of the charge parity (C) and the total angular momentum (the spin, as the ground states of Ps have no orbital angular momentum). Hence, the possibility in principle to justify the complete degeneration of the ground spin states of a superpositronium, taking into account the oscillations in the mirror world, may be associated with the relativistic transformation of the angular momentum. Indeed, if we postulate random mirror-world wandering in the three-dimensional space with velocity $|V| \sim c$ relative to the ground laboratory (observer) and if the relation between the walk step Δ (and the time Δ/c) and the ^{T}Ps$|^{T}$Ps$'$ (stroke indicates belonging to the mirror world) lifetime is favorable, the averaged (over this time interval) value of spin seen by the observer is $\langle(S = 0)\rangle = (S = 1)'(|V|^2/c^2)^{1/2}$ [33];

14. S. L. Glashow due to the presence of the isolated virtual photon $\widetilde{\gamma}$ in the dynamics of the orthopositronium, postulated (outside the context of the violation of P- and CP-symmetries) the possibility of o-Ps oscillations in the mirror world. The difference in understanding the nature of the mirror world discussed herein as past a new (additional) $G\hbar/ck$-physics and the *mirror Universe* by Glashow (the "mirror world"), rejected by himself in comparing the alleged consequences with the experimental data available at the time [34], is that the *energy* and *action* in the $G\hbar/ck$-mirror world of a new (additional) $G\hbar/ck$-physics have *negative sings*. In addition, the mirror world of $G\hbar/ck$-physics (with the negative sign) is realized *locally* (in the atom of long-range action) through the double-valued ($\pm$) Planck mass $M_\mu = M_{U^\pm} = \pm M_{Pl} = \pm(\hbar c/G)^{1/2}$ (development of Gliner's ideas);

15. A. D. Linde [35] earlier proposed an independent concept of antipodal symmetry of energy and action in the mirror world relative to the observable Universe. The $G\hbar/ck$-physics is substantiated by this concept. Expansion of the Standard Model includes the double-valued nature of the Planck's constant $\pm\hbar$;

16. L. B. Okun considered the possibility of "... the existence of many-particle states with anomalous permutation symmetry [...] in the relativistic case, it leads to non-positive energy or non-locality" (ferbons/parastatistic) [36];

17. G. A. Kotelnikov [37]: "It was shown that equations of electrodynamics are invariant with respect to the operation of changing the value the speed of light".
The double-valued nature of the speed of light $\pm c$ was realized in $G\hbar/ck$-physics. Two of the three superconstants of physics are double-valued $G, \pm\hbar, \pm c$.
We have noted the fact that $\pm\hbar$ and $\pm c$ are included in the structure of all quantum-relativistic physical constants with odd exponents, i.e. in the form of the positive-definite product of $(\pm\hbar)^{2k+1} \otimes (\pm c)^{2\kappa+1}$ (where k and κ are equal to 0 or an integer) as a phenomenon of the *antipodal cosmological invariance* (*ACI phenomenon*) *of the fundamental physical constants*: dimensionless constants of physical interaction — $\alpha = e^2/\hbar c$ (electromagnetic), $\alpha_g = Gm^2/\hbar c$ (gravitat.), $\alpha_W = G_F m^2/\hbar c$ (weak), Planck values — mass $M_{Pl} = (\hbar c/G)^{1/2}$, length $l_{Pl} = (\hbar G/c^3)^{1/2}$, time $t_{Pl} = (\hbar G/c^5)^{1/2}$ and all the rest. This means that mirror-world physics ("on the outside of the light cone") may be regarded as an extension of the Standard Model;

18. A. Yu. Andreev and D. A. Kirzhnits [38]: "Not quite simple and rather obscure relations between the concept of 'instability' and 'tachyons' are discussed".
This work has defined the physical status of the double-valued $\pm$ four-dimensional space-time "on the outside" of the light cone. At the time of publication, the authors could not give up the phenomenology and the term *tachyon*. The key word is *instability*. The only realization is the β^+-orthopositronium oscillating in the mirror world. In the final state of the topological quantum transition under the β^+-decay of ^{22}Na, β^+-o-Ps breaks the light barrier due to presence of the isolated virtual photon $\widetilde{\gamma}$ in its dynamics. An *atom of long-range action with a nucleus* takes over from the counterproductive phenomenology "tachyon".
The β^+-decay of $p \to n + e^+_\beta + \nu$ (in the atomic nucleus) in the earth laboratory (g = 981 cm/s^2) involves physical interactions of all types: *strong* — $p \to n$, *electromagnetic* — p, e^+_β, *weak* — ν (*electroweak*) and *gravitational* one. That is why "instability" in the context of the β^+-decay (of the $\Delta J^\pi = 1^\pi$ type) must be accompanied by a unified field reaction (generalized displacement current) ad modum the displacement current in electrodynamics.
The space-like structure of the unified field displacement current (an atom of long-range action with a nucleus) was postulated instead of the counterproductive phenomenology "tachyon";

19. L. B. Borissova and D. D. Rabounski [39]: Using the method of chronometric invariants (physical observable values, A.L. Zelmanov, 1956), "... the possibility of co-existence of short-range and long-range action has be studied" as an extension of GR.
Mathematical prediction of the existence of the third form of matter in the zero-space (zero particles) has given rise to construction of the phenomenology of the additional one notoph mode of β^+-o-Ps annihilation

(see items 5,7,10 above);

20. J. M. Fröhlich ("Planck's Hypercube" [40]): following the logic and intuition of **Max Planck** (1900/1906), reattributes Boltzmann's constant k to the status of the fundamental constants $c, G, \hbar$, which determined the *cube of physical theories* (G. Gamov, D. Ivanenko, L. Landau, M. P. Bronstein/1928, and A. Zelmanov/ 1967–1969), thus opening the opportunity of the *four-dimensional generalization of the cube*.
The formulation of the double resonance concept (Appendix in [15]) predicts dependence of intensity of β^+-o-Ps (I_2) on temperature in the "β^+-decay ^{22}Na — neon ($\sim$ 9% ^{22}Ne)" system to be studied in the range — $30°\text{C} < T < +30°\text{C}$.
This remind on lecture [40]. If there was destructive criticism of the Planck's Hypercube concept in [41], lecture [40] would hardly be noticed, as it was published in a non-peer-reviewed journal (it is absent in the Science Citation Index);

21. A. D. Sukhanov and O. N. Golubeva [42]: "We show that the quantum statistical mechanics (QSM) describing quantum and thermal properties of objects has only the sense of particular semiclassical approximation. We propose a more general (than QSM) microdescription of objects in a heat bath taking into account a vacuum as an object environment; we call it $\hbar$-k-dynamics";

22. L. V. Prokhorov [43]: "On Planck Distances Physics. Universe as a Net", "On Physics at the Planck Distance. Strings and Symmetries".

These ideas and results obtained by theoreticians (items 1 to 22) were included in the wording of the Standard Model extension phenomenology, as the isotope effect in neon (the increased β^+-orthopositronium component I_2 in the sample depleted by an isotope of ^{22}Ne [14]; 1.85 ± 0.1 factor) is on 6-7 order of magnitude greater than estimated in the Standard Model (by isotopic shift of atomic energy levels).

The main motives for extending the Standard Model to explain the anomalies in the "β^+-decay ^{22}Na – neon ($\sim$ 9% ^{22}Ne)" system [2–6, 9, 14, 15] are determined by three concepts — vacuum-like state of matter (see item 4 [19] above), complete relativity (see item 11 [29, 30] above) and development of the idea of β^+-o-Ps oscillations in the mirror world [15] ([34]).

It is surprising that, in the XIX century, the genius of Sir W. R. Hamilton (1806-1865) linked the Standard Model of physics of XX century (the Hamiltonian method) and its alleged expansion in XXI century, since quantitative harmonization of lifetime anomaly β^+-o-Ps in the "β^+-decay ^{22}Na — neon ($\sim$ 9% ^{22}Ne)" system is based on the phenomenology of the *atom of long-range action with nucleus*. This spacelike structure in the final state of β^+-decay is represented by bound Hamiltonian chains/cycles (paths contain each node of the graph once).

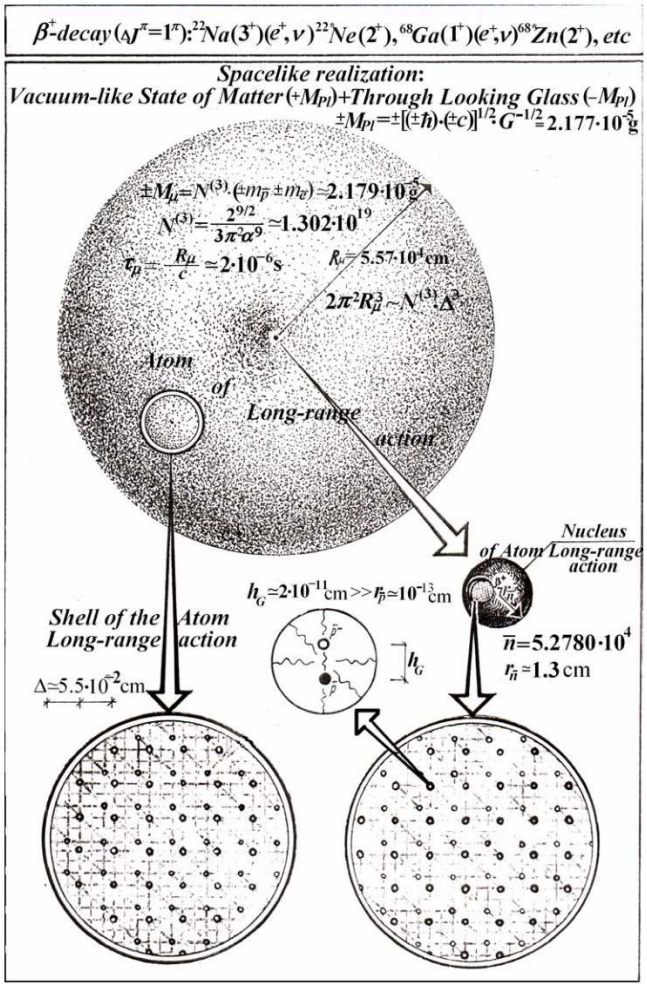

Fig. 2: "Microstructure" of the vacuum-like state of matter (*VSM/mirror world*); h_G is vertical displacement of double-valued sublattices $U^{\pm}$ in the gravitational field of the Earth.

The Planck mass $M_\mu = M_{U^\pm} = \pm M_{Pl} = \pm(\hbar c/G)^{1/2}$ g is regarded as a space-like structure (the number of nodes in *atom of long-range action* and radii is $N^{(3)} \cong 1.302 \times 10^{19}$, $R_\mu \cong 5.57 \times 10^4$ cm, in the nucleus $\bar{n} \cong 5.2780 \times 10^4$, $r_{\bar{n}} \cong 1.3$ cm). It is assumed that each node contains elementary charges of all physical interactions ($\bar{p}^+$, $\bar{p}^-$, $\bar{e}^-/\bar{e}^+$, $\bar{\nu}/\bar{\bar{\nu}}$ with their double-valued $\pm$ masses). In these assumptions, the Planck mass is calculated with high accuracy using the fine structure constant α [15].

Unlike the *gravitational* (G) and *electromagnetic* (α) *interactions* with infinitive ranges ($r_G, r_\alpha = \infty$), the ranges of the *weak* ($r_W = 10^{-16}$ cm) and *baryon* ($r_{str} = r_{\bar{p}} \sim 10^{-13}$ cm) *interactions* are *ultramicroscopically* small. Since $+M_{Pl}$ and $-M_{Pl}$ move in the gravitational field vertically and in opposite directions and diverge to a distance of $h_G = 2g\tau^2_{0-Ps}/2 = 2 \times 10^{-11}$ cm over the lifetime of β^+-o-Ps (up to 142 ns), the weak and baryon charges are decompensated (opened) in the nodes of *vacuum-like state of matter/VSM* ($+M_{Pl}$) as $h_G \gg r_W, r_{\bar{p}}$ (Fig. 2).

The rate of self-annihilation of β^+-*o*-Ps (in non-resonant conditions) is exceeded by $(0.19 \pm 0.02 \div 0.14 \pm 0.023)$ % (see footnote in Page 12) due to the amplification factor as result of β^+-*o*-Ps oscillations on $\bar{n} \cong 5.2780 \times 10^4$ nodes of the space-time structure of the *nucleus of atom of long-range action* [15] (parallel acts of annihilation)

$$B\left(\beta^+ - {}^{\mathrm{T}}\mathrm{Ps}\right)\bar{n} \to \gamma^{\circ} U^+ = 3.5 \times 10^{-8} \times 5.2780 \times 10^4 \cong 1.9 \times 10^{-3}(0.19)\%$$

(see item 12 above).

In the fourth dimension of space-time outside the light cone, the $+M_{Pl}$ lattice has the properties of an *absolutely rigid body*. Electrical charges in the nodes of $\bar{p}^+/\bar{p}^-$, $\bar{e}^-/\bar{e}^+$ lattices are balanced as a result of the infinite range (the Coulomb barrier is absent in the VSM nodes). Exchange of *quasiprotons* in the nodes of the *VSM* lattice with protons of the atomic nuclei of the gas surrounding the source of positrons becomes possible. In the case of neon, nuclear gamma-resonance (the Mössbauer Effect) is realized in the "β^+-decay ^{22}Na — neon ($\sim 9\%$ ^{22}Ne)" system.

Appearance of protons (quasi-particles $\bar{p}$) in each node of the $+M_{Pl}$ lattice and bonding of atoms with ^{22}Ne nuclei in the "β^+-decay ^{22}Na — neon ($\sim 9\%$ ^{22}Ne)" system is the response to β^+-decay ^{22}Na. This is similar to the displacement current, but having the space-like structure.

The difference between the masses of the neutron and proton $\Delta m_{np}c^2 = m_n c^2 - m_p c^2 = 1.2933317 \pm 0.0000005$ MeV is exceeding energy of the marker γ_n-quantum ("start": $^{22*}\mathrm{Ne} \xrightarrow{E_{\gamma n}=1.274577\,\mathrm{MeV}} {}^{22}\mathrm{Ne}$; $\Delta m_{np}c^2 - E_{\gamma_n} = 18.7547$ keV).

There was an idea to link the difference $\Delta m_{np}c^2 - E_{\gamma_n} = 18.7547$ keV with response energy resonance in the topological quantum transition under β^+-decay ^{22}Na, because the kinetic energy of neon atoms from gaseous phase "freeze" on the $+M_{Pl}$ lattice during the β^+-*o*-Ps lifetime, and the final-state neutrino also participates in "vertical" ($\updownarrow$) oscillations and gains the additional (topological) mass ($m^{\mathrm{eff}}_{\nu_e}$)

$$^{22}\mathrm{Na}(3^+) \to {}^{22*}\mathrm{Ne}(2^+) + e^+_{\beta} + \nu_e + U^{\pm}.$$

Then $\Delta m_{np}c^2$ exceeding E_{γ_n} may be presented as follows

$$\Delta m_{np}c^2 - E_{\gamma_n} = \frac{3}{2}\, k\, T\bar{n} + m^{\mathrm{eff}}_{\nu_e} = 18.7547\ \mathrm{keV},$$

where $\frac{3}{2} kT\bar{n} = 0.038 \times 5.2780 \times 10^4 \cong 2$ keV, $m^{\mathrm{eff}}_{\nu_e} \cong 16.75$ keV.

The effective mass of the neutrino $m^{\mathrm{eff}}_{\nu_e}$ is equal to the mass heavy 17-keV neutrino as a possible result of mixing "horizontal" generation of neutrinos (a brief review of the 17-keV neutrino problem is described in monograph [44]). The dramatic history of experimental studies of 17-keV neutrinos is similar to the history of the β^+-orthopositronium problem [44, 45].

All the anomalies in the "β^+-decay ^{22}Na — neon ($\sim 9\%$ ^{22}Ne)" system — blurred shoulder and variability of the observed β^+-orthopositronium intensity (I_2) (up to factor 2) [9, 14] — are explained by the assumption of existence of the temperature-dependent resonance I_2. The inert gas temperature (the laboratory temperature) was not monitored in lifetime spectra measurements [2–6, 14].

Submitted on October 5, 2016 / Accepted on October 19, 2016

References

1. Tao S.J., Green J.H., and Celitans G.J. *Proc. Phys. Soc.*, 1963, v.81, 1091.
2. Osmon P.E. *Phys. Rev.*, 1965, v.B138(1), 216.
3. Goldanskii V.I. & Levin B.M. Institute of Chemical Physics, Moscow (1967): in *Atomic Energy Review*, v.6, IAEA, Vienna, 1968; in *Table of Positron Annihilation Data*, Ed. By B. G. Hogg, C. M. Laidlaw, V. I. Goldanskii and V. P. Shantarovich, pages 154, 171, 183.
4. Canter K.F. and Roellig L.O. *Phys. Rev.*, 1975, v.A12(2), 386.
5. Mao A.C. and Paul D.A.L. *Canad. J. Phys.*, 1975, v.53(21), 2406.
6. Coleman P.G., Griffith T.C., Heyland G.R. and Killen T.L. *J. Phys.*, 1975, v.B8(10), 1734.
7. Griffith T.C. and Heyland G.R. *Phys. Rep.*, 1978, v.39(3), 170.
8. Coleman P.G., Griffith T.C., Heyland G.R. and Killen T.L. *J. Phys.*, 1975, v.B8(10), L185.
9. Marder S., Huges V.W., Wu C.S., and Bennett W. *Phys. Rev.*, 1956, v.103(5), 1258.
10. Levin B.M. and Shantarovich V.P. *Khim. Vys. Energ.* (*High Energy Chem. USSR*), 1977, no.11, 382.
11. Campeanu R.I., Dubau J. *J. Phys.*, 1978, v.B11, L567.
12. Levin B.M. *Sov. J. Nucl. Phys.*, 1981, v.34(6), 917.
13. Levin B.M., Shantarovich V.P. Anomalies of Positron Annihilation Lifetime Spectra in Gaseous Neon. *ICPA-7*, sect. D38, January 6–11, 1985, New Delhi, India.
14. Levin B.M., Kochenda L.M., Markov A.A., and Shantarovich V.P. *Sov. J. Nucl. Phys.*, 1987, v.45(6), 1119.
15. Levin B.M. About extension of the Standard Model of Physics; see Appendix: About physical nature "resonance conditions" in the lifetime annihilation spectra of the positron (orthopositronium) from β^+-decay ^{22}Na in gaseous neon. http://science.snauka.ru/2013/01/3279
16. Vallery R.S., Zitzewitz P.W., and Gidley D.W. Resolution of the Orthopositronium-Lifetime Puzzle. *Phys. Rev. Lett.*, 2003, v.90(20), 203402.
17. Kotov B.A., Levin B.M., and Sokolov V.I. Orthopositronium: On the possible relation of gravity to electricity. arXiv: quant-ph/0604171.
18. Landau L.D. Collected Papers, 1965, 800–802.
19. Feynman R. *Acta Phys. Pol.*, 1963, v.24, 697 (*Conference on Relativistic Theories of Gravitation*, July 1962).
20. Hoyle F., and Narlikar J.V. *Proc. Roy. Soc.*, 1964, v.A282, no.1389, 178.
21. Gliner E.B. *Sov. Phys. JETP–USSR*, 1966, v.22, 378.
22. Ogievetskii V.I., Polubarinov I.V. *Sov. J. Nucl. Phys.*, 1967, v.4, 156.
23. Iverson G.J., and Mack G. *Phys. Rev.*, 1970, v.D2(10), 2326; *Ann. Phys.*, 1971, v.B64(10), 211.
24. Lyuboshits V.L., Podgoretskii M.I. *Sov. Phys. JETP–USSR*, 1971, v.33(1), 5.
25. Golfand Yu.A., Likhtman E.P. *JETP Lett.*, 1971, v.13(8), 323.
26. Hawking S.W., Ellis G.F.R. The Large Scale Structure of Space-Time. Cambridge University Press, 1973.

27. Synge J.L. *Proc. Roy. Ir. Acad.*, 1974, v.A74(9), 67.
28. Levin B.M., Sokolov V.I. arXiv: quant-ph/0702063.
29. Andreev A.F. *JETP Lett.*, 1973, v.17(8), 303; *Sov. Phys. JETP–USSR*, 1974, v.38(4), 648.
30. Andreev A.F. *JETP Lett.*, 1982, v.36(3), 100.
31. Fayet P. and Mezard M. *Phys. Lett.*, 1981, v.B104(3), 226.
32. Di Vecchia P., Schuchhard V. *Phys. Lett.*, 1985, v.B155, 427.
33. Levin B.M. *Phys. At. Nucl.*, 1985, v.58(2), 332.
34. Glashow S.L. *Phys. Lett.*, 1986, v.B167, 35.
35. Linde A.D. *Phys. Lett.*, 1988, v.B200, 272.
36. Okun L.B. *Sov. J. Nucl. Phys.*, 1988, v.47(4), 752.
37. Kotelnikov G.A. *Izvestiya VUZov*, 1992, no.12, 69 (*in Russian*).
38. Andreev A.Yu., Kirzhnits D.A. *Phys. Usp.*, 1996, v.39(10), 1071.
39. Borissova L., Rabounski D. Fields, Vacuum, and the Mirror Universe. 2nd edition, Svenska fysikarkivet, Stockholm, 2009; Rabounski D., Borissova L. Particle Here and Beyond the Mirror. 3rd edition, American Research Press, Rehoboth (NM), 2012.
40. Fröhlich J. *Phys. Blätter*, 2001, B57(7/8), 53.
41. Okun L.B. On the Article of G.Gamov, D.Ivanenko, and L.Landau "World Constants and Limiting Transition". *Phys. At. Nucl.*, 2002, v.65(7), 1370; Cube or hypercube of natural units. arXiv: hep-ph/0112339; in: Michael Marinov memorial volume *Multiple Facets of Quantization and Supersymmetry*, Ed. by M. Olshanetsky, A. Vainshtein, World Scientific Publishing, 2002, 670–675.
42. Sukhanov A.D., Golubjeva O.N. *Physics of Elementary Particles and Atomic Nuclei*, 2010, v.41(7).
43. Prokhorov L.V. *Physics of Elementary Particles and Atomic Nuclei*, 2007, v.38(3), 696; 2012, v.43(1), 4.
44. Klapdor-Kleingrothhaus H.V., Staudt A. Teilchenphysik ohne Beschleunger. B. G. Teubner, Stutgart, 1995.
45. Levin B.M. arXiv: quant-ph/0303166.

Half-Century History of the Project of New (Additional) $G\hbar/ck$-Physics

Boris M. Levin

Semenov Institute of Chemical Physics, Russ. Acad. Sci, Moscow (1964–1987)
In cooperation with Konstantinov Institute of Nuclear Physics, Russ. Acad. Sci., Gatchina (St. Petersburg) (1984–1987)
Ioffe Physical-Technical Institute, Russ. Acad. Sci., St. Petersburg (2005–2007)
E-mail: bormikhlev@yandex.ru

The origins of fundamental knowledge, which were mentioned by the genius of Pushkin, are closed in the history of science like in lens focus. This paper survey the 50-years history of studying the orthopositronium anomaly, where the author spent decades on the substantial experiments and further analysis among the experiments made by other experimental groups in different countries throughout the world.

Oh, how much of wondrous discoveries
Enlightenment Spirit preparing for us
And Experience the son of difficult errors
And genius, the paradoxes' friend,
And Case — the got of all inventions.

A. S. Pushkin, 1829

. . . Enlightenment spirit. . .

A single (as one might think) yet fundamental (!) phenomenon — **the annihilation of positrons emitted by a ^{22}Na isotope (and the like) in positron beta decay in inert gases** — combines all the types of physical interactions, such as: **strong/nuclear** interaction (transformation of a *proton* into a *neutron* in a *neutron-deficient atomic nucleus* with emission of a *positron* and a *neutrino*); **electromagnetic** interaction (electrically charged *proton* and *positron* with magnetic moments); **weak** interaction (emission of *neutrino*); and **gravity** interaction, since experiments have only been made in *ground-based* laboratories so far.

Therefore, if we come to think of it, we should not exclude the special role of the half-century *observations of anomalies in neon* (1956–2003) in making a *unified description of physical interactions* (*unified field theory*). Furthermore, these observations are only possible with *monoatomic* gases, which are the closest to the ideal gas status [1].

This idea is relevant against the backdrop of stagnation in fundamental physics (since mid-1970s), as Standard Model (SM) formulated in the same period has led to development of idea started by Einstein (with no final success through) and for the first time worded by Faraday (in respect of then known gravity and electromagnetism) [2]. The idea was given an official status in the XX century. It was the idea of all the fundamental interactions (the Theory of Everything).

The constructive idea presented by the new (additional) $G\hbar/ck$-physics Project could not emerge a priori. The signs of *new physics* in the experimental data on the beta-decay positron annihilation in inert gases were recorded for the first time by experimentalists involved in solving the issues of orthopositronium/parapositronium with a chemical-physical (or physical-chemical) "pedigree".

However, it would be impossible to implement the idea without the results achieved by fundamentalist theoreticians in their independent efforts on expanding SM [1]. It is clear why the phenomenology of the $G\hbar/ck$-physics Project finalized among experimenters a decade ago cannot get through to implementation of the *Decisive Experiment Project* [4], despite being based on the giant effect exceeding the SM estimate by 6–7 orders of magnitude [3].

Nevertheless, there is another reason, which the prominent ethologist Konrad Lorenz described as one of "*the civilised man's eight deadly sins*". It is *indoctrinability of the "Big Science"* (susceptibility to fashion and stereotypes).

"...never before have the manipulators had at their disposal such clever advertising techniques or such impressive mass media as today. [...]

However, the worst effect of fashion ... can be observed in the realm of science. It is mistake to suppose that all professional scientists are free from the cultural diseases that are the subject of this treatise. [...] "Big Science" in no way implies a science concerned with the most important things on our planet, nor is it the science of the human psyche and intellect: it is exclusively that science which promises money, energy, or power... [...] The special danger of fashionably indoctrination in the field of science lies in the fact that it leads too many, though fortunately not all modern scientists, in a directions exactly opposite to that of the real aim of all human striving for truth — the aim for the better self-knowledge" [5].

In 1970s, K. Lorenz still retained hope for overcoming the "*mortal*" contradictions. In another essay of this, we can feel the spirit of the Rome Club ("*sustainable development*") founded in those years:

"I believe that we can see the true sings that self-consciousness begins to awaken in the cultural humanity, based on scientific knowledge. [...] **Until now, there has never been a rational self-study of human culture on our planet**, just like there was no objective, in our opinion, natural science before Galileo' s times. [...]

Of course, the position of mankind is now more dangerous than it has ever been in the past. However, thinking found by our culture due to its natural science potentially gives it a

change to escape death that befell all the high cultures in the past. This is the first time in world history" [6].

The first (and only so far) constructive response by theorists to the unique information on the positron (orthopositronium) annihilation anomalies, received by "quiet physics" (without accelerators of ultrahigh-energy particles) after they created the mathematical theory of the existence of the *third form of matter* [7], is that the experimental data was understood by the authors as subject for application of their fundamental theory [8]. Through paradoxical expansion of the general relativity, they "... studied the possibility of coexistence of short-range and long-range actions", using the method of chronometric invariants (physical observable values, A. L. Zelmanov, 1956). The theoretical (mathematical) prediction of the existence of the third form of matter (*zero-particles*) in the *zero-space* became an additional incentive for building the phenomenology of new (additional) $G\hbar/ck$-physics on the way to justifying the anomalies in neon.

And experience the son of difficult errors...

The start (1964) of assumption of a new range of time spectrometry (up to 200 ns) at the Department of Matter Structure of the Institute of Chemical Physics Academy of Sciences USSR/DMS IChP in Moscow (led by Professor V. I. Goldanskii) to study the annihilation of beta-decay positrons in physical media with the large void volume (gases or porous solids) coincided with the publication of a work by P. E. Osmon from Columbia University, New York, presenting comparative data on annihilation of quasi-free positrons (from the Na-22 isotope) in all inert gases at pressures of several atmospheres and room temperature [9].

Here is the abstract of this work:

"Positron lifetime spectra have been measured in helium, neon, argon, krypton, and xenon at pressures of a few atmospheres. The annihilation rates of the free positrons are found to be time-dependent. Physical reasons, based on the strong correlation between energy and age of a positron, are suggested for this time dependence. Three parameters describing the main features of the free-positron spectrum are separated from the data, for each gas, and tabulated".

Neither the abstract, nor the article itself contains any reference to the characteristic feature of *neon* lifetime diagrams. Lifetime diagrams show a nonexponential feature of this area of the lifetime spectra — the so-called *shoulder*. Its manifestation is generally enhancing from helium to xenon along with the increasing atomic number of gas Z. However, *neon* stands out — the shoulder in its diagrams is blurred or nonexistent at all.

It was decided to repeat the observation in the *helium-neon-argon* area to verify the said distinctive feature of neon. The blurring effect in the shoulder of neon was confirmed. The result were published (1967) in the departmental Newsletter of the Institute of Instrument Engineering, which provided time range converter into digital vernier type code up to 200 ns for lifetime spectrometer, and in Tables [10].

V.I.Goldanskii discussed the results at international meetings. Later on, several laboratories took up measurements with neon and confirmed the neon shoulder blur [11–14].

As we known, polyatomic impurities in inert gas influence the dynamics of positron moderation under the positronium formation threshold due to inelastic energy losses on the background of elastic moderation in inert (monoatomic) gas. Therefore, the difference in shoulder parameters between experimental data obtained in different laboratories could be attributed to differences in residual polyatomic impurities in neon samples used in the experiments [9–14], despite the fact that neon had the *ultra-high purity* grade in all the experiments.

However, an analysis of all the experimental data showed that this cannot explain the observed differences in shoulder parameters in neon. In our measurements, using *the same sample of neon* in a wide pressure range (16 atm to 32 atm), the product of the shoulder length t_s and the gas pressure p (the constant for ideal gas [1]) differ almost twofold (from 500 ns atm to 900 ns atm); in [10] these results are only represented by upper limit of 900 ns atm). The true result (500÷900) ns atm was reported by V. I. Goldanskii (see [11]*, [14]†). At the same time, according to our measurements, the shoulder lengths in helium and argon remain constant (with in the experimental errors) [10].

A decade after the shoulder blur in neon had been confirmed, a hypothesis was published that the marker gamma-quantum of lifetime spectrometer is collectivized under special conditions of the system described as "**beta-decay of a Na-22 isotope** $\xrightarrow{\text{positron+neutrino}}$ **excited Ne-22** (the source of the marker gamma-quantum of the lifetime spectrometer/ "start") **in gaseous neon with natural isotope composition (~9% of the Ne-22 isotope)**" [15].

Two decades later, a comparative critical experiment was made on separated neon isotopes [3]. The experiment confirmed the hypothesis and opened up the prospects for expanding SM and building the phenomenology of $G\hbar/ck$-physics.

The project of new $G\hbar/ck$-physics was surprisingly supported by the results of the Michigan group (University of Michigan, Ann Arbor) for absolute measurement of the lifetime (the reciprocal of the self-annihilation rate) of an orthopositronium (1982–1990). Two methods (with buffer gases and in vacuum) revealed that the self-annihilation rate of an orthopositronium is exceeded by ($0.19 \pm 0.02 \div 0.14 \pm$

*"Aside from the presence of the prompt component, it is very difficult to discern any nonexponential region of the spectrum. Goldanskii claims to see a shoulder in his room-temperature spectra, (ρt_s = 500–900 nsec amagat), but he states that it is considerably weaker than that which occurs in helium and is difficult to locate".

†"The only other evidence for the shoulder comes from the work Goldanskii and Levin reported by Hogg et al. [10] to have a width in the range 500–900 ns amagats".

0.023) percent compared with the calculated value (quantum electrodynamics/QED), which has reached the accuracy of $1.6 \times 10^{-4}\%$ by now. As we see, the deviation of the experimental data from the theory was recorded at the level of 10σ (standard deviation)!

These groups of H.M. Randal Laboratory at the University of Michigan led by Professor A. Rich (1937–1990) were the world leaders in the orthopositronium lifetime absolute precision measurements. The irony is that the article titled "*Resolution of the Orthopositronium-Lifetime Puzzle*" [16], published by the Michigan group in Phys. Rev. Lett., and disavowed the results of the group's previous measurements (1982–1990), which were in conflict with the theory, and thus "closed" the problem for the scientific community.

In the modified method, an auxiliary electric field was introduced *vertically* in the measurement chamber [16]. A sequential analysis, taking into account all the information available, showed that previously found discrepancy between the theory and the experiment would be preserved with a *horizontal* direction of the auxiliary electric field [17].

In all fairness, Work-2003 had a constructive role too. Its destructive conclusions made it possible to find and substantiate the manifestation of the fundamental connection between *gravity* and *electricity*, which was the cause of the wrong conclusion by the Michigan group, who did not have all the experimental data available by the time.

The shoulder shape is influenced by intensity of the orthopositronium component I_2, since the **orthopositronium component follows the component of annihilation of quasi-free positrons on the time axis** in lifetime spectra. This can cause the shoulder blurring and problems with anomalies of beta-decay positrons (from Na-22) annihilation in neon [3,9–13], because the **laboratory temperature was not taken into account in all of this measurements**.

It is also worth nothing that there is an abnormally high share of positrons forming a positronium in gaseous neon — $(55 \pm 6)\%$ — obtained on the energy spectrum of the annihilation gamma-quanta with Cu-64 as the source of positrons [18] in contrast to half the value — $(28 \pm 3)\%$ — obtained by a lifetime method with Na-22 as the source of positrons.

And genius, the paradoxes' friend...

The blatant paradox in the perspective of justification on the hypothesis of collectivization of Ne-22 nuclear excitation ($\cong$ 1.28 MeV) by nuclei of Ne-22 atoms with natural isotopic composition ($\sim$ 9%) in the macroscopic volume of the measuring chamber at the final stage of the beta-decay of Na-22 nucleus was confirmed by comparing the lifetime spectra of neon samples — a natural one and a sample depleted by Ne-22 isotope [15]. As said above, the effect of changing I_2 was 6–7 orders of magnitude higher than the estimate of SM.

Now we can exclude the general suggested version of the determining role of the residual polyatomic gas impurities.

The paradox is that, in experimental conditions [3], the Mössbauer effect (nuclear gamma-resonance) takes place for a sufficiently hard gamma-quantum ($\cong$ 1.28 MeV) of the excited daughter Ne-22 nucleus, located on the solid positron source, and nuclei of Ne-22 atoms staying in gas at room temperature. As we known, the Mössbauer Effect is possible in condensed media (solids: crystalline, amorphous, or powder one).

Most likely, this paradoxical formulation of the issue was due to the fact that two group of experimenters were working alongside at DMS IChP in Moscow (from beginning 1960s) led by V.I. Goldanskii — "positron group" (the group of Chemistry of New Atoms) and "Mössbauer group" (the Mössbauer Effect laboratory). The groups met at general workshops, making presentations and passively sharing information and ideas.

The concept of zero-space (zero-particles) as an extension of the *general relativity* [7] has set a framework for overcoming the paradox through introduction of the four-dimensional space-time on the *outside* of the light cone into fundamental physics.

But how shall we implement this program on a quantitative level, when compared with the experimental data?

The collective genius of famous and prominent theorists, who independently sought (each for their own reasons) to go beyond SM, determined the development of a phenomenology of new (additional) $G\hbar/ck$-physics [1]. The search for unique and rarely-cited works of theorists with high index of citing continued for two with half decades (1987–2012) following publication of the critical experiment results [3].

An analysis of the paradoxical experimental situation has led to the conclusion that the macroscopic volume of the double-valued ($\pm$) four-dimensional space-time of the final state of positron beta-decay of $\Delta J^{\pi} = 1^{\pi}$ type is filled with bonded Hamiltonian chains/cycles of the *nucleus* of the atom of long-range action (with a number of nodes $\bar{n} \cong 5.2790 \times 10^4$) and the *atom of long-range action* as a whole ($N^{(3)} = 1.302 \times 10^{19}$) [1].

Summing up this phenomenology, we can say that two fundamental (mathematical) abstractions — the *material point* (*inside* the light cone) and *absolutely rigid body* (*outside* the light cone) — will determine the relevant expansion of SM (the *unified quantum field theory*).

A decisive experiment in the study of the supposed temperature resonance I_2 in the range $-30^{\circ}\mathrm{C} < T < +30^{\circ}\mathrm{C}$ (see [4], Appendix) will finally clarify the issue of anomalies of positron (Na-22) annihilation in gaseous neon.

And case — the God of all inventions

One might think that the sacral line by Pushkin is a poetic paraphrase of a revelation from the New Testament, the Apostle Paul to the Romans 11:33, "*Oh, the depth of the riches and wisdom and knowledge of God! How unsearchable are*

His judgments and His ways!" The deep thought received a lapidary form — "*The ways of God are inscrutable*".

Fundamental physics is the search for Truth, for understanding of the basic of Existence — the space-time (quantitative criteria of cause-and-effect relationship, *experiment and theory*).

However, since the mid-1970s, physics suffers a profound crisis. At no time in history there was such a long stagnation of fundamental knowledge, when the issue was formulated (e.g. *How does the supersymmetry manifest itself? What is the nature of dark matter/dark energy? What is the mainstay of consciousness? And others???*), but they had no solutions. This breaks the formation of fundamentally new technologies. That cannot not have globally destructive social consequences.

There is a high measure of confidence, that crisis could be overcome for a long time. A decade before the physicists understood the heuristic importance of supersymmetry, there was made an experiment [9, 10], which laid the foundation for the study of anomalies in the system described as "**beta-decay of a Na-22 isotope $\xrightarrow{\text{positron+neutrino}}$ excited state of Ne-22 isotope (the source of the marker gamma-quantum of the lifetime spectrometer/"start") in gaseous neon with natural isotopic composition (~9% of Ne-22 isotope)** — "resonance conditions" [15]". Later on, this anomaly was linked to the anomaly of the positronium share in neon (55 ± 6)% under nonresonance conditions (with Cu-64 as the source of positrons) [16].

All of this have prepared the ground for the introduction of space-like object physics (i.e., on the outside of the light cone) in the fundamental context.

Physics is one, but the now prevailing stereotype — the increased interest in ultra-high energies as a prospect for overcoming stagnation — and neglect of the unique data received by "quiet physics", does not promise to overcome stagnation. The existence of the quantum-field resonance as a consequence of the existence of a *nucleus of the atom of long-range action* is possible, if energy $m_p \times \bar{n} \cong 50$ TeV (where m_p is proton mass), which is half order of magnitude greater than the energy of the colliding proton beams of the Large Hadron Collider. It is very distant, if not illusory prospect...

The core of the Project of New (Additional) $G\hbar/ck$-physics was the critical experiment [3]. It was the result of previous work in many laboratories [9–13], an independent breakthrough by theorists to the double-valued ($\pm$) four-dimensional space-time [7], which virtually legalized the results of independent theoretical searches for the way to go beyond Standard Model by the methods of the *general relativity* [19] and the *quantum field theory* ([20] and [21]).

Setting a decisive experiment promises a breakthrough to the *unified field theory* based on expansion of the Hamiltonian method by including the Hamiltonian chain/cycle [1].

Submitted on October 5, 2016 / Accepted on October 19, 2016

References

1. Levin B.M. *Progress in Physics*, 2017, v.13, issue 1, 11–17.
2. Faraday M. The Bakerian Lecture. *Philosophical Transactions*, 1851, 1.
3. Levin B.M., Kochenda L.M., Markov A.A., and Shantarovich V.P. *Sov. J. Nucl. Phys.*, 1987, v.45(6), 1119.
4. Levin B.M. http://science.snauka.ru/2013/01/3279 (Appendix).
5. Lorenz K. Die acht todsünden der zivilisierten Menshheit. R. Piper & Co., München, 1973.
6. Lorenz K. Die Rückerte des Spiegels: Versuch einer Naturgeschichte menschlichen Erkenners. R.Piper & Co., München, 1973.
7. Borissova L.B., Rabounski D.D. The theory of movement of particles in four-dimensional space-time. Lomonossov Workshop, Moscow, 1997 (*in Russian*); Rabounski D.D. Three form of existence of matter in four-dimensional space-time. Lomonossov Workshop, Moscow, 1997 (*in Russian*).
8. Borissova L., Rabounski D. Fields, Vacuum, and the Mirror Universe. 2nd edition, Svenska fysikarkivet, Stockholm, 2009; Rabounski D., Borissova L. Particle Here and Beyond the Mirror. 3rd edition, American Research Press, Rehoboth (NM), 2012.
9. Osmon P.E. *Phys. Rev.*, 1965, v.B138(1), 216.
10. Goldanskii V.I. & Levin B.M. Institute of Chemical Physics, Moscow (1967): in *Atomic Energy Review*, v.6, IAEA, Vienna, 1968; in *Table of Positron Annihilation Data*, Ed. By B. G. Hogg, C. M. Laidlaw, V. I. Goldanskii and V. P. Shantarovich, pages 154, 171, 183.
11. Canter K.F. and Roellig L.O. *Phys. Rev.*, 1975, v.A12(2), 386.
12. Mao A.C. and Paul D.A.L. *Canad. J. Phys.*, 1975, v.53(21), 2406.
13. Coleman P.G., Griffith T.C., Heyland G.R. and Killen T.L. *J. Phys.*, 1975, v.B8(10), 1734.
14. Griffith T.C. and Heyland G.R. *Phys. Rep.*, 1978, v.39(3), 170.
15. Levin B.M. and Shantarovich V.P. *Khim. Vys. Energ.* (*High Energy Chem. USSR*), 1977, no.11, 382.
16. Vallery R.S., Zitzewitz P.W., and Gidley D.W. Resolution of the Orthopositronium-Lifetime Puzzle. *Phys. Rev. Lett.*, 2003, v.90(20), 203402.
17. Levin B.M. arXiv: quant-ph/0303166.
18. Marder S., Huges V.W., Wu C.S., and Bennett W. *Phys. Rev.*, 1956, v.103(5), 1258.
19. Gliner E.B. *Sov. Phys. JETP–USSR*, 1966, v.22, 378.
20. Andreev A.F. *JETP Lett.*, 1973, v.17(8), 303; *Sov. Phys. JETP–USSR*, 1974, v.38(4), 648.
21. Glashow S.L. *Phys. Lett.*, 1986, v.B167, 35.

Probing Quantum Memory Effects in the Single Photon Regime

Carlos Belmonte[1], Frederik Vanden Berghe[1], Krassimir Panajotov[1,2], Thomas Durt[3*]

[1]B-Phot. Vrije Universiteit Brussel Pleinlaan 2, 1050 Brussel, Belgium.
[2]Institute of Solid State Physics, 72 Tzarigradsko Chaussee blvd., 1784 Sofia, Bulgaria.
[3]Aix Marseille Université, CNRS, Centrale Marseille, Institut Fresnel, UMR 7249, 13013 Marseille, France.
*Corresponding author: thomas.durt@centrale-marseille.fr

In this paper we study correlations present in experimental random series extracted from a Quantum Optical Random Number generator conceived and implemented in our lab. In particular we study the manifestations of inertia/memory effects. This study is realized in the single photon regime.

1 Introduction

We learn from classical and quantum physics that the future properties of a physical system are determined by its instantaneous, present state. This is reminiscent of the so-called Markov property in statistics, according to which* *"...the conditional probability distribution of future states of the process, given the present state and all past states, depends only upon the present state and not on any past states..."*

In previous papers (see [5] for a survey), one of us (T. D.) studied the possibility that quantum correlations exhibit non-Markovian features [4], in other words that quantum correlations would be endowed with an intrinsic, non-standard memory effect. Actually, several experiments were realized in the past, in different contexts, in order to test the possibility of such memory effects [2–4, 7]. These experiments aimed at testing hidden variable models (both local and non-local models [5]) which predicted the appearance of non-standard correlations between measurement outcomes collected at different times (different places in the case of non-local models [2]). We shall not enter in the detail of these experiments and models here, but instead we shall focus on the results of a statistical test that we developed in the past in order to characterize quantum random number generators that were developed at the Université Libre de Bruxelles (U.L.B.) and Vrije Universiteit Brussel (V.U.B.). We developed this test, from now on denoted the Histogram Inertia Indicator (H.I.I.) test in order to reveal whether histograms constituted from data measured at different times were correlated to each other.

Besides the aforementioned hidden variable models, we found inspiration in the idea of morphic resonance expressed and developed by Rupert Sheldrake [17] according to which the evolution of species and development of life in general are characterized by memory effects having as a consequence that new shapes/patterns tend to behave as attractors for other shapes/patterns. In a previous paper we showed that mixing Sheldrake's ideas and hidden variable models led to the prediction of observable non-standard memory effects (see [4] section 3: Sheldrake and Smolin's Models, and a Related Experimental Proposal).

*Quoted from Wiktionary.

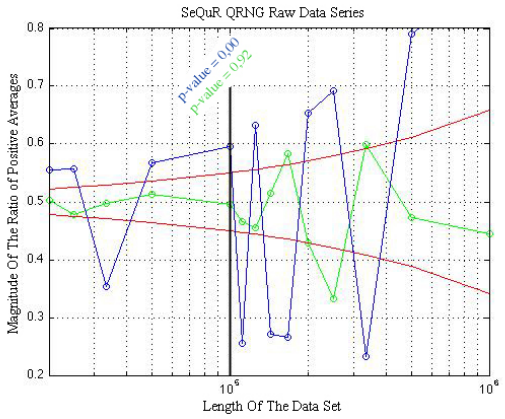

Fig. 1: SeQuR QRNG - Raw Data: A "near zone" effect is clearly present in the SeQuR data (blue graph). Successive histograms, each drawn from 1000 sequential random values, exhibit a manifest tendency to resemble each other. The green graph represents the same test on a Matlab pseudo-random series. The red lines represent the boundaries that are assigned to "perfect" random series. The plotted p-values confirm the results in graphical form. (quoted from [19])

Our main goal, when we developed the H.I.I. was to try and reveal whether quantum histograms would exhibit memory effects. It can be seen as an attempt to extrapolate the extent of validity of Sheldrake's ideas to the quantum realm.

A last source of inspiration was provided by the evidence for annual periodicity in decay data [9, 10] that has been revealed a few years ago. It has been suspected that this periodicity cannot be explained by environmental effects such as temperature, humidity, pressure, *etc* [11], nor is there a correlation with the Sun-Earth distance after re-analysation of the data [13].

All these observations suggest that there could exist some "regularity in randomness", some "hidden" pattern, a non-standard memory effect characterized by correlations between data collected at different times. This is a very upsetting and at the same time challenging idea which deserves to be considered seriously, from a foundational perspective [2–5, 7].

In particular we noticed the presence of an intriguing memory effect already some years ago [19], at the level of a random optical signal measured in the continuous counting

regime (see section 2.3). The data were delivered to us by colleagues from the U.L.B. developing a prototype of ultra-fast quantum optical random number generator [6]. Essentially, this device amplified fluctuations of the intensity delivered by a laser source. The results plotted at the level of Fig. 1 reveal for instance a clear deviation from the theoretical boundaries (in red) associated to a fully random process (without memory effect). We also checked in the same work [19] that Fourier filtering and/or Faraday filtering diminishes the effect, but does not suppress it totally. Our interpretation of these observations is that these correlations could be partially due to an external mechanism, and partially due to the internal memory of the device (here the light detector which is acting in the continuous (many photons) regime).

It was not clear however, uniquely on the basis of the observations, to decide whether the external source of the correlations had to be attributed solely to electromagnetic pollution (GSM devices, FM radio channels and so on) or whether it was necessary to resort to a universal memory effect in order to explain our observations.

Therefore we decided to test experimentally similar memory effects in the low intensity (single photon) regime, which was made possible by the development of quantum random number generators (QRNG) active in the low intensity (discrete counting) regime *in situ* in our labs and based on the random character of time delays between clicks collected with a single photon avalanche detector at the output of an attenuated laser source. The corresponding generator, the so-called Parity Quantum Optical Random Number (PQORN) generator has been described in a separate publication [6] and is briefly described in section 3.1 (see also Fig. 2).

As we shall describe in the present paper, we applied the H.I.I. test to the raw data generated with our PQORN generator. This program is triply challenging in our eyes because, as far as we know, nobody tested in the past the existence of memory effects by the same method, and *a fortiori* no such test has been achieved so far in the low intensity regime. Last but not least, if the memory effect revealed by the H.I.I. indicator is universal, its detection provides a criterion for discriminating physical randomness from pseudo-randomness which is a very challenging idea.

The paper is structured as follows. We describe in section 2 a new statistical test, the H.I.I. test, introduced in [19] aimed at measuring and/or revealing memory effects (section 2.1), as well as the corresponding p-value (section 2.2). Our methods are also relevant in the framework of random number generation because the H.I.I. test and the associated p-value are thus useful tools in order to characterize randomness.

Before scrutinizing (making use of the tests described in section 2) the existence of memory effects at the level of the PQORN generator (section 4), we investigated more in depth the correlations which appear in the high intensity regime at the level of our single photon detectors (section 3.2). These correlations are *a priori* not of quantum nature but they are induced by the dead time of the detector. As we show in section 4, in the high intensity regime, and only in this regime, the H.I. memory effect is present.

We also studied whether similar memory effects still exist beyond the near zone regime studied in section 4.1, and in particular whether non-local in space (section 4.2) and time (section 4.3) memory effects (previously denoted Spatial and Temporal Long Range Memory effects) can be measured at the level of our device. The last section is devoted to the conclusions and to the interpretation of the collected results.

2 The near-zone H.I.I. test

2.1 Qualitative test

In order to derive a statistical test aimed at revealing memory effects, we approached the problem as follows [19]: Each histogram of a given data sample – given it is not too large

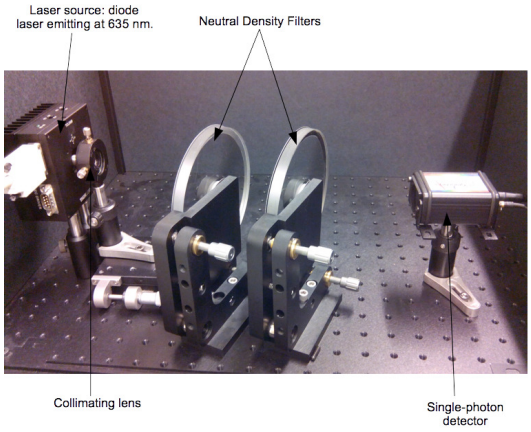

Fig. 2: Detailed setup for the near-zone experiment. It is composed of a laser source, two neutral density filters and a single photon detector. The same setup, supplemented with a nanosecond resolution clock constitutes the Parity QORNG.

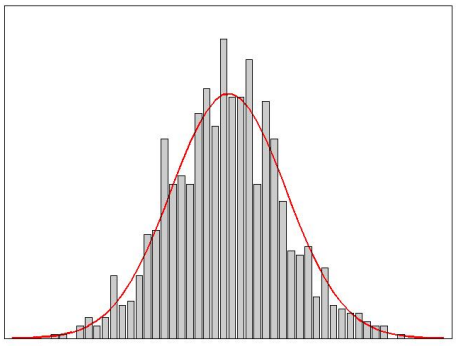

Fig. 3: Fluctuations of a sample histogram - constructed from 1 000 gaussian distributed random data values - around the line of the average histogram computed from a data sample of 10 000 000 gaussian distributed random values.

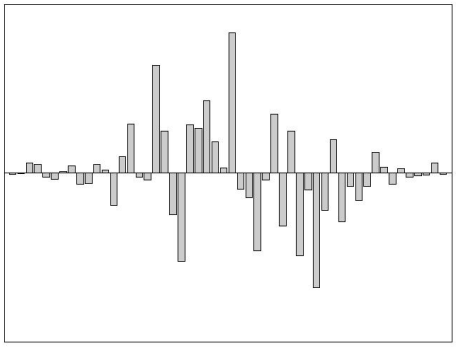

Fig. 4: The difference $\tilde{H}$ of a sample histogram H with the average histogram.

– fluctuates around the average histogram, which is obtained from a very large data sample, *cfr*. Fig. 3. For each histogram H we compute its difference with the mean histogram. This leaves us with a new normalized histogram $\tilde{H}$ in which each value can either have a positive of a negative value, depending whether that value is observed more or less often than in average, as shown in Fig. 4. Thereafter, we introduce a quantitative "resemblance" value r as follows. Consider $\tilde{H}_i$ and $\tilde{H}_j$ two neighboring histograms.

$$r_i = \sum_{\alpha} \tilde{H}_{i_\alpha} \tilde{H}_{j_\alpha} \quad \text{(with } j = i + 1\text{)} \tag{1}$$

with α the corresponding value of the histogram at this entry. Remark that we are working with histograms where values can be both positive and negative. Consequently, the inproduct r can be either positive or negative. The following interpretation can now be given to r:

- r **is large and negative**: Both histograms seem to be inverse of each other for most of the entries. The histograms have no near zone effect. Instead this suggests an anti- or complementary- "near-zone" effect.
- r **is close to zero**: Both histograms have approximately as much resemblance as difference. Again no "near zone" effect is observed.
- r **is large and positive**: Both histograms have the same shape for most of their entries. A "near zone" effect is then observed.

Considering that the random sequence of length n is divided in M data samples of length N, this analysis leaves us with $\lfloor \frac{N}{1000} \rfloor - 1$ values of r for each of the M samples, since we choose each histogram to be created from 1000 random values. Fig. 5 depicts graphical results after calculating all r-values.

This is only the first part of the investigation since, as one can deduce from Fig. 5, often, not much can visually be said about a possible "near-zone" effect. Therefore, it is appropriate to perform a statistical treatment of the data.

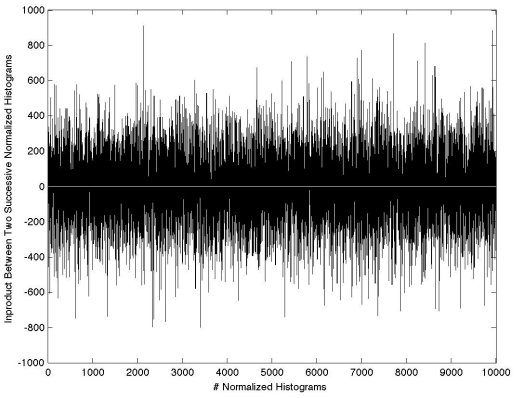

Fig. 5: Example graph of 9 999 inproducts between 10 000 successive histograms obtained from a data sample of $N = 10^7$ values.

Let us start by taking the average of all r inproducts:

$$\bar{r} = \frac{\sum_{i=1}^{\frac{N}{1000}-1} r_i}{\frac{N}{1000} - 1} . \tag{2}$$

Since the analysis is performed on M data samples of length N, each of the M samples now leaves us with one value of $\bar{r}$. These M average values $\bar{r}$ provide us with a qualitative indication of a "near zone" effect that we choose to express through the ratio of positive averages of $\bar{r}$, i.e.

$$\frac{\#\bar{r}_{pos}}{M} \tag{3}$$

with $\#\bar{r}_{pos}$ the amount of $\bar{r} \geq 0$. Note that the sign of $\bar{r}$ can be regarded as a Bernoulli process, or as a bit sequence with for example a bit value of 1 corresponding to a positive value and a bit value of 0 to a negative one. In a perfectly random process the ratio between them should be close to $1/2$ with a deviation depending on M, the amount of data samples. In order to determine the magnitude of this deviation we consider the law of large numbers to derive the boundaries:

$$\frac{\#\bar{r}_{pos}}{M} \sim \frac{1}{2} \pm \frac{\sigma_{bit}}{\sqrt{M}} = \frac{1}{2}\left(1 \pm \frac{1}{\sqrt{M}}\right) \tag{4}$$

with M the amount of data samples or the amount of values $\bar{r}$. For a data set of length n, $M = \lfloor \frac{n}{N} \rfloor$ so that the boundaries also depend on N.

It is expected for perfect random processes that the magnitude of the ratio of positive averages $\bar{r}$ will remain confined within the boundaries plotted in Fig. 6. One expects that sporadically $\bar{r}$ will be found outside the boundaries but in the case that it will remain persistently outside the boundaries we must suspect that the random sequence is biased. Considered so, we now have at our disposal a qualitative test aimed at testing the presence of the near zone effect. In the next section, we shall also derive a quantitative criterion, in the form of a p-value.

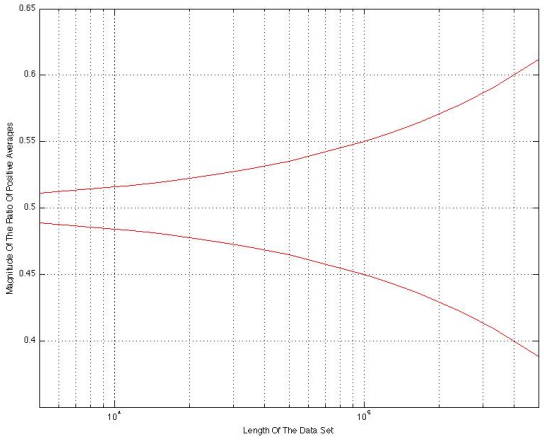

Fig. 6: Boundaries for the fluctuations of the ratio of positive averages $\bar{r}$ depending on M, the amount of data samples tested. Since a very large data sample is divided in M subsamples of length N, M decreases as N increases and consequently, the fluctuations also depend on the size N of the subsamples.

2.2 Derivation of a p-value for the near-zone H.I.I. test

The standard randomness tests (*e.g.* the NIST or Die Hard tests [12,16]) deliver their results through a so-called p-value. Typically, $p \in [0,1]$ is the probability of obtaining a test result at least as extreme as the one that was actually observed, assuming that the null hypothesis is true, *i.e.* the tested sequence is considered random. A p-value ≥ 0.01 indicates that the tested series of bits is random with a confidence interval of 99%. While the near-zone H.I.I. test described in the previous section is of qualitative nature and delivers its results in a graphical way, we shall now show how to connect a p-value to the different values in the graph of this near-zone H.I.I. test.

Recall that the value of $\bar{r}$ from (2) can be regarded as a Bernoulli process or conversely as a random walk if one considers a positive value of $\bar{r}$ as the value $+1$ and a negative value of $\bar{r}$ as -1. Consider the sequence $X = X_1, X_2, \ldots$ of values ± 1 in accordance to positive or negative values of $\bar{r}$. We define S_M as the sum

$$S_M = X_1 + X_2 + \ldots + X_M \tag{5}$$

with M the amount of values of $\bar{r}$ (see discussion at (2) and (3)). Compute the test statistics

$$Z = \frac{|S_M|}{\sqrt{2M}}\,. \tag{6}$$

Making use of the law of large numbers, the p-value can be shown [19] to be equal to

$$p\text{−value} = \operatorname{erfc}\left(\frac{Z}{\sqrt{2}}\right). \tag{7}$$

2.3 Near zone memory effect in the continuous counting regime

Some years ago [19], we investigated the existence of a memory effect at the level of an optical random number generator the SeQuR QRNG, acting in the continuous regime. Essentially, the device amplifies the fluctuations of the intensity delivered by a laser source [6]. We considered the decimal random data delivered by the detector. The tested results show clear similarities in the successive histograms from the data samples. This can be observed in Fig. 1, quoted from [19]. This analysis clearly indicates the presence of an inertia or memory effect in the signal. Let us now consider discrete data collected with single photon detectors.

3 Randomness in the low photon number regime

3.1 Parity QORNG

The *Parity QORNG* exploits the random nature of the distribution of clicks in a single photon detector. It is based on the parity of the time (in nanoseconds) for which the events (clicks) occur. If this time is even, the bit will be zero; if this time is odd, the bit will be one. The set-up to carry out this method consists of an attenuated laser source coupled to a single-photon detector (Fig. 2). The detector is coupled to a buffer via an acquisition card synchronized with a clock of high resolution (1 nanosecond).

As has been shown in [6], the principal advantages with this method are 1) that it requires to use only one photon-detector to generate a random number and 2) that even in the high intensity regime it delivers random series of very high quality*.

Before we characterize the H.I. effect, let us study the physical correlations exhibited by the single photon detectors of the parity QORNG.

3.2 Study of correlations due to dead-time of detectors

3.2.1 Successive clicks in one single-photon detector

In this section we will check the statistical properties of the data acquired in single-photon detectors in various regimes. These regimes are reached by modifying the attenuation of our two tunable attenuators (Fig. 2), from almost no attenuation at all to a high attenuation.

Before going further it is worth recalling that the single-photon detector is characterized by a dead time (that is to say the lapse of time during which the photon-detector will be off after detecting a photon) in the range of 45 to 50 ns. The resolution time of the acquisition card is 1 ns, therefore every 1 ns a datum will be acquired, while the maximum data that the acquisition card can memorize is 750 000 ns, after which the memory of the acquisition card is full.

*For instance bit series obtained from the PQORNG successfully pass [6] the NIST battery of standard randomness tests (frequency test, parity test, spectral test, entropy test and so on).

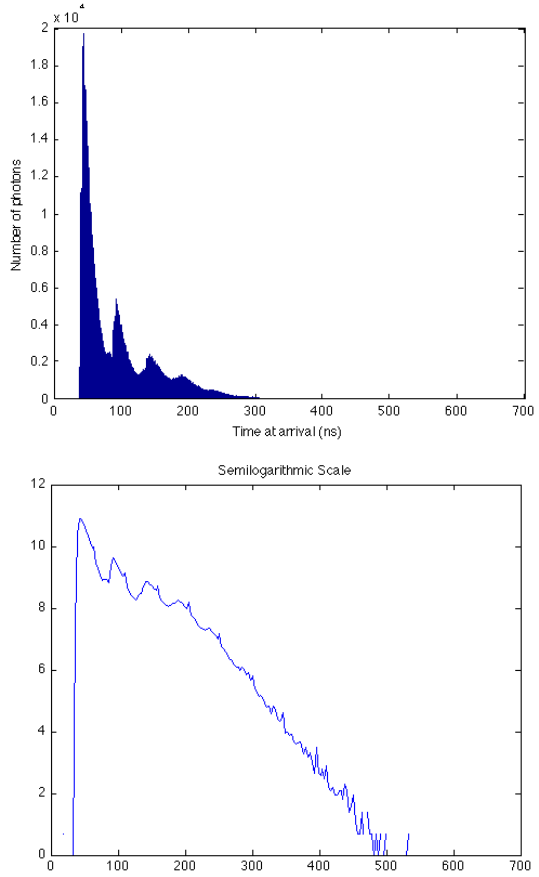

Fig. 7: Statistics of time arrival between photons in the high intensity regime. Average time between photons estimated to be more or less 36 ns.

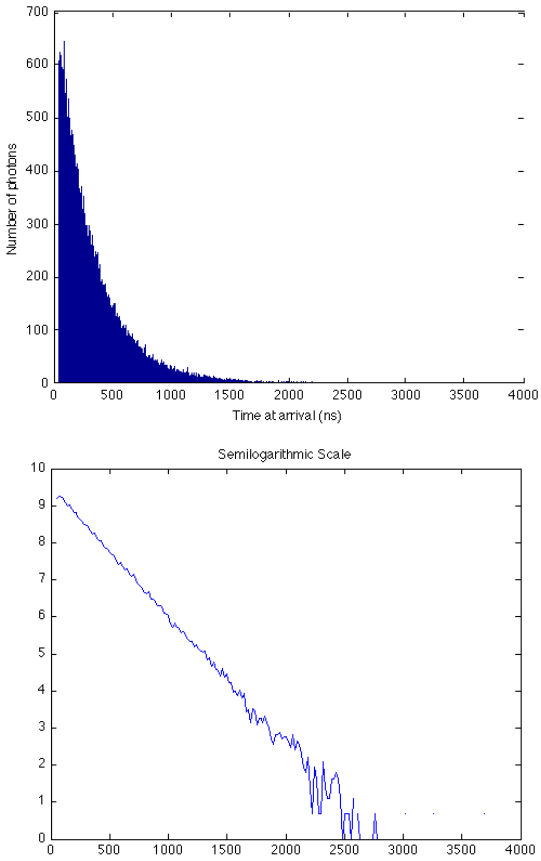

Fig. 8: Statistics of time arrival between photons in the low intensity regime. Average time between photons estimated to be more or less 294 ns.

Taking into account the specifications above, we performed a study of the time arrival between two photons in different regimes changing the attenuation. For instance, in the high intensity regime (low attenuation regime) we observe a distribution of delay times between clicks plotted in Fig. 7 which is contaminated by the correlations induced by the dead-time of the detector (as revealed by the presence of peaks separated by 45 ns). From the tail of the semi-logarithmic plot, we can infer the average time between two photons, which would be exactly the slope of the straight line if the distribution was Poissonian, which corresponds to a dead time equal to zero.

If in turn we work in a low intensity regime, for which the average time between two clicks is quite larger than the dead time of the detectors, we observe a nearly Poissonian distribution, as can be seen from Fig. 8. The single noticeable difference with a Poisson distribution is the null probability to measure successive clicks in a time smaller than the dead time (here 45 ns).

3.2.2 Simultaneous clicks in two single-photon detectors

In order to check the departure from the Poisson distribution, we estimated another parameter which is the number of simultaneous counts in two detectors placed at the output of a beamsplitter. When two photons arrive at the exact same time to the beamsplitter, there exist four possible scenarios (Fig. 9):

1. Both photons are detected by the photon-detector A.
2. Both photons are detected by the photon-detector B.
3. Photon A is detected by the photon-detector A and photon B is detected by the photon-detector B.
4. Photon A is detected by the photon-detector B and photon B is detected by the photon-detector A.

The probability of obtaining a single photon during a unit-period of time is (in case of a perfectly Poissonian distribu-

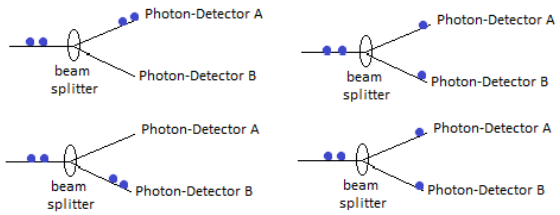

Fig. 9: Possibilities that two photons are detected by two photon-detectors.

tion):

$$P(\text{single}) = \frac{1}{\text{average time between photons}} \tag{8}$$

The probability of obtaining two photons at the input of the beamsplitter is then:

$$P(\text{pair}) = \left(\frac{1}{\text{average time between photons}}\right)^2 \frac{1}{2!} \tag{9}$$

Henceforth, the probability that two photons arrive during a same temporal window unity in the two photon-detectors can be calculated theoretically:

$$P(\text{double count}) = \left(\frac{1}{(\text{average time between photons})^2 \cdot 2!}\right)\frac{1}{2}$$

The average number of double clicks obeys therefore

$$N(\text{double counts}) = \left(\frac{\text{total number of photons}}{\text{average time between photons} \cdot 2!}\right)\frac{1}{2}$$

In the high intensity regime we found a significant departure from the Poisson distribution:

- Total number of photons $\approx 640\,000$.
- Average time between photons ≈ 21 ns.
- Simultaneous clicks in the 2 photon-detectors = 4 999.

$$\left(\frac{640\,000}{21 \cdot 2!}\right)\frac{1}{2} \approx 7\,619 \tag{10}$$

In the low intensity regime we found a better agreement:

- Total number of photons $\approx 184\,000$.
- Average time between photons ≈ 141 ns.
- Simultaneous clicks in the two photon-detectors = 272.

$$\left(\frac{184\,000}{141 \cdot 2!}\right)\frac{1}{2} \approx 326 \tag{11}$$

This confirms that when the dead time is small compared to the average time between two photons, the statistics of counts is Poissonian in good approximation, which fits with the standard quantum prediction for a coherently attenuated laser source. From this point of view, the limit of low intensities corresponds to the genuinely quantum regime, while in the high intensity regime (for which the dead time is comparable to the average time between two photons) quantumness is spoiled by correlations induced by the dead time mechanism of the detector.

Incidentally, our study also confirms that we nearly always operate in the single photon regime; the probability to have two photons or more in the same interval of acquisition (one nanosecond) being at most of the order of 10^{-2}, even in the "high" intensity regime.

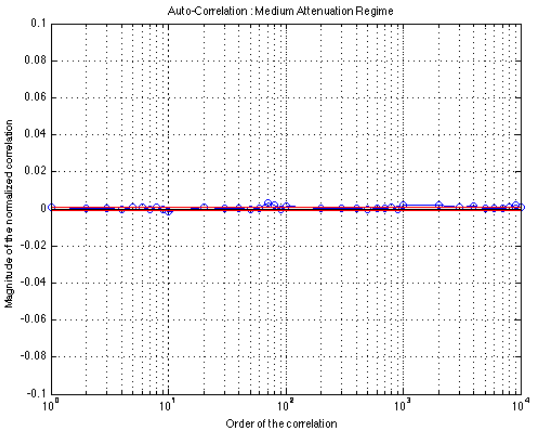

Fig. 10: Autocorrelation for the low intensity regime.

4 Characterization of the PQORN generator using the H.I.I. test

4.1 Near-zone temporal memory effect

The existence of a near-zone temporal memory effect would be revealed through the fact that similar histograms are significantly more probable to appear in the nearby (neighbouring) intervals of the time series of the results of measurements.

Using the setup in Fig. 2, we measured this effect in the two different regimes, the low intensity regime and the high intensity regime (they were defined in terms of the dead time at the end of the previous section).

To determine whether the effect is present, we make use of the H.I.I. test described in section 2, which delivers a p-value and a graph for a fast visual appreciation. We applied a level of significance of 0.01 for the p-value, hence if the p-value delivered is lower than the level of significance, we assumed that the presence of a significant memory effect gets confirmed by experimental data. Similarly, if the curve provided by the test remains outside the boundary curves, we assume that the existence of a memory effect is experimentally confirmed. We also used a standard auto-correlation test [6, 12, 16] to corroborate the results of the H.I.I. test.

4.1.1 Low intensity regime

We firstly measured the effect in the (highly attenuated) low intensity regime. We observed no correlation in this regime, as it is shown in Fig. 10. The H.I.I. test gives us the option to choose arbitrarily the sample length, which optimally ought to be of the order of the memory time of the H.I. effect. We selected four different sample lengths of 100, 300, 500 and 1000; and for each choice of a sample length, we tested the possible existence of a memory effect with the first, the second, the fifth and the tenth neighbour. For instance selecting 100 as a sample length, the reference sample runs from 1 to 100, the first neighbour sample from 101 to 200, the second neighbour one runs from 201 to 300, the fifth neighbour sam-

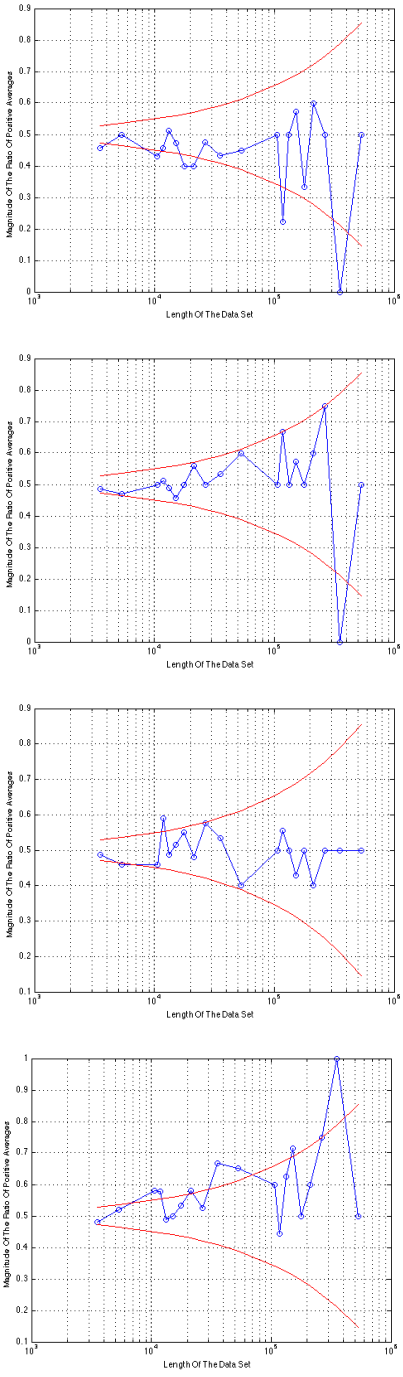

Fig. 11: Memory effect for the low attenuation regime with sample length of 100 for the first(a), the second (b), the fifth(c) and the tenth neighbour (d).

ple runs from 501 to 600 and so on. As is clear from Fig. 11, no memory effect is present in the low intensity regime. The result is also confirmed by similar plots obtained for sample lengths of 300, 500 and 1000 that we do not reproduce here in order not to overload the presentation. The corresponding p-values are gathered in Tab. 5. All the p-values are larger than

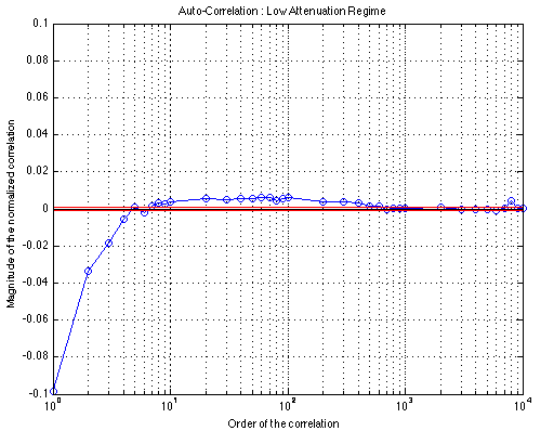

Fig. 12: Autocorrelation for the high intensity regime.

0.01, thus we can safely conclude that there is no memory effect in the low intensity regime, confirming the information provided by the graphics. These p-values are obtained by averaging all p-values associated to one "graphical" test.

4.1.2 High intensity regime

We measured again the correlations in the high intensity (weakly attenuated) regime and Fig. 12 shows that in this regime a strong auto-correlation prevails until the bit 600 approximately. We also measured the memory effect in the same way as for the low intensity regime, *i.e.* for different sample lengths (100, 300, 500 and 1000) and different neighbours (1^{st}, 2^{nd}, 5^{th} and 10^{th}). From Figs. 13, 14, 15 and 16, it can be seen that for a sample length of 100, the H.I. effect is present. On the other hand, for a sample length of 1000, the experimental curve stays inside the red boundaries most of the time. Actually, when two samples separated by less than say 1000 bits are compared, the memory effect is present, otherwise there is no H.I. effect. These results are corroborated by the auto-correlation (Fig. 12) which is strong until the bit 600 approximately. They also fit with the average p-values shown in Tab. 6.

4.2 Long range spatial H.I.-like correlations

In a previous paper [4], one of us (T. D.) predicted that similar histograms are highly probable to appear at different geographical points at the same time on the basis of a genuine quantum hidden variable model incorporating the morphic resonance concept of Sheldrake [17]. We conceived a new experiment in order to study this prediction, based on the setup of Fig. 17, which is composed of two sub-setups (sub-setup A and sub-setup B). Each sub-setup consists of one source, one neutral density filter and one photodetector and is equivalent to the set-up described in the previous section that we used for testing the near-zone effect. The two sources are launched at the same time. In a first time we implemented the same H.I.I.

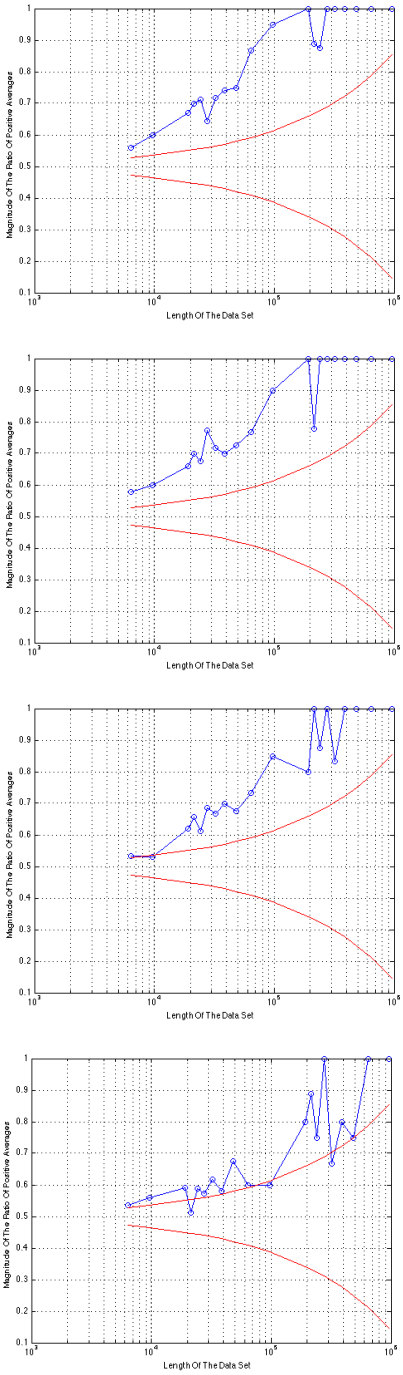

Fig. 13: Memory effect for the high intensity regime with sample length of 100 for the first (a), the second (b), the fifth (c) and the tenth neighbour (d).

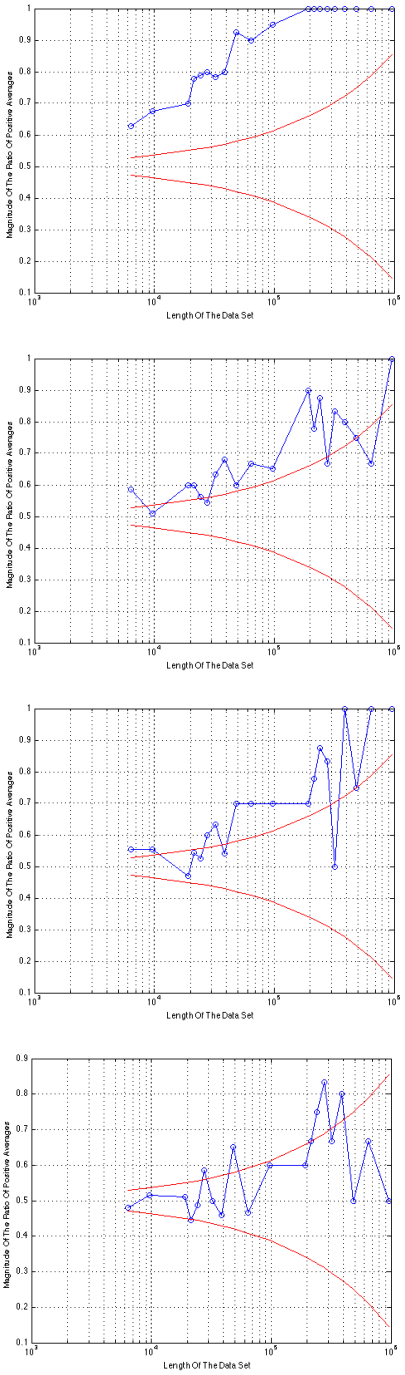

Fig. 14: Memory effect for the high intensity regime with sample length of 300 for the first (a), the second (b), the fifth (c) and the tenth neighbour (d).

test as in section 4.1 separately for each detector in order to check that each individual subset-up exhibits the near-zone memory effect. This can be seen for instance at the level of Tab. 1. The period of the near-zone memory effect is of the order of 500 clicks, as is corroborated by the auto-correlation tests in Figs. 18a and 18b.

In a second time, we adapted the H.I.I. test in order to be able to detect H.I.-like correlations between the two subset-ups. We have thus to compare the random series of time delays obtained in one photodetector (series A) with the random series obtained in the other photodetector (series B). Comparing both of them will determine whether the histograms are

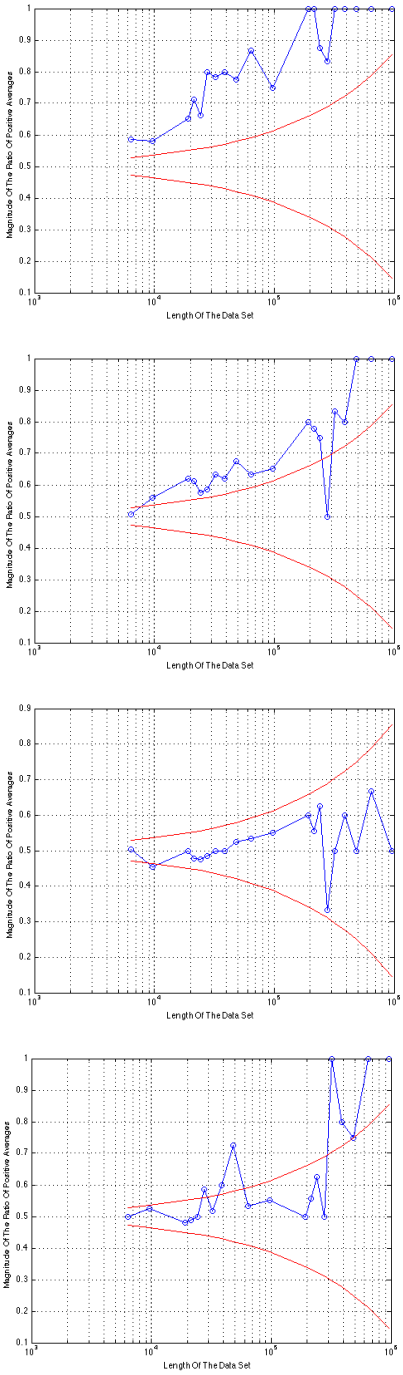

Fig. 15: Memory effect for the high intensity regime with sample length of 500 for the first (a), the second (b), the fifth (c) and the tenth neighbour (d).

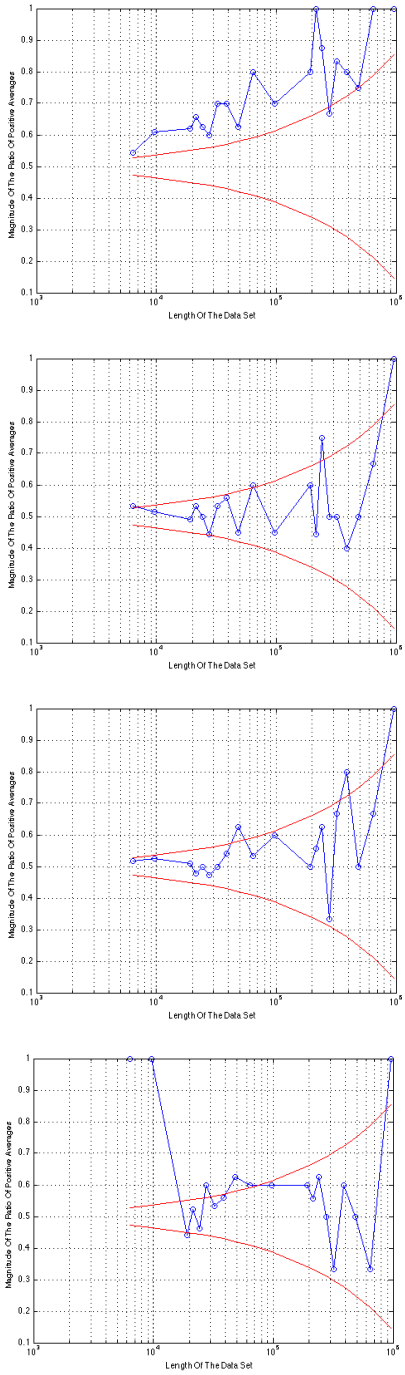

Fig. 16: Memory effect for the high intensity regime with sample length of 1000 for the first (a), the second (b), the fifth (c) and the tenth neighbour (d).

similar or not. In order to do so, a fixed sample length is selected (in our case, 100, 300, 500 and 1000) and we compare the histogram built from samples of this length extracted from series A with the corresponding histograms from series B, *i.e.* sample 1-100 of series A with the sample 1-100 of series B. We also compared neighbour histograms, like we did in section 4. This time we compare one histogram of series A with the neighbours of series B, *i.e.* for the first neighbour, sample 1-100 of series A with sample 101-200 of series B. We extended this procedure for the second, third, fifth, tenth and twentieth neighbour too. The results are encapsulated in Tab. 7. The average p-values are always quite larger than

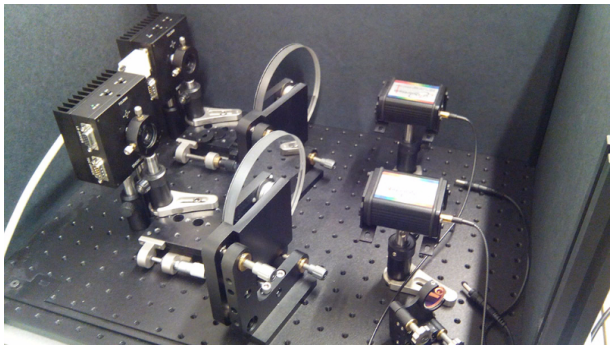

Fig. 17: Double set-up for detecting long range spatial H.I.-like correlations.

0.01, for all the cases, which shows that no observable spatial H.I.-like effect is present at the level of our experimental setup, even in the high intensity regime where individual setups exhibit a near zone memory effect. We checked by similar methods that in the low intensity regime no spatial H.I.-like effect is present. In both regimes we also scrutinized the graphical presentations of the test results (that we do not reproduce here in order not to overload the presentation), which confirmed the conclusions already drawn from the estimate of the p-values.

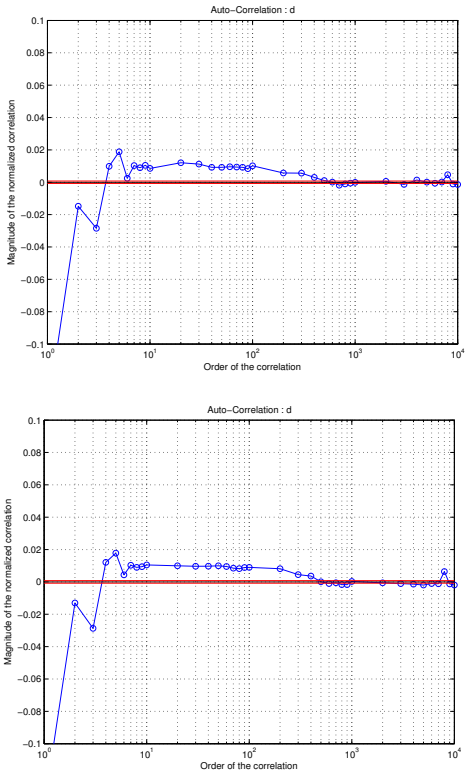

Fig. 18: Correlation for the data obtained in the two different photondetectors. Fig. (a) and Fig. (b) present a strong correlation.

Sample Length: 100	A	B
1 neighbor	0.0036	0.0033
2 neighbor	0.0071	0.0036
3 neighbor	0.0367	0.0094
5 neighbor	0.4984	0.3224
10 neighbor	0.4746	0.3269
20 neighbor	0.3191	0.3168

Tab. 1: p-values for the two sub-setups with a sample length of 100 bits for different neighbours (first, second, third, fifth, tenth and twentieth.

4.3 Long range temporal memory effects

The aforementioned periodic modulation of radio-active emission with a period of about 365 days [9, 10], suggests that the phenomenon has a cosmophysical origin. We therefore investigated the possibility to generalize these observations in the case of a quantum signal. We focused on the 24-hour period experiment due to the large amount of time that we would have spent in tracking yearly memory effects. The 24-hour period would be an indication of the existence of an external agent that influences the object of study, most probably the rotation of the Earth. Our aim was to probe the existence of this effect at the level of the quantum signal obtained from our QRNG. For our experiment we used the same setup as in the near-zone experiment in section 4. It consists again of a laser source, a collimating lens, two neutral density filters and one avalanche photo-diode.

In February 2015, we realized a series of experiments, after having synchronized our computer clock with an atomic clock from the nist.gov website* in such a way that all the measurements were automatized. Then, the runs were performed at exactly the same time every day for three consecutive days and we performed 20 different experimental runs with an interval of 20 second between each of them†.

We estimated, based on the slope of the semi-logarithmic plot of the histogram of delay times, the average time delay and we found that the drift was small, with average times comprised in the interval 45-52 ns. Thereafter we estimated the individual H.I.I. p-values which measure the cross-correlations between the samples of days 1 and 2, of days 2 and 3, and of days 1 and 3. The results are encapsulated in Tab. 2.

*The procedure for doing so is available on the website http://www.nist.gov/pml/div688/grp40/its.cfm

† We learn from wikipedia that... *"A synodic day is the period it takes for a planet to rotate once in relation to the body it is orbiting. For Earth, the synodic day is known as a solar day, and is about 24 hours long. The synodic day is distinguished from the sidereal day, which is one complete rotation in relation to distant stars. A synodic day may be "sunrise to sunrise" whereas a sidereal day can be from the rise of any star to the rise of the same star on the next day. These two quantities are not equal because of the body's movement around its parent"...* Henceforth we expect a difference between the sidereal and synodic (solar) day to be of the order of 24x3600/365 second, more or less 240 second. Our measurements cover 400 second, which allows us to address at the same time the synodic and sidereal periods

Total number of p-values: 3380
Day 1 Day 2
Number p-values < 0.01 = 272
Number p-values < 0.1 = 978
Day 2 Day 3
Number p-values < 0.01 = 284
Number p-values < 0.1 = 980
Day 1 Day 3
Number p-values < 0.01 = 221
Number p-values < 0.1 = 988

Tab. 2: Statistics of "pathological" p-values, from consecutive random series separated by 24 or 48 hours.

Total number of p-values: 8000
Day 1 Day 2
Number p-values < 0.01 = 123
Number p-values < 0.1 = 1195
Day 2 – Day 3
Number p-values < 0.01 = 152
Number p-values < 0.1 = 1201
Day 1 – Day 3
Number p-values < 0.01 = 104
Number p-values < 0.1 = 1185

Tab. 3: Statistics of "pathological" p-values, from pseudo-random series.

There were 13 runs each day and from each pair of runs we extracted twenty p-values (each of these values is associated to a point on a graph similar to, for instance, the plots in Fig. 11). By doing so, for each pair of days, we were able to estimate 13 times 13 times 20 = 3380 p-values from the cross-correlations between samples extracted at different days.

In order to properly calibrate the statistical distribution of p-values we did two things:

A) we generated sixty runs of Poisson distributed time series characterized by an average time of the order of 50 ns. The duration of each series was the same as the duration of each experimental run. We arbitrarily assigned a day to each of them, according to the rule 1-20 → day 1, 21-40 → day 2, 41-60 → day 3. Then we considered the 400 (20 times 20) cross-correlations between the data "extracted at different days" and estimated the corresponding p-values, following the same algorithm already used for establishing Tab. 2. The results are encapsulated in Tab. 3.

B) We also estimated through the same method the H.I. cross-correlation between samples that were measured in June 2014 and those measured in February 2015. Here again there were three runs of 13 samples, measured at different days, after a period of the order of 24 hours each time, and also in the high intensity regime, but the timing of the data collected in June 2014 was not automated. We estimated correlations between data measured in days 1, 2 and 3 in June 2014 and those measured in days 1, 2 and 3 in 2015. The results are summarized in Tab. 4.

Total number of p-values: 3380
Day 1 in June 2014 Day 1 in February 2015
Number p-values < 0.01 = 112
Number p-values < 0.1 = 578
Day 2 in June 2014 Day 1 in February 2015
Number p-values < 0.01 = 82
Number p-values < 0.1 = 526
Day 1 in June 2014 Day 3 in February 2015
Number p-values < 0.01 = 91
Number p-values < 0.1 = 521

Tab. 4: Statistics of "pathological" p-values, from consecutive random series measured in June 2014 and February 2015.

For obvious reasons, we consider that the statistical distribution of "pathological" p-values which appears in Tabs. 3 and 4 is representative of uncorrelated data. Indeed, pseudo-random series do not exhibit any memory effect, and we do not expect that data measured in June 2014 and February 2015 are correlated. This is confirmed by a comparison of those tables: if we consider the occurrence of p-values smaller than 0.1, we find a probability of the order of 0.15 in each case*.

On the contrary, in Tab. 2 the occurrence of p-values smaller than 0.1 is of the order of 0.29, twice more, which reveals the existence of a systematic memory effect, persisting after 24 hours. We consider therefore that our observations confirm the existence of long range temporal H.I.-like correlations of periodicity of the order of 24 hours, which appears, at least in our eyes, to be a very surprising result.

5 Conclusions and discussions

In this paper we studied the H.I. effect, which, roughly, would manifest itself through a tendency of random series to present analogous departures from their mean statistical behaviour. This tendency would possibly characterize data collected in the same temporal interval (what we denoted the near zone memory effect) but could present non-local features (non-local in time and/or space), what we denoted the long range temporal (resp. spatial) memory effect.

Our main goal was to study experimentally whether or not a memory effect of the H.I. type was present in the single photon regime. We developed a new, self-cooked algorithm, described in section 2 in order to realize this objective.

*At first sight we ought to expect 0.1 instead of 0.15, but we must have in mind that the p-value derived by us corresponds to a situation where the sign of the parameter r defined at the level of (1) was negative in exactly fifty percent of the cases and positive in fifty percent of the cases, which is of course an assumption that is not always strictly verified. From this point of view, the p-value defined by (7) ought not to be considered as an exact p-value but still plays the role of a valuable indicator.

Sample Length	1^{st} Neighbor	2^{nd} Neighbor	5^{th} Neighbor	10^{th} Neighbor
100	0.4762	0.6031	0.6048	0.3997
300	0.4515	0.5647	0.4537	0.5269
500	0.5323	0.3049	0.4101	0.4614
1000	0.4105	0.4745	0.5121	0.2665

Tab. 5: p-values extracted from the H.I. test for the low intensity regime for different sample lengths and different neighbours.

Sample Length	1^{st} Neighbor	2^{nd} Neighbor	5^{th} Neighbor	10^{th} Neighbor
100	0.0037	0.0043	0.0219	0.1005
300	0.0033	0.1100	0.1489	0.4066
500	0.0042	0.1098	0.6511	0.4410
1000	0.0304	0.4866	0.4876	0.3305

Tab. 6: Parity Method: Results of the file generated with the Split Method applying the NIST test battery.

Sample length	0^{th} neighbour	1^{st} neighbour	2^{nd} neighbour	3^{rd} neighbour	5^{th} neighbour	10^{th} neighbour
100	0.4330	0.5725	0.4067	0.4844	0.4530	0.5348
300	0.4608	0.5303	0.2870	0.2363	0.3765	0.3965
500	0.4508	0.4930	0.5378	0.4623	0.3572	0.0361
1000	0.5029	0.4965	0.4373	0.3953	0.2483	0.1399

Tab. 7: p-values when series A and B are compared for different sample length (100, 300, 500 and 1000 bits) for different neighbours (first, second, third, fifth, tenth and twentieth.

Our conclusions are the following:

A) The near-zone H.I. memory effect is well present in the single photon regime, but only in the high intensity regime (for which the dead time is comparable to the average time between two photons). As we discussed in section 3.2, the limit of low intensities (when the dead time is quite larger than the average time between two photons) corresponds to the genuinely quantum regime, and in this regime no memory effect is present. This goes in the sense of the conclusion [19] drawn from the study of the SeQuR QORNG, for which the H.I. effect could be explained in terms of external electromagnetic pollution, combined with an internal memory time (inertia) of the photodetector. The persistence of H.I.-like correlations after 24 hours (that we address below) is however more difficult to explain. Anyhow, we can safely conclude from our experiments and our analysis that "pure" quantum random series, collected in the low intensity single photon regime do not exhibit any kind of observable H.I.-like correlation.

B) We were unable to observe manifestations of a long range spatial memory effect but detected a systematic tendency indicating the possible presence of the long range temporal memory effect, even after 24 hours. Our preliminary result ought to be of course confirmed by supplementary studies. The door remains thus open for what concerns the "daily" effect. It is worth noting that, even if this effect gets definitively confirmed, its interpretation is not straightforward. It is well-known for instance that some noises in nature (and in particular at the surface of our planet) exhibit a 24 hours period. It could be that the daily memory effect merely reveals this feature.

In any case, we hope that, beside contributing to a better understanding of fundamental aspects of quantum randomness*, our study also brings new tools aimed at characterizing randomness in general. We actually consider that the H.I.I. test provides a new statistical test, complementary to the standard NIST tests, and in particular to the auto-correlation test.

As we have shown (*e.g.* in section 4.1.2), at the level of physical random number generators, when auto-correlation is present, the H.I. effect is most often present too, which is already remarkable in itself and suggests the existence of a universal memory effect.

Moreover, as shown in section 4.3, the long range temporal H.I. effect provide an example where the H.I.I. test reveals a systematic tendency, even in absence of auto-correlation (we checked for instance that the auto-correlation between data collected at different days (1,2,3) was uniformly flat).

We are still far away from one of our initial motivations, which was to be able to discriminate between physical randomness and pseudo-randomness thanks to the H.I.I. test†,

*In particular the main motivation of one of us (T. D.) was to investigate possible memory effects at the level of the quantum statistics, and finds its place in a series of works centered around this question [2–5, 7]

†In certain cases, pseudo-randomness can be revealed by measuring the

and the low intensity case provides a counterexample to the mere possibility of doing so in general, but at least, our measurements confirmed that the H.I. effect is present in nature in various regimes. In particular it is weakened but still present after a delay of 24 hours, which is very amazing. Therefore we are intimately convinced that it is important to pursue these investigations. For instance it would be interesting in the future to compare results obtained with our algorithm and those obtained by Shnoll and coworkers, making use of a quite different algorithm [8,14,18], and applying it to noise [15], not to quantum signal as we did, which addressed relatively short series of data (of the order of 30 clicks only), contrary to ours, where we systematically made use of the law of large numbers in order to estimate p-values.

Last but not least, it would be interesting to study the appearance of the H.I.-effect at various temporal and spatial scales, the present work constituting only a first probe in this direction.

Acknowledgements

Support from the B-Phot team, to his leader Hugo Thienpont, and the ICT Impulse Program of the Brussels Capital Region (Project Cryptasc) is acknowledged. Sincere thanks to Marco Bischof for drawing attention of one of us (T.D.) on Shnoll's work, some years ago.

Submitted on August 16, 2016 / Accepted on October 9, 2016

References

1. Calude C. S., Dinneen M. J., Dumitrescu M., and Svozil K. Experimental Evidence of Quantum Randomness Incomputability. *Physical Review A*, 2010, v. 82 (022102).
2. Durt T. About the Possibility of Supraluminal Transmission of Information in the Bohm-Bub Theory. *Helvetica Physica Acta*, 1999, v. 72, 356.
3. Durt T. Do Dice Remember? *International Journal of Theoretical Physics*, 1999, v. 38, 457.
4. Durt T. Quantum Mechanics and the Role of Time: Are Quantum Systems Markovian? *International Journal of Modern Physics B*, 2012, v. 26 (27&28), 1243005.
5. Durt T. Do Quantum Dice Remember? in Aerts D., Aerts S., and de Ronde C., eds. Probing the Meaning of Quantum Mechanics. World Scientific, Singapore, 2014, 1–24.
6. Durt T., Belmonte C., Lamoureux L-P., Panajotov K., Vanden Berghe F., and Thienpont H. Fast Quantum-Optical Random-Number Generators. *Physical Review A*, 2013, v. 87, 022339.
7. Durt T., Mathevet R., Robert J., and Viaris de Lesegno B. Memory Effects in Atomic Interferometry: A Negative Result, in Aerts D., Czachor M., Durt T., eds. Entanglement, Non-linearity, Quantum Structures and New Experiments, 2000, 165–204.
8. Fedorov M. V., Belousov L. V., Voeikov V. L., Zenchenko T. A., Zenchenko K. I., Pozharskii E. V., Konradov A. A., and Shnoll S. E. Synchronous Changes in Dark Current Fluctuations in Two Separate Photomultipliers in Relation to Earth Rotation. *Astrophysics and Space Science*, 2003, v. 283, 3–10.
9. Fischbach E., Buncher J. B., Gruenwald J. T., Jenkins J. H., Krause D. E., Mattes J. J., and Newport J. R. Time-Dependent Nuclear Decay Parameters: New Evidence for New Forces? *Space Science Review*, 2009, v. 145, 285–335.
10. Jenkins J. H., Fischbach E., Buncher J.B., Gruenwald J. T., Krause D. E., and Mattes J. J. Evidence of Correlations Between Nuclear Decay Rates and Earth-Sun Distance. *Astroparticle Physics*, 2009, v. 32, 42–46.
11. Jenkins J.H., Mundy D.W., and Fischbach E. Analysis of Environmental Influences in Nuclear Half-Life Measurements Exhibiting Time-Dependent Decay Rates. *Nuclear Instruments and Methods A*, 2010, v. 620 (2–3), 332–342.
12. Marsaglia G. The Marsaglia Random Number CDROM Including the Diehard Battery of Tests of Randomness, 1995, http://www.stat.fsu.edu/pub/diehard/.
13. Norman E. B., Browne E., Shugart H. A., Joshi T. H., and Firestone R. B. Evidence Against Correlations Between Nuclear Decay Rates and Earth-Sun Distance. *Astroparticles Physics*, 2009, v. 31, 135–137.
14. Panchelyuga V. A., Kolombet V. A., Panchelyuga M. S., and Shnoll S. E. Local-Time Effect on Small Space-Time Scale. arXiv: physics/0610137.
15. Rabounski D. and Borissova L. General Relativity Theory Explains the Shnoll Effect and Makes Possible Forecasting Earthquakes and Weather Cataclysms. *Letters to Progress in Physics*, 2014, v. 10 (2), 63–70.
16. Rukhin A., Soto J., Nechvatal J., Smid M., Barker E., Leigh S., Levenson M., Vangel M., Banks D., Heckert A., Dray J., and Vo S. Statistical Test Suite for Random and Pseudorandom Number Generators for Cryptographic Applications. NIST Special Publication, 2001, v. 800-22.
17. Sheldrake R. Une nouvelle science de la vie. Eds. du Rocher, Monaco, 1985.
18. Shnoll S. E., Colombet V. A., Pozharskii E. V., Zenchenko T. A., Zvereva I. M., and Konradov A. A. Realization of Discrete States During Fluctuations in Macroscopic Processes, *Physics-Uspekhi*, 1998, v. 43 (2), 1025–1035.
19. Vanden Berghe F. Quantum Aspects of Cryptography: From Qutrit Symmetric Informationally Complete Projective Operator Valued Measure Key Encryption to Randomness Quality Control. Ph.D. thesis, Vrije Universiteit, Brussels, 2011.

algorithmic complexity of a pseudo-random series, which delivers by then a criterion for discriminating quantum randomness from pseudo-randomness because, as has been shown elsewhere [1], quantum random series are incompressible.

Relativity and the Luminal Structure of Matter

Andrew Laidlaw

Calle Cuesta de los Cubos 17, Velez de Benaudalla, 18670, Spain

It is shown that Lorentz Invariance is a wave phenomenon. The relativistic mass, length contraction and time dilation all follow from the assumption that energy-momentum is constrained to propagate at the speed of light, c, in all contexts, matter as well as radiation. Lorentz Transformations, and both of the usual postulates, then follow upon adopting Einstein clock synchronisation. The wave interpretation proposed here is paradox free and it is compatible with quantum nonlocality.

1 Introduction

> *"But the division into matter and field is, after the recognition of the equivalence of mass and energy, something artificial and not clearly defined. Could we not reject the concept of matter and build a pure field physics? What impresses our senses as matter is really a great concentration of energy into a comparatively small space. We could regard matter as the regions in space where the field is extremely strong. In this way a new philosophical background could be created."* — Einstein & Infeld [1].

Modern Physics relies heavily on relativistic wave equations, especially the d'Alembert, Helmholtz and Dirac [2] equations, that feature either propagation at the characteristic velocity, c, or a velocity operator of constant modulus equal to c [3]. There are also many Lorentz covariant classical field theories in the literature, including nonlinear theories with subluminal soliton solutions that serve as candidate models for the fermions. [4–10] are just a few to illustrate the diverse range of approaches. This Article shows that the first, necessary step towards achieving Einstein's dream of a pure field physics is to recognise that, whether it appears as radiation or as matter, energy is a propagative phenomenon.

We shall consider the basic mechanics of luminal wave systems, *i.e.* systems of waves that propagate at c. Adapting the Newtonian momentum equation, $p = mv$, for use with constant speed luminal waves and then applying universally accepted basic principles of mechanics to luminal waves leads to a general structural analysis of luminal wave systems that is inherently relativistic without asserting any principle of relativity. The usual relativistic mechanics of matter can thus be interpreted as the basic mechanics of subluminally moving systems constructed entirely from luminal waves.

The proposed luminal wave ontology provides new perspectives on many issues including the Dirac velocity operator, angular momentum quantisation, the structure of Electromagnetics [11], gravity [12], the existence of nonlocal relations between observables, and interference phenomena in matter beams. The plan of the Article is as follows:

Section 2 defines the basic principles of mechanics that are regarded as universally accepted and identifies the simple general relationship that governs the connection between inertial frames for systems of luminal wave momenta. Section 3 shows that the usual relativistic momentum equation for particles applies to systems of luminal wave momenta. Section 4 derives the (forward) relativistic transformation of wave momenta in a form that is useful for analysing wave systems as a whole. Section 5 extends the results to any kind of luminal wave system, provided a wave vector in the direction of propagation can be defined, linear momentum is locally conserved, and propagation is luminal. In particular, linear superposition is not required so the method is applicable to nonlinear wave systems with subluminal soliton solutions.

For luminal waves the speed of propagation is, by definition, fixed and any luminal wave model of a subluminal massive particle is immediately subject to the kinematic constraint that, when the speed of the particle changes, the speed of its constituent wave components does not. Sections 6 and 7 show that length contraction and time dilation are the consequences of this kinematic constraint, so luminal systems display all the usual relativistic phenomena.

Section 8 addresses the question how the physical phenomena of length contraction and time dilation constrain the coordinate transformations. Selleri [13, 14] has shown that, subject mainly to the use of Einstein clock synchronisation, Lorentz Transformations follow directly from length contraction and time dilation, which are derived here from the basic principles of mechanics without making any further assumptions. As discussed in Subsection 8.2, the proposed wave interpretation is also equipped with a readily observable preferred frame, eliminating the paradoxes associated with the usual, relativist interpretation.

It remains only to point out, in Section 9, that any form of non-luminal structure for the massive particles is implausible, hence the conclusion reached is that the relativistic phenomena imply the luminal structure. Finally, Section 10 outlines the reasons why Lorentz Invariance does not preclude nonlocal relations between observables in this pure field context.

2 Basic physics of luminal waves

2.1 The basic principles of Mechanics

The usual classical field approach to mechanics in wave systems begins by choosing wave or field equations. Any analy-

sis is immediately limited to the mechanics of one particular kind of wave system. We would identify various solutions to the chosen equations, which are in general expressed as spatial distributions of some field variables. Field energy and momentum densities must be induced from these field variables. After evaluating the spatial integrals of the energy and momentum densities we would arrive at expressions for the momenta and energies of the wave solutions and we could begin the mechanics.

Unfortunately, in many circumstances we do not know what equations to use, much less their solutions. Moreover, the great variety of Lorentz covariant wave equations suggests that relativistic mechanics is a general feature that many wave systems have in common. What kind of wave systems? As mentioned in the introduction, the leading relativistic wave equations feature the characteristic velocity, suggesting that, when the field energy-momentum in a wave system is constrained to propagate at c (i.e. luminally), then the system displays the usual relativistic mechanics.

Therefore, instead of taking the usual fields approach to mechanics let us take a *mechanics* approach to *fields*, applying the basic principles of mechanics directly to a field energy-momentum density that propagates at c. The universally accepted principles to rely upon can be stated as follows:

1. The momentum of an object is defined as the product of its inertia times its velocity. Similarly, field momentum density is the product of inertia density and velocity.
2. Momentum is conserved. Field momentum is locally conserved.
3. The principle of local action means that wave objects, as defined below, may interact with each other only in regions of space where they overlap.
4. The force acting on an object is equal to its rate of change of momentum.
5. The resulting change in the energy of the object is given by the work integral.
6. Energy is conserved. Field energy is locally conserved.

Here 'wave object' means: some set of functions on a 3-space*, which together induce a field momentum density, $\vec{\rho_p}(x, y, z, t)$, that propagates luminally according to a unique unit wave vector, $\hat{\mathbf{k}}(x, y, z, t)$ and whose spatial integral, $\int\int\int_{-\infty}^{+\infty} \vec{\rho_p}(x, y, z, t)\, dxdydz$, is finite.†,‡,§

*That is, spatial distributions of field variables.

†In addition to inducing the field momentum density, the space functions that define wave objects in a nonlinear field theory may also act as sufficient causes for any interactions that there may be.

‡Note that infinite plane waves are not wave objects.

§Neither the propagation of the space functions nor their relation to the linear momentum density are specified here. This allows for wave objects with intrinsic field angular momentum and, more generally, the definition accommodates two kinds of internal evolution, via the internal movements of an otherwise invariant set of functions and via their individual time evolutions.

We are interested in the mechanics of systems that comprise multiple wave objects. This begins with non-interacting systems, where the wave objects are not presently interacting with each other. The next Subsection focusses on the case where each object's unit wave vector, $\hat{\mathbf{k}}(x, y, z, t)$, is a constant vector, independent of x, y, z and t. The momentum density distribution of such wave objects moves through space in a self similar form at c. We shall refer to this special kind of wave object as a light flash.

2.2 Application to light

Consider a source that simultaneously emits a set of N light flashes in various directions. The development here can be applied to any kind of light flashes, including individual photons, short segments of laser beams, or collimated beams in general, monochromatic or not. We require only that each flash propagates at c, carrying a finite linear momentum in a well-defined direction in space.

Let the i^{th} light flash carry linear momentum $\mathbf{p}_i$. According to the first basic principle, momentum equals the product of inertia and velocity and the wave inertia of the i^{th} light flash is therefore defined as $m_i = p_i/c$, where $p_i = |\mathbf{p}_i|$ is the magnitude of the momentum of the i^{th} light flash, also called the 'scalar momentum':

$$p_i = m_i\, c\,. \tag{1}$$

This Article is essentially a consistent application of the basic mechanics principles, using (1) in place of the familiar $p = mv$, where the speed v is a variable. Note that, *prima facie*, the inertia, m_i, of a wave propagating in a well-defined direction in space has nothing to do with the mass of a particle. However, we use the symbol m_i because, unless they ALL propagate in the same direction, the total inertia of a set of N waves will be found to correspond to the usual, relativistic particle mass. The time differential of (1) is:

$$\frac{dp_i}{dt} = c\,\frac{dm_i}{dt}\,. \tag{2}$$

Having fixed the propagation speed, c, changes of the scalar momentum are thus associated with changes of the wave inertia. It will become clear in Sect. 8 that the inertia changes we will be discussing throughout this Article are in fact frequency changes. Such changes may be due to a change of observer or they may be physical changes due to any forces that are acting on the wavefield.

In general, if a force acts on a light flash then, since (2) is the force component parallel to the light flash's motion, the work integral is:

$$W = \int_{p_s}^{p_f} \frac{d\mathbf{p}}{dt}\cdot d\mathbf{s} = \int_{m_s}^{m_f} c\,\frac{dm}{dt}\,cdt = (m_f - m_s)\,c^2\,, \tag{3}$$

where subscripts s and f refer to the words 'start' and 'finish'. The radiation reaction force that acts on a light flash

reflected by a moving mirror is an example that highlights the role of the work integral in a basic mechanics calculation*. According to the fifth basic principle, the work done equals the energy change, and we may assume that a light flash that has zero momentum requires zero energy, so the energy of the i^{th} flash is:

$$E_i = m_i c^2 = c p_i . \quad (4)$$

According to the second basic principle, momentum is conserved so the total momentum of a set of N wave objects is given by the vector sum over their momenta:

$$\mathbf{P} = \sum_{i=1}^{N} \mathbf{p}_i . \quad (5)$$

Suppressing the summation range henceforth, we write the total inertia as $m_e = \sum_i m_i$. The total energy of the set is then:

$$E = \sum_i c p_i = m_e c^2 . \quad (6)$$

According to the (first and second) basic principles, the velocity of the centre of inertia of a system of objects is the inertia weighted average velocity, $\mathbf{V} = \sum_i m_i \mathbf{v}_i / \sum_i m_i$, so that:

$$\mathbf{V} = \frac{\sum_i \mathbf{p}_i}{m_e} \Rightarrow \mathbf{P} = m_e \mathbf{V} . \quad (7)$$

For a relativistic analysis, these basic Equations (1) - (7) must be good for any observer, however, since we intend *inter alia* to show it, no principle of relativity will be asserted *a priori*. Consider an incremental change that affects the system of light flashes as a whole. For example, an incremental change in the condition of motion of the observer would alter all his observations of the $\mathbf{p}_i$. Similarly, a single observer considering light flashes emitted by otherwise identical sources that are in different conditions of motion will find different values for the $\mathbf{p}_i$. Since these two cases are not *a priori* assumed equivalent, consider the latter one, and consider, specifically, two otherwise identical sources moving at velocities $\mathbf{v}$ and $\mathbf{v} + d\mathbf{v}$ in the inertial frame of a single inertial observer.

This scenario closely corresponds to applying a Lorentz boost to a system of wave momenta. We may write the momenta of the light flashes as $\mathbf{p}_i$ and $\mathbf{p}_i + d\mathbf{p}_i$ respectively and their totals as $\mathbf{P}$ and $\mathbf{P} + d\mathbf{P}$. We are interested in how the $d\mathbf{p}_i$ are related to $d\mathbf{P}$. As shown in Appendix 2, this is determined by the relevant known facts, the relativistic Doppler shift and aberration phenomena, which together imply:

$$d\mathbf{p}_i = \frac{p_i}{m_e c} d\mathbf{P} . \quad (8)$$

We are assuming neither Special Relativity nor the relativity principle by referring to these phenomena. Indeed, while Lorentz Transformations correctly imply each of them, there exist other coordinate transformations [13] that also correctly predict these observables [15]. Because (8) is a direct consequence of the phenomena themselves, it necessarily applies to any theory that correctly accounts for them†.

It is nonetheless relevant to consider what, if anything, the facts here are introducing over and above the basic principles stated above. If our coordinate transformations are to be linear and homogeneous, as is usually assumed, then $d\mathbf{p}_i$ will be linear in p_i. Similarly, when considering the case of a single light flash, (the case $N = 1$), $d\mathbf{p}_i$ should be linear in, and parallel to, any incremental change of momentum of the light source, $d\mathbf{P}_{LS}$, prior to emission. Since the same applies to each of the light flashes in our system it follows that $d\mathbf{p}_i \propto d\mathbf{P}$ and we can safely assume that: $d\mathbf{p}_i = \alpha_i p_i \, d\mathbf{P}$.

Eq. (8) means that all the weights, α_i, are the same, $\alpha_i = \alpha$. Summing over i gives $\alpha = 1/m_e c$ (since $\sum_i d\mathbf{p}_i = d\mathbf{P}$). In particular, under an incremental momentum boost of the whole system, the momentum shifts, $d\mathbf{p}_i$, applied to the various wave momenta, $\mathbf{p}_i$, depend linearly on their energies but not on their directions of propagation, $\hat{\mathbf{k}}_i$.

The next two sections show how (8) governs the connection between inertial frames for systems of luminal wave momenta. In order to avoid asserting the relativity principle, the boost will not presently be associated with a change of observer. It will turn out to work relativistically, but for the present purposes the incremental momentum boost, (8), has only the restricted meaning of an incremental change $d\mathbf{v}$ in the velocity of a light source, the result of which is to add $d\mathbf{P}$ to the total wave momentum by adding wave momentum $d\mathbf{p}_i$ to each of the N constituent light flashes‡.

3 The relativistic momentum

This section shows that systems of luminal wave momenta that are connected by incremental momentum boosts obey the usual relativistic momentum equation for particles.

In subsection 2.2, the incremental change in the scalar momentum of the i^{th} light flash, dp_i, is given by the component of $\mathbf{dp}_i$ parallel to $\mathbf{p}_i$, which is:

$$dp_i = d\mathbf{p}_i \cdot \frac{\mathbf{p}_i}{p_i} .$$

Substituting (8) in this gives $m_e c \, dp_i = \mathbf{p}_i \cdot d\mathbf{P}$. Noting that $\sum dp_i = c \, dm_e$, summing over i gives $c^2 m_e dm_e = \mathbf{P} \cdot d\mathbf{P}$, and integrating this we obtain the common expression for the invariance of the 4-momentum:

$$m_e^2 c^2 = P^2 + m_0^2 c^2 , \quad (9)$$

*See Appendix 1, which shows that the ratio of reflected and incident momenta is the square of the relativistic doppler shift.

†When Appendix 1 is generalised to the case of non-normal incidence, the result is the product of the two relativistic Doppler shift and aberration operations involved. The basic principles are thus arguably sufficient to derive (8) by themselves, although the analysis is tedious.

‡Note that we do not need to assume that $d\mathbf{V} = d\mathbf{v}$

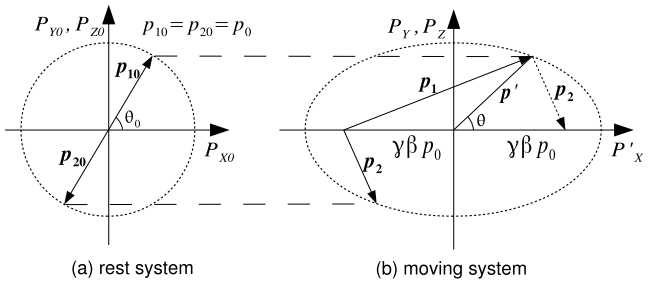

Fig. 1: Binary light flash systems whose centers of inertia are (a) at rest (b) moving at speed $V = \beta c$.

where m_0 is the value of m_e for $P = 0$. Let $\beta = V/c$ as usual so β is a +ve real number in the interval $[0, 1]$. The basic equations of relativistic mechanics, $\mathbf{P} = \gamma m_0 \mathbf{V}$ and $m_e = \gamma m_0$, where $\gamma = 1/\sqrt{1-\beta^2}$, follow upon substituting (7) into (9).

4 Wave system transformations in momentum space

In this section we show how the momenta of individual wave objects in a multi-object wave system transform under the action of (8).

By analogy to the usual comoving frame for massive particles, let us define the rest frame of a multi-object wave system as the (unique) inertial frame for which the right hand side of (5) vanishes. This definition is convenient, but not essential. Given the definition, let us now adopt the perspective of a single inertial observer who compares systems of light flashes emitted by two otherwise identical sources in different conditions of motion such that he considers one system's centre of inertia to be at rest, i.e. $\mathbf{P} = 0$ in (5) and $\mathbf{V} = 0$ in (7), and the other's to be moving at speed V in the x-direction, so that, from Section 3, $P = \gamma m_0 V$.

Let us refer to these two systems of light flashes as the 'rest system' and the 'moving system' respectively. We shall use a 0 subscript to refer to rest system momenta, so $\mathbf{P}_0 = \sum_i \mathbf{p}_{i0} = 0$. The analysis is expressed in momentum coordinates and it does not involve anything about spatial relations between the waves until Section 6.

The simplest case of a compound wave system where $\mathbf{P}_0 = 0$ consists of 2 light flashes of equal scalar momentum, $p_{10} = p_{20} = p_0$, propagating in opposite directions, as shown in Fig. 1a. The moving system is shown in Fig. 1b, where the x-components of the wave momenta, $\mathbf{p}_{10}$ and $\mathbf{p}_{20}$, have been modified in accordance with (8) so that the centre of inertia moves at speed V in the x-direction.

In Fig. 1a, $m_0 = (p_{10} + p_{20})/c = 2p_0/c$. Recalling from Section 3 that $m_e = \gamma m_0$, the sum of scalar momenta in the moving system of Fig. 1b is:

$$p_1 + p_2 = m_e c = 2\gamma p_0 \,, \tag{10}$$

whilst the total momentum, $\mathbf{P} = m_e \mathbf{V}$, is the vector sum of momenta:

$$\mathbf{P} = \mathbf{p}_1 + \mathbf{p}_2 = \frac{2\gamma p_0}{c}\mathbf{V} = 2\gamma\beta p_0 \,\hat{\mathbf{i}} \,.$$

Consider the vector $\mathbf{p}'$ in Fig. 1b, where $\mathbf{p}_1 = \mathbf{P}/2 + \mathbf{p}'$ and $\mathbf{p}_2 = \mathbf{P}/2 - \mathbf{p}'$. Using the law of cosines, its magnitude, p', is such that:

$$p_1^2 = p'^2 + (\gamma\beta p_0)^2 + 2\gamma\beta p_0 p' \cos\theta \tag{11}$$

$$p_2^2 = p'^2 + (\gamma\beta p_0)^2 - 2\gamma\beta p_0 p' \cos\theta \,, \tag{12}$$

where θ is the angle $\mathbf{p}'$ makes with the x-axis. Upon eliminating p_1 and p_2 from (10)-(12) we find that $p' = p'(\theta)$ is the ellipsoid:

$$p'(\theta) = \frac{p_0}{\sqrt{1-\beta^2\cos^2\theta}} \,. \tag{13}$$

Writing the momenta in component form as $\{p_{ij}\}_{i=1,2\,;\,j=x,y,z}$, (13) is then the ellipsoid:

$$(p'_x/\gamma)^2 + p_{iy0}^2 + p_{iz0}^2 = p_{i0}^2 \,,$$

where $p'_x = p_{1x} - \gamma\beta p_{10} = -(p_{2x} - \gamma\beta p_{20})$, so that the moving system momenta satisfy the following equation:

$$\left(\frac{p_{ix} - \gamma\beta p_{i0}}{\gamma}\right)^2 + p_{iy0}^2 + p_{iz0}^2 = p_{i0}^2 \,. \tag{14}$$

Eq. (14) is here derived only for the case N=2, however this equation also covers the general case, as we shall now show. Consider as initial condition an arbitrary system of light flashes, comprising a number $N \geqslant 2$ of wave momenta of scalar momentum p_{i0}, whose directions of propagation are distributed in space such that $\mathbf{P}_0 = \sum_i \mathbf{p}_{i0} = 0$ and $\sum_i p_{i0} = m_0 c$. In the rest system components are such that:

$$p_{ix0}^2 + p_{iy0}^2 + p_{iz0}^2 = p_{i0}^2 \,. \tag{15}$$

The example for $N = 2$ above suggests that after (8) acts on the set, bringing the total momentum to $\mathbf{P} = \gamma m_0 V \,\hat{\mathbf{i}}$, then (14) applies to the moving system momenta. Fig. 2 shows the moving system momenta when all the rest system scalar momenta are the same, i.e. $p_{i0} = p_0$ for all i. Differentiating (14) with respect to β gives:

$$\frac{dp_{ix}}{d\beta} = \gamma\,(p_{i0} + \gamma\beta p_{ix}) \,. \tag{16}$$

Expanding the first term in (14) and using $\gamma^2\beta^2 = \gamma^2 - 1$ gives:

$$p_i = \frac{p_{i0} + \gamma\beta p_{ix}}{\gamma} \,. \tag{17}$$

From $P_x = \gamma m_0 V$, we also have $dP_x = \gamma^3 m_0\, dV$, so that:

$$dp_{ix} = \frac{dp_{ix}}{dV} dV = \frac{dp_{ix}}{d\beta}\frac{dP_x}{\gamma^3 m_0\, c} \,. \tag{18}$$

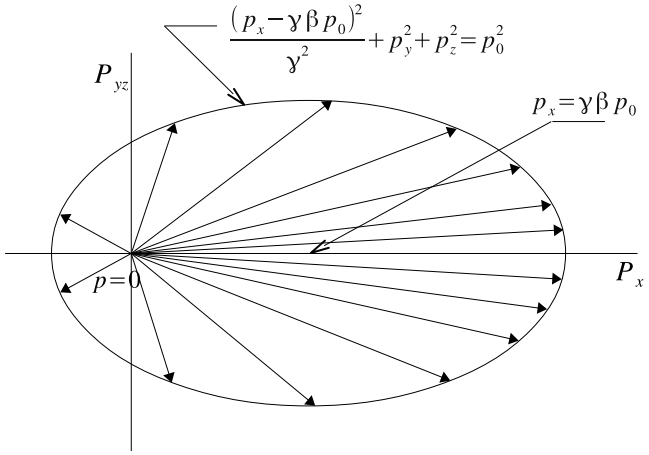

Fig. 2: Individual momenta in an isotropic wave system modified such that $V = \beta c$.

Finally, substituting (16) and (17) in (18):

$$dp_{ix} = \frac{p_i}{\gamma m_0 c} dP_x ,$$

which is the x-component of (8). Due to the choice of coordinates, the y and z components of momentum were unaffected, so the ellipsoidally modified distribution (14) is generated by the action of (8) on our arbitrary initial condition as expected. Comparing (14) and (15), the components of the moving system wave momenta are:

$$p_{ix} = \gamma(p_{ix0} + \beta p_{i0}) \;\; ; \;\; p_{iy} = p_{iy0} \;\; ; \;\; p_{iz} = p_{iz0} . \qquad (19)$$

Note that these physical transformations due to changes in the condition of motion of a light source are identical to Lorentz Transformations of wave momenta between different reference frames in standard configuration. However, as we are not asserting the Principle of Relativity there is no guarantee (so far) that our analysis works relativistically, and (19) corresponds only to the forward transformations of wave momenta in relativity theory.

We can now calculate the relative velocity of the i^{th} light flash, which is to say its velocity relative to the centre of inertia of the system, which our observer considers to be moving at V in the x-direction. The total velocity of the i^{th} flash has components $\{v_{ij} = c p_{ij}/p_i\}_{i=1..N\,;\,j=x,y,z}$. Using $\gamma^2\beta^2 = \gamma^2 - 1$ with (17) and (19), it is readily shown that the relative velocity, $\mathbf{v}_{ri}$, has components*:

$$v_{rix} = v_{ix} - V = \frac{c p_{ix0}}{\gamma p_i} \; ; \; v_{riy} = v_{iy} = \frac{c p_{iy0}}{p_i} \; ; \; v_{riz} = v_{iz} = \frac{c p_{iz0}}{p_i} .$$

If $\mathbf{v}_{ri}$ makes the angle ϑ_i with the x-axis, then:

$$\tan\vartheta_i = \frac{\sqrt{v_{riy}^2 + v_{riz}^2}}{v_{rix}} = \gamma \tan\vartheta_{i0} , \qquad (20)$$

*Since $\mathbf{V}$, $\mathbf{v}_i$ and $\mathbf{v}_{ri}$ are all referred to the same observer

where ϑ_{i0} is the corresponding angle in the rest system. Sect. 6 shows how this basic kinematic relationship leads to length contraction in 'pure field' models of the massive particles where all the field energy propagates luminally. Such models are discussed in the next section.

5 Luminal wave models of matter

Up to this point the analysis has dealt with systems of light flashes emitted by identical sources in different conditions of motion. No functional description of the light flashes was required, neither as photons nor as solutions to any particular wave equation. The fact that these systems obey the usual relativistic momentum equation for particles strongly suggests that the massive particles should also be thought of as luminally propagating field systems. This Section shows how the basic mechanics principles can be applied quite generally to compound, interacting systems of wave objects that are commensurate with modelling subluminally moving systems.

5.1 Compound wave systems

At any point in a system of disjoint light flashes (*i.e.* whose momentum densities do not overlap), there is a single field momentum density associated to a well defined unit wave vector. In principle, this field momentum density could be induced from a set of space functions in accordance with the definition of a wave object, so the entire system can be thought of as a single wave object, but there are also wave systems that cannot be represented as single wave objects.

Consider instead a system of N light flashes that propagate towards each other. When the field momentum densities of the various light flashes meet and overlap, the physical situation is inevitably such that there are multiple waves coexisting at the same place, propagating in different directions†. Since the set of space functions that comprises a wave object only induces a single momentum density at each point, when wave objects collide the luminal wave description necessarily involves multiple wave objects coexisting at the same place and time.

We shall now see that interactions between these distinct entities are required in order to construct luminal wave models of subluminally moving matter.

5.2 Forces, field variables and superposition

The force operating on a wave object is, by definition, equal to its rate of change of momentum, which is to say the space integral of the rate of change of its momentum density‡. Momentum is locally conserved, so forces necessarily manifest

†Note that the vector addition of two non-collinear luminal wave vectors is not a luminal wave vector because there is no wave actually propagating at c in the direction of the resultant vector.

‡There is also generally a rate of change of a wave object's momentum density at every fixed point due to the movement of the object, but the space integral of such changes obviously vanishes.

as reciprocal local exchanges of momentum between the momentum densities of the participating wave objects. These exchanges necessarily sum to zero locally as well as globally, so 'local action' can only mean that the objects' momentum densities must overlap. Now, when the momentum density distribution of a wave object changes then so must the field variables that induce it, so the essential nature of forces in a wave theory is to modify wave objects.

In a compound wave system formed by intersecting light flashes, if there were no forces between wave objects, then the momentum distributions pertaining to each object would not change as they move through each other, the same space functions could be retained for each wave object throughout the encounter and it is reasonable to think of each object's field variables as being the same as if it were by itself. A linear field theory is then appropriate. In Electromagnetics, for example, the wavefields interact with charges but not with each other. The chosen field variables, **E** and **H**, are force fields defined by the force that the wavefield exerts on a standard reference system, a 1 coulomb point charge. The global values of these field variables are given as linear superpositions of the *disjoint* values pertaining to individual wavefields.

In linear field theory, wave components evolve independently of each other, there are no interactions amongst the waves and any superposition must dissipate unless all of the wave vectors are parallel, in which case the motion of the centre of inertia of the wave group is $V = c$. Electromagnetic field models of subluminal massive particles are thus excluded. The idea that a finite subluminal image can be formed as an interference pattern can also be excluded as it requires infinite wave trains, which requires infinite energy. Therefore, the construction of luminal wave models for the massive particles requires multiple distinct wavefields that share the same space and interact with each other to form bounded systems, which is to say they form wave solitons.

When the wavefields in a model do interact with each other, the forces that are actually operating on a given wave object still superpose (by definition). However, as mentioned above, the definition of force also implies that wave objects are distorted under interaction. If the wave object is defined by force field variables, as in Electromagnetics, then its force fields (which are propensities to exchange momentum as opposed to actual forces) are not the same under interaction as would be the case if it had been disjoint. Furthermore, if a wave object in an interacting system persists in a self-similar form then that form depends in an essential way on the forces that are operating on it. It is obviously counterfactual to consider such an object as if it were disjoint from the others that are actually present. If they were not present, it would be a different object.

Overall, once we include interactions between wave objects, the global values of field variables cannot be expressed as a linear superposition of disjoint values so a nonlinear theory is required. If the chosen field variables are force fields, then global values are by definition still given as a linear superposition, but this is a linear superposition of *conjoint* values that correspond to actual transfers of wave momentum from one object to another.

Of course one might choose other field variables besides force fields. With water waves for example the vertical displacement of the water surface is commonly used as a field variable. Such alternatives also do not generally superpose linearly. Whatever field variables we may choose and however they may induce it, the field momentum density is locally conserved. As we shall see in the next two sections, the field momentum density is also the physical basis for any mechanical quantities that we may observe including not just momenta but also lengths and times.

5.3 Wave trajectories

Whereas a field variables description immediately confronts us with some unknown nonlinearity, we can focus directly on the inherently linear field momentum density by considering a wave trajectories description. This kind of description is often useful in Electromagnetics, where it arises from the field variables description as follows. Electromagnetic waves in a vacuum obey the well known d'Alembert wave equation:

$$\left\{\nabla^2 - \frac{1}{c^2}\frac{\partial^2}{\partial t^2}\right\}\psi = 0\,, \tag{21}$$

where $\psi(x, y, z, t)$ may be any component of either the Electric field **E** or the Magnetic field **H**. Electromagnetic waves involve both Electric and Magnetic fields and the linear momentum density is $\vec{\rho}_p = \mathbf{S}/c^2$, where the Poynting vector $\mathbf{S} = \mathbf{E}\times\mathbf{H}$ is aligned with the wave vector, **k** (which by definition points in the direction of propagation). The field lines of the wave vector trace out well defined trajectories at the ray velocity $v_{ray} = c$ (in vacuo) [16,17], and the linear momentum carried by the Electromagnetic wave propagates along these trajectories at the characteristic velocity.

Any luminal wave theory, linear or nonlinear, has a wave vector pointing in the direction of propagation, and once we have a wave vector, the wave trajectories description works as in Electromagnetics.

5.4 Closed wave systems

Whether we consider a subatomic particle or some macroscopic object, it is a basic premise that the energy that constitutes a persistent subluminally moving system must remain in the same general vicinity as the object. From the perspective of a luminal wave model where the energy is moving at c, any trajectory of the wave vector will remain bound to the system because any wave trajectory that leaves the system bleeds energy from it. Therefore, when considering luminal wave models for matter, we shall restrict our attention to closed trajectory systems, where the trajectories may or may not form closed loops, but any given trajectory remains within some finite distance of the centre of inertia of the system.

5.5 Towards coordinate transformations

In order for wave trajectories to remain bound to a subluminally moving centre of inertia they must be curved. Therefore, the unit wave vector for any given wave object in a closed system must be position dependent and may in general also be time dependent. Consequently, space functions that describe light flashes, where the unit wave vector is constant (see for example [18–20]), are unsuitable for describing closed systems, so we cannot think that the massive particles are constructed of light flashes. Therefore, we now require the incremental momentum boosts to operate directly on the momentum densities.

Eqs. (1) - (7) can be rewritten in terms of momentum densities, however it is more convenient to preserve the notation by converting momentum densities into momenta as follows. Let the entire space be divided into small regions of dimension $\delta x = \delta y = \delta z = \delta l$, where δl is sufficiently small that any of the momentum densities, $\overrightarrow{\rho}_{pi}(x, y, z, t)$, can be considered constant within each region so that $\overrightarrow{\rho}_{pi}(x, y, z, t)\,\delta l^3$ is a linear momentum propagating at c in a definite direction in space. Introducing a new subscript, k, to label the regions, we write the linear momentum of the i^{th} field in the k^{th} region as $\mathbf{p}_{ik}(t) = \overrightarrow{\rho}_{pi}(\mathbf{r}_k, t)\,\delta l^3$, where $\mathbf{r}_k$ is the position vector to the centre of the k^{th} region. Since the space integral of the momentum boost must recover (8) for all possible light flashes, the incremental momentum boost operating on the $\mathbf{p}_{ik}$ can only be:

$$d\mathbf{p}_{ik} = \frac{p_{ik}}{m_e c} d\mathbf{P}\,, \tag{22}$$

where $\mathbf{P} = \sum_k \sum_i \mathbf{p}_{ik}$, $p_{ik} = |\mathbf{p}_{ik}|$ and $m_e = \frac{1}{c}\sum_k \sum_i p_{ik}$, and the rest goes through as before.

The rest system in Sect. 4 could be a particle or any macroscopic system that is comoving with the observer. The moving system's internal momenta, $\mathbf{p}_{ik}$, are related to the $\mathbf{p}_{ik0}$ by (19), with an additional k subscript inserted. The system's momentum is $\mathbf{P} = \gamma m_0 \mathbf{V}$, where the velocity of the centre of inertia of the wavegroup, $\mathbf{V}$, is simply the observed velocity of the system. The relative velocity we developed at the end of the last section, $\mathbf{v}_{rik} = \mathbf{v}_{ik} - \mathbf{V}$, describes the internal movements of the system as seen by an observer who considers it to be moving at $\mathbf{V}$.

Since internal movements obviously change in response to changes in the observed velocity, neither the shape nor the internal evolution of a subluminally moving wave system can be assumed to be velocity independent so that, in order to determine coordinate transformations, we must first calculate the impacts this has on rulers and clocks constructed from luminal wave energy.

Before moving onto the analysis of length contraction and time dilation in luminal wave models let us contrast (22) with the Newtonian concept of a force field acting on a point-like massive particle. According to the fourth basic principle, the force acting on an interacting field is, by definition, equal to its rate of change of momentum*. It might appear at first blush that:

$$\frac{d\mathbf{p}_{ik}}{dt} = \frac{p_{ik}}{m_e c}\frac{d\mathbf{P}}{dt} \tag{23}$$

and the left hand side of (23) should be interpreted as the force acting on the i^{th} wave object in the k^{th} region when the total externally applied force acting on the particle is $\mathbf{F} = d\mathbf{P}/dt$. Such a dynamic interpretation requires making unreasonable extraneous assumptions, including not least a uniform applied field. This is unnecessary for our analysis, for which (22) applies to the relationship between systems in steady state conditions, before and after (but not necessarily during) some physical process that results in an incremental boost to the system's momentum. A one-to-one correspondence between the momentum densities of rest and moving systems is assumed, but without such an assumption no inherently relativistic structure would be possible because we could never equate a boost with a change of observer.

6 The Lorentz-Fitzgerald contraction

This section shows that closed wave trajectory systems contract in the direction of motion. This is easily understood by considering the special case of a rest system where the wave vector is transverse to the direction to the centre of inertia so that the system evolves under rotations and any wave trajectory exists on the surface of a sphere. Such systems are of particular interest because the usual interpretation [21] of the little group of transformations that preserves the linear momentum of a particle in Special Relativity is that rest particles evolve under the action of elements of the rotations group.

Consider a system of concentric spherical surfaces constructed about the rest system's centre of inertia, which we shall assume is at the origin. Given the abovementioned condition, all rest system wave trajectories through a given point, $\mathbf{r}_{k0}$, lie instantaneously in the tangent plane at that point to the sphere of radius r_{k0}. Without loss of generality, let us consider the trajectories passing through a point in the xy plane where the tangent plane makes the angle θ_0 with the x-axis, as shown in the top left of Fig. 3. The wave momentum along a trajectory lying in this plane has components in the form $p_{x0} = p_0 \cos\theta_0 \cos\phi_0$, $p_{y0} = p_0 \sin\theta_0 \cos\phi_0$, $p_{z0} = p_0 \sin\phi_0$, where ϕ_0 is the angle the trajectory makes with the xy plane. Note that this is just the component form of any of the $\mathbf{p}_{ik0}$. The i and k subscripts can be omitted without ambiguity: p_{x0} means p_{ikx0} and so on. Using (19), the components of the corresponding wave momentum in the moving system are:

$$p_x = p_0\gamma(\cos\theta_0 \cos\phi_0 + \beta)\ ;\ p_y = p_{y0}\ ;\ p_z = p_{z0}\,.$$

The moving system momenta for different values of ϕ_0 are not coplanar. As shown in the top right of Fig. 3, they lie on

*Donev and Tashkova [20] have also developed this within a field variables approach to luminally propagating bivector fields.

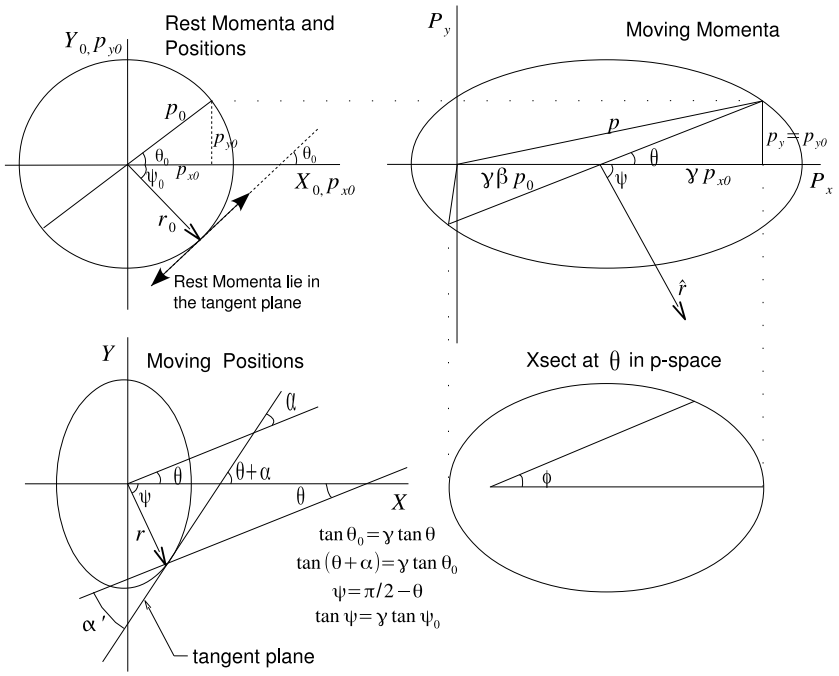

Fig. 3: Momenta and Positions in Rest and Moving Luminal Wave Particle Models.

a conical surface whose vertex is at the origin of momentum coordinates, and whose base is the intersection of the plane at angle θ, where $\tan\theta = \tan\theta_0/\gamma$, with the moving system momentum distribution. This elliptical intersection is shown in the bottom right of Fig. 3.

The (total) velocity for each of these momenta has components of the form $\{v_j = cp_j/p\}_{j=x,y,z}$, where p is given by (17):

$$p = \frac{p_0 + \gamma\beta p_x}{\gamma} = \frac{p_0}{\gamma}\left(1 + \gamma^2\beta(\cos\theta_0\cos\phi_0 + \beta)\right). \quad (24)$$

The group velocity is $V\hat{\mathbf{i}}$, so using (24) the relative velocity components are:

$$v_{rx} = \frac{cp_x - pV}{p} = \frac{cp_0\cos\theta_0\cos\phi_0}{\gamma p},$$

$$v_{ry} = \frac{cp_0\sin\theta_0\cos\phi_0}{p} \text{ and } v_{rz} = \frac{cp_0\sin\phi_0}{p}.$$

The ratio $v_{ry}/v_{rx} = \gamma\tan\theta_0$ is independent of ϕ_0 (and ϕ), so the velocities that lay in a given tangent plane in the rest system transform into relative velocities lying in a corresponding moving plane, tangent to the moving trajectory system*. Let α be the angle between the plane at θ and the tangent plane, as shown in the bottom left of Fig. 3. The moving system tangent plane makes the angle $\alpha + \theta$ with the x-axis, where $\tan(\theta+\alpha) = v_{ry}/v_{rx} = \gamma\tan\theta_0 = \gamma^2\tan\theta$. Using the angle sum trigonometric relations we obtain:

$$\tan\alpha = \frac{\beta^2\sin\theta\cos\theta}{1 - \beta^2\cos^2\theta}. \quad (25)$$

The set of all tangent planes defines the surface up to a scale factor. Due to rotational symmetry we can anticipate being able to write the equation describing this surface in the form $r = r(\psi)$, where ψ is the angle from the position vector to the x-axis. For any function $r(\psi)$ the angle between the tangent plane and the plane transverse to the radius vector is:

$$\tan\alpha' = \frac{1}{r}\frac{dr}{d\psi}. \quad (26)$$

Consider as trial function the ellipsoid:

$$r(\psi) = \frac{\lambda}{\sqrt{1 - \beta^2\sin^2\psi}}, \quad (27)$$

for which

$$\tan\alpha' = \frac{\beta^2\cos\psi\sin\psi}{1 - \beta^2\sin^2\psi}, \quad (28)$$

independent of the scale parameter λ. With $\psi = \pi/2 - \theta$, this is identical to (25), which therefore describes an ellipsoid of revolution (27), such that the plane at θ is transverse to the position vector, $\mathbf{r}$, shown in the bottom left of Fig. 3.

*Recall that we showed in Section 4 that the relative velocity of any trajectory is rotated by the kinematic relation $\tan\vartheta = \gamma\tan\vartheta_0$, where ϑ was the angle $\mathbf{v}_r$ makes with the x-axis. We now see the consequence of the little group: Locally flat surfaces formed by sets of trajectories at a given point in the rest system transform into locally flat moving surfaces, rotated so that the tangent of the angle the moving surface makes with the x-axis is $\gamma\tan\theta_0$, where θ_0 is the angle the rest system surface makes with the x-axis.

The scale factor, λ, is readily found by inspection. The moving system equatorial plane is the plane $x = Vt$ and $\psi = \pi/2$. The tangent plane at any point in the equatorial plane is parallel to the x-axis so the $d\mathbf{p}_{ik}$ at these points lie in the tangent plane. Therefore the equatorial tangent planes are not altered by the action of (22). Therefore the radius of a circumferential trajectory in the equatorial plane is invariant under the dimensional transformation (27), and $\lambda = r_0/\gamma$, where r_0 is the radius of the spherical surface in the rest system.

The result is that, for our rest observer, any wave trajectory in the moving system lies on the surface of an ellipsoid moving along the x-axis at speed V and of the form:

$$r(\psi) = \frac{r_0}{\gamma\sqrt{1-\beta^2\sin^2\psi}}\,. \tag{29}$$

The moving system wave trajectories are thus compressed by the factor γ in the direction of motion. Let us now consider general wave trajectories that are not confined to the surfaces of spheres in the rest system. The analysis above shows that any short segment of the general trajectory is rotated so that the ratio of its dimensions parallel and transverse to V is suppressed by γ. Since this applies to every segment it applies to entire trajectories and since we have already identified specific trajectories whose transverse dimensions are invariant, the same scale factor applies to the general case.

Closed luminal wave trajectory systems are thus physically compressed by the factor γ in the direction of motion so that any macroscopic physical objects, including rulers, that are constructed entirely from luminal wave energy undergo the usual Lorentz-Fitzgerald length contraction.

7 Time dilation

It can be seen from (7) and Fig. 2 that any movement of a closed luminal wave system through space is the result of correlations amongst the directions of propagation of the internal momenta, $\hat{\mathbf{k}}_i(x, y, z, t)$. On the other hand, if all the trajectories of a wave system were exactly parallel the spatial configuration of the system would not change and there would be no internal evolution. Just as correlations are necessary for movement in space, decorrelations are necessary for evolution in time. There is a direct tradeoff involved, so some form of time dilation is an inevitable consequence of constructing variable speed particles from fixed speed waves.

We shall now show that internal processes in wave systems slow down according to $dt/dt_0 = 1/\gamma$. The analysis is similar to the standard analysis of a light clock.

With respect to the rest system's wave trajectory system, consider any closed trajectory formed by n segments, where the i^{th} segment has length l_{i0} and makes the angle θ_{i0} with the x-axis. The speed on all segments is $v_0 = c$ so the period around the closed trajectory is $T_0 = \frac{1}{c}\sum_{i=1}^{n} l_{i0}$, where T_0 is the time elapsed on a clock in the rest frame to traverse the trajectory in the rest system. Lengths in the rest system may be written in component form such that:

$$l_{i0}^2 = l_{ix0}^2 + l_{iy0}^2 + l_{iz0}^2\,.$$

Let the trajectory system now move in the x-direction at speed V. Given the length contraction, x-components contract by the factor γ and the corresponding relationship is:

$$l_i^2 = \frac{l_{ix0}^2}{\gamma^2} + l_{iy0}^2 + l_{iz0}^2\,.$$

It is readily shown that:

$$l_i^2 = l_{i0}^2(1-\beta^2\cos^2\theta_{i0})\,. \tag{30}$$

The moving and rest system angles are related by $\tan\theta_i = \gamma\tan\theta_{i0}$, from which it is easily shown that:

$$\frac{\cos\theta_i}{\cos\theta_{i0}} = \sqrt{1-\beta^2\sin^2\theta_i}\,. \tag{31}$$

The relative velocity on the i^{th} segment in the moving system, v_{ri}, is constrained by:

$$(v_{ri}\cos\theta_i + V)^2 + v_{ri}^2\sin^2\theta_i = c^2\,, \tag{32}$$

which leads to: $v_{ri} + V\cos\theta_i = c\sqrt{1-\beta^2\sin^2\theta_i}$, from which, using (31):

$$v_{ri} = \frac{l_{ix0}\,c\,(1-\beta\cos\theta_{i0})}{\gamma l_i\cos\theta_{i0}}\,.$$

The time taken to traverse the i^{th} segment in the moving system is $l_i/v_{ri} = l_i^2/v_{ri}l_i$, so, using (30), we may write the period elapsed on clocks in the rest system for traversals around the Lorentz contracted moving system trajectory as:

$$T_0^V = \sum_{i=1}^{n}\frac{l_i^2}{v_{ri}l_i} = \frac{\gamma}{c}\sum_{i=1}^{n} l_{i0}(1+\beta\cos\theta_{i0})\,.$$

Since $\sum_i l_{i0}\cos\theta_{i0} = 0$ it follows that $T_0^V = \gamma T_0$. It might be argued that trajectories need not form closed loops, but a path that crosses a given plane transverse to $\mathbf{V}$ must eventually either recross the same plane or become confined to a smaller region, in which it must either routinely recross a transverse plane or become confined to an even smaller region and so on. In steady state, the trajectories can only be transverse or regularly recross a transverse plane. The analysis above also covers open paths between points in the same transverse plane, for which the condition $\sum_i l_{i0}\cos\theta_{i0} = 0$ is also fullfilled. The time between such crossing points dilates by γ. We conclude that the internal processes of a luminal wave system slow down by the factor γ. The argument from internal processes to real world clocks is well established [23], and tested [24–26], so moving clocks will run slow according to the usual relation $dt/dt_0 = 1/\gamma$.

A similar tradeoff occurs in the Dirac Equation. Consider the equation for the time dependence of the velocity operator in the Heisenberg representation of the Dirac theory [22]:

$$\overrightarrow{\alpha}(\mathrm{t}) = \left(\overrightarrow{\alpha}(0) - \frac{\mathbf{p}}{\mathrm{H}}\right)\exp\left(-2i\mathrm{H}t\right) + \frac{\mathbf{p}}{\mathrm{H}}\,, \qquad (33)$$

where $\mathbf{p}$ and H are both constants, $c = 1$ and the group velocity is $\mathbf{p}/\mathrm{H} = \mathbf{v}_g = const.$. The first term on the right is routinely interpreted to represent the internal movements of the electron, the 'Zitterbewegung'. Since $\overrightarrow{\alpha}$ has real eigenvalues, its quantum mechanical expectation, $< \Psi \mid (\overrightarrow{\alpha}(0) - \mathbf{v}_g) \mid \Psi > / < \Psi \mid \Psi >$, varies with v_g as $\sqrt{1 - v_g^2}$. In other words, the Zitterbewegung slows down by a Lorentz factor as the group velocity increases.

Whilst we can now write down a constant overall rate of spatiotemporal evolution for a single observer as $c^2dt^2 = c^2dt_0^2 - d\mathbf{x}_0^2$, Lorentz Transformations do involve an additional ingredient, Einstein clock synchronisation, which will be the focus of the next Section.

8 Coordinate transformations

We have shown length contraction and time dilation as physical effects in luminal wave models subject to the basic mechanics Eqs. (1) - (7) and the incremental momentum boost generator (22). The analyses were constructed from the perspective of a single observer so the principle of relativity, covariance, coordinate independence, and coordinate transformations were *all* irrelevant.

Let us now focus on the question of how these physical phenomena of length contraction and time dilation constrain the coordinate transformations. Selleri has studied this question in some detail [13, 14]. He considered three assumptions, namely: length contraction, time dilation and constancy of the 2-way velocity of light. He showed that any two of these assumptions both implies the third and constrains the coordinate transformations between a preferred rest frame, $S_0 = (x_0, y_0, z_0, t_0)$ and a frame $S = (x, y, z, t)$ in standard configuration moving with speed v to the following form:

$$x = \frac{(x_0 - \beta c t_0)}{\sqrt{1-\beta^2}}\,;\; y = y_0\,;\; z = z_0\,;$$

$$t = \sqrt{1-\beta^2}\; t_0 + e_1(x_0 - \beta c t_0)\,,$$

where $\beta = v/c$ and e_1 is a synchronisation parameter.

Setting $e_1 = -\beta/(c\sqrt{1-\beta^2})$ corresponds to the usual Einstein clock synchronisation convention and reduces this to the Lorentz Transformation. Our coordinate transformations are therefore Lorentz Transformations and the relativity principle and the constant speed of light for all observers are therefore results, not postulates. It is also now finally clear that the wave inertia changes we have analysed are frequency changes corresponding to the relativistic Doppler shift, as opposed to, say, amplitude changes.

8.1 Other synchronisation protocols

Selleri also discusses alternative clock synchronisation protocols, especially the case $e_1 = 0$ which corresponds to using Einstein synchronisation in a preferred rest frame, and setting clocks in the moving frame to coincide with nearby clocks in the rest frame at $t = 0$. Both sets of observers agree that clocks in the moving system run slow, and they also agree on the simultaneity of spatially separated events. The transformations in this case, known as the inertial transformations, were first found by Tangherlini [27]. The empirical consequences of inertial transformations have been shown to comply with experimental evidence in a wide variety of situations [28]. As far as the present article is concerned, Appendix 2 derives (8) from the relativistic Doppler shift and aberration results, which apply equally well to inertial transformations [15], and therefore so do the structural consequences developed above.

Selleri and others have advanced various arguments in favour of absolute simultaneity [29–34] (notably a simplified analysis on the rotating platform), but nothing that questions the Lorentz form within the domain of inertial frames. Inertial transformations do not preserve the line element, $ds^2 = c^2dt^2 - dx^2 - dy^2 - dz^2$, the physical laws are frame dependent, the inverse transformation is different, the relative velocity of the origin of S as seen by S_0 does not equal the relative velocity of S_0 as seen by S and the inertial transformations do not form a group [14]. In short, they fail to deliver elegant and simple analysis in most physical situations.

The conventional nature of the Einstein protocol has, of course, always been stipulated in relativity theory but Selleri has shown something important: Like the choice between Cartesian and Spherical coordinates, the choice of a clock synchronisation protocol really is only a matter of convenience. Provided they use it consistently, physicists solving problems on a rotating platform and engineers developing GPS satellite networks (which use an inertial clock synchronisation protocol) can use whatever protocol is most effective.

The self-evident fact remains that the events that happen in the world cannot depend on the coordinate systems we use to describe them. Coordinate independence is one of the most powerful practical tools for the development of new physics. Other coordinate transformations may be empirically adequate, but special status is rightly afforded to Lorentz Transformations on the basis of symmetry and utility, not uniqueness, and what we have shown is that their 'natural habitat' is field theory.

8.2 Objective simultaneity and the preferred frame

An immediate consequence of the Einstein synchronisation protocol is that observers in relative motion find themselves in disagreement over intrinsically objective facts such as the rates of their respective clocks and the temporal ordering of spacelike separated events.

Philosophical relativism sought to leave these conflicts unresolved on the basis, ultimately, that a preferred frame cannot be observed. This approach induces numerous paradoxes that have been criticised for over a century [35]. More recently, Hardy [32] and Percival [33, 34] have each shown that relativity of simultaneity when combined with quantum nonlocality leads to more than just conflicts between different observers. It leads to manifest contradictions for individual observers.

Percival's double Bell paradox, for example, considers two EPR/Bell experiments in relative motion. According to relativity of simultaneity, a temporal loop can be constructed by using the measurement results in one arm of each experiment to select the measurement axis in the corresponding arm of the other experiment. Given the quantum predictions for individual EPR/Bell experiments, he showed that an observable measurement result is, on at least some occasions, inverted by the loop becoming equal to its own opposite which is a manifest contradiction.

The long standing loopholes [36] in EPR experiments finally having been closed [37], it can no longer be argued that the quantum predictions are somehow "wrong" when they correctly predict the experimental outcomes. Instead, one must simply admit what good sense always demanded: When two observers disagree about an objective fact, they cannot both be right. The temporal loop relativistically assumes that each observer's view of the temporal order of the relevant events is indeed "true", which is impossible because their views are mutually exclusive.

Therefore, we must admit a distinction between the real physical state of affairs and how things appear to a given observer. Two different concepts of simultaneity, apparent and objective, arise. Apparent simultaneity is what appears to observers using a given clock synchronisation protocol. Provided the protocol corresponds to a definite value for the synchronisation parameter, e_1, apparent simultaneity is sufficient for making valid predictions — an essential consideration since Physics expresses itself in terms of observable quantities*. Relativistic simultaneity is just the apparent simultaneity for observers who use the Einstein protocol and there is no need to assert the truth value of this clock synchronisation protocol (which would imply that the forbidden double-Bell temporal loop is real).

As far as objective simultaneity is concerned, the foregoing wave analyses have shown that motion induces objective changes in clocks and rulers that are constructed entirely from luminal waves. A unique preferred frame, in which these devices are undistorted, can now be identified in two different ways, because an observer's velocity relative to either (a) the medium in which waves propagate or (b) the universe as a whole can be determined from Doppler effects in the wave interpretation.

Of course, the nett observed Doppler shift for a given source and detector depends only on their relative velocity and the direction to the source, so that we cannot isolate the detector's velocity. However, with a large number of sources lying in different, random directions whose individual masses and conditions of motion are independent of the direction in space, we can determine the detector velocity relative to the centre of mass of the group as a whole. Similarly, measurements on an *a priori* isotropic radiation bath are sufficient [38] to determine the detector velocity relative to the rest frame of the bath, as defined in Section 4.

As discussed in [12] and references therein, two important cases have already been studied, namely the anisotropies of (1) the Cosmic Microwave Background Radiation (CMBR) [38, 39], which gives Earth's velocity relative to the medium and (2) the angular number density of observable astronomical objects [40], which gives Earth's velocity relative to the rest of the universe. In both cases, an identical velocity dipole of magnitude ~ 350 km/sec is observed!

It is anticipated that future observations on other isotropic radiation baths will show the same anisotropy and the same velocity dipole. Variations in the average red shift of distant galaxies as a function of the direction in space constitute a further example that can be tested in the future to confirm this prediction. Note that these results are at odds with the relativist interpretation.

Within the wave interpretation of Lorentz Invariance, we see from Section 2 that the momentum density distribution of a system whose centre of inertia has zero velocity relative to the medium has no bias in any given direction, and, with Sections 6 and 7, we can now safely state that clocks in this condition of motion really do run faster, rulers really are longer and so on. The existence of this preferred frame is implied by the wave analysis and its observability provides the essential empirical basis for asserting at last that objective simultaneity coincides with the Einstein simultaneity of observers at rest in the CMBR frame. The wave interpretation presented here has therefore eliminated all the paradoxes associated with Special Relativity without sacrificing any of the practical benefits of Lorentz symmetry, whilst also covering a wider range of observables.

However, this interpretation assumes a wave ontology, with energy constrained to propagate at c. The idea of matter as constructed from some form of energy that does not propagate at c is considered, and rejected, in the next Section.

9 Non-luminal structures

It is of course possible that wave propagation slows down or stops altogether under interaction, so that the wave energy is transformed into some ill-defined notion of 'substance'. Nothing prevents applying the same basic mechanics principles to such non-luminal structures, however once we intro-

*Note that the quantum predictions for EPR experiments are insenstitive to the temporal order of the Bell measurements, so they cause no difficulty.

duce entities that do not move at c, an immediate casualty is the work integral connection between momentum and energy. We would have no choice but to re-define inertia as being fundamentally velocity dependent.

Such a flexible approach to so pivotal a definition might raise eyebrows if it were not for the fact that this particular step is an integral part of Special Relativity. So, let us assume that we could somehow make sense of the relativistic inertia in its own right, as we have done in this Article but on some other grounds that are also independent of Special Relativity.

As far as the structure of particles is concerned, without the concept of internal movements it would not seem possible to provide any account of internal processes (such as muon decay for example). Likewise, the fact that the massive particles possess angular momentum implies the existence of internal movements*. Let us consider internal movements at speeds other than c. To illustrate the difficulties this causes, we shall also assume that we can somehow produce Lorentz contracted moving system trajectories on other grounds that are also independent of Special Relativity.

We must still use (32), with v_i^2 replacing c^2 on the RHS, to connect the total and relative velocities on the i^{th} segment (as both are referred to the same observer). If v_i were the same in the moving and rest systems, then clearly the periods would not dilate by γ, and yet we know that for any physical system, not just luminal systems, periods must dilate by γ under Lorentz Transformations.

The resolution is most easily seen from Special Relativity. If the total speed, v_{i0}, on the i^{th} segment as seen by a comoving observer is such that $v_{i0} \neq c$, then for observers in other frames, $v_i \neq v_{i0}$ and must in general be calculated according to the relativistic composition of velocities:

$$\mathbf{v}_i = \frac{\mathbf{V} + \mathbf{v}_{i0\parallel} + \sqrt{1-\beta^2}\,\mathbf{v}_{i0\perp}}{1 + \frac{\mathbf{V}\cdot\mathbf{v}_{i0}}{c^2}} .$$

Now as we Lorentz boost a particle in the frame of a single observer, there are two possibilities. If $v_{i0} = c$, then $v_i = c$ for all i independent of the condition of motion of the particle, and structural models incorporating length contraction and the relativistic momentum are readily available. Sect. 8 showed that these phenomena imply Lorentz Transformations, whose elegance and simplicity therefore has a coherent explanation based on the very definition of momentum as inertia times velocity, $p = mc$.

Alternatively, if $v_{i0} \neq c$ the total velocities of internal movements, $\mathbf{v}_i$, must depend on both the particle velocity and the orientation of individual segments in the above complicated manner. Why? The elegance and simplicity of Lorentz Transformations then has at its very foundations an implausibly inelegant, complex structure. We are left reasoning in a circle from Lorentz Transformations to the composition of velocities to the proposition that such complex structures are necessary as the basis for our simple coordinate transformations and we have no physical basis for either length contraction or the relativistic momentum. Ockham's razor insists that we reject nonluminal structures.

Therefore, we must conclude that, in the comoving frame, Lorentz invariant structural models of the massive particles should have internal movements at, and only at, c.

10 Does local action imply retarded interaction?

Local action is the single most basic, self-evident principle in Physics — interaction requires colocation. Both Newton and Einstein agreed. This section considers the logic of interaction at a distance, subject to local action, but from a pure field perspective where mass energy propagates luminally.

In Classical Physics it was taken for granted that matter emits field, leading to the idea that the far fields of a particle propagate away from it at c. It then follows that long-range interactions between particles are retarded and the unavoidable consequence is that there can be no causal relations between space-like separated events. On the other hand, Quantum Mechanics predicts instant causal correlations at a distance and experiments replicate these predictions [41–43]. However, if matter and field are one and the same, as Einstein suggested, then the idea that matter emits field is meaningless. We need to consider whether or not the far fields propagate away from the centre of inertia in a pure field particle model.

Section 6 considered a rest system that evolves under rotations, corresponding to Special Relativity's little group. Note that the radius of the rest system sphere was not relevant — the analysis applies to any radius, and there is no good reason, neither in our analysis nor in Special Relativity, to distinguish between the near and far fields of a particle. The distinction in Electromagnetics between the 'attached' field [44] and the 'body' of the particle is arguably incompatible with Special Relativity because it implicitly introduces (radial) field movements that contravene the little group.

Consistent with Einstein's view that relativity theory renders the division into matter and field 'artificial', our luminal wave structure implies that particles are unbounded with far fields that propagate transverse to the radius† rather than radially away from a 'body'. There is then no good reason to presume that local action implies retarded interaction.

The long range interaction between two particles, A and B, depends on the colocation of their respective fields. It is an integral over all space, dominated by terms close to the two centres, but any far fields of A that become colocated with the B particle's centre of inertia did not travel there from A's centre of inertia. They are part of the extended wave system that is comoving, as a whole, with the A centre of inertia so one

*The quantisation of angular momenta is also readily explicable as a wave phenomenon [12, 20].

†As is also consistent with Electromagnetics' radial Coulomb field because $\mathbf{E}$ and $\mathbf{H}$ are each transverse to the momentum density $\mathbf{S}/c^2$, whilst $\mathbf{H}$ fields cancel in the rest particle due to balanced movements.

might anticipate that the direct impact of A's far fields on the observed location of the B particle would be instantaneous, while the reaction impact on the observed location of the A particle might be retarded.

However, it is more apposite simply to observe that field theory problems are usually formulated and solved on whole regions evolving subject to local action at all points in parallel. The idea of a local realist wave ontology is inherently Lorentz invariant, but waves are inherently distributed. They run on correlations at a distance sustained by strictly local actions. Distributed interactions between distributed waves can have distributed impacts, occurring simultaneously in different places. Waves exemplify Redhead's conclusion that ontological locality does not rule out instant relations between observables [45]. Trajectories in local realist wave systems display entanglement as shown in [16], where a Madelung decomposition of the Helmholtz wave equation shows that it contains Bohmian mechanics' nonlocal quantum potential within it. Therefore, quantum nonlocality and entanglement can perhaps be interpreted as locally realistic wave phenomena. With specific reference to the EPR paradox [46], the Bell Inequalities [47] depend on a causality analysis that uses light cones emanating from point events [48], presuming a one to one correspondence with point-like 'beables' [49], but for inherently distributed systems like waves neither beables nor events can be presumed to be point-like.

11 Discussion

Since massive particles have finite energy, the volume integral of the field energy density must not diverge as $r \to \infty$. The $1/r^2$ long range force fields for the charged particles imply a $1/r^4$ energy density asymptote for both charged and neutral particles in luminal wave models [12]. The energy density integral does not then diverge as $r \to \infty$ so finite but unbounded luminal wave structures are compatible with the usual basic physics. They appear as pointlike particles because the field energy is highly concentrated near the centre. For example, according to a $1/r^4$ energy density asymptote the maximum energy density for a particle with the mass of an electron, at the radius $r \sim 4 \times 10^{-13} m$, is $\sim 400,000$ times greater than that at a radius of 0.1 Angstrom unit.

Unlike Electromagnetics, nothing prevents the method in this Article from applying to the fermions. A wide range of candidate models for the massive particles, in the form of subluminal soliton solutions found in typically nonlinear field theories, have been reported in the literature. The appearance of Lorentz covariance in so many disparate field models is no coincidence as they are all subject to the same basic kinematic constraints used in Sects. 2 - 7 to show that Lorentz invariance is the consequence of constructing subluminally moving particles from fields that are constrained to propagate luminally.

While the constraints are simple, the structures of soliton solutions are generally not simple. For example, evolution under rotations does not imply spherical symmetry and nor does it imply that the particle rotates as a whole in a simple manner, like a solid ball. Due to the kinematic constraint, trajectories at different radii necessarily evolve at different angular rates and, similarly, wave trajectories at various points on the same spherical surface in the rest system generally rotate about different axes.

12 Conclusions

This Article has developed a particularly simple hypothesis: Energy-momentum propagates at c. It has shown why subluminally moving physical systems, including observers' measuring devices, then display time dilation and length contraction, so that an underlying luminal wave reality, although objective, presents a Lorentz covariant "spacetime" to its observers. Neither the Relativity Principle nor the invariance of the observed speed of light were assumed. These two cornerstones of relativity theory were shown as results, not put in as postulates.

This 3D+t reality also entails a preferred frame that has been observed in practice in at least two independent ways, providing a natural definition of objective simultaneity. All the paradoxes formerly associated with Special Relativity's subjective notions of reality are thus removed, and, unlike Special Relativity, the proposed luminal wave interpretation of Lorentz invariance is consistent with all the relevant facts.

Although the Lorentz covariance of luminal wave systems was perhaps already familiar, the basic mechanics underlying Lorentz symmetry remained unnoticed for over a century. The discovery of this direct link between wave systems and relativistic mechanics has wide ranging implications for the interpretation and unification of modern physics.

Rather than replacing Newtonian Mechanics, Einstein's relativistic mechanics is the natural step accompanying the shift in our founding physical ideas from particle to wave concepts. The wave packet is reformed by giving explicit recognition to the conservation of momentum between wave components and particles, which can now be seen as widely distributed systems with instantly correlated far fields. Quantum nonlocality can be understood within this framework whilst general covariance is readily incorporated, conceptually and analytically, with a refractive medium approach to gravity [12] that produces the relevant phenomena without the raft of problems flowing from the usual field equations.

Hopefully, this article has highlighted the absence of any good reason to presume that any non-propagative form of mass-energy exists. It's not so much the introduction of a new hypothesis, as the removal of an old one — the idea of matter as a distinct ontological class in its own right.

Submitted on November 18, 2016 / Accepted on November 21, 2016

References

1. Einstein A., Infeld L. Evolution of physics: The growth of ideas from early concepts to relativity and quanta. 1961, Simon and Schuster, New York, 242-243.
2. Dirac P.A.M. The theory of the electron (parts 1 and 2). *Proceedings of the Royal Society in London A*, 1928, v. 117, 610 and v. 118, 351.
3. Breit G. An interpretation of Dirac's Theory of the electron. *Proceedings of the National Academy of Sciences USA*, 1928, v. 14, 553.
4. Bellazini J., Benci V., Bonanno C., Micheletti A.M. Solitons for the nonlinear Klein-Gordon equation. 2007, arXiv: math.AP/0712.1103v1.
5. Finkelstein R.J. A Field Theory of knotted solitons. 2007, arXiv: hep-th/0701124v2.
6. Radu E., Volkov M.S., Existence of stationary, non-radiating ring solitons in field theory: knots and vortons. 2008, arXiv: hep-th/0804.1357v1.
7. Moret-Bailly J. Electromagnetic solitons and de Broglie's "double solution". *J. of Theoretics*, 2003, v. 5-5, 11. arXiv: math-ph/0201002v1.
8. Borisyuk D., Faber M., Kobushkin A. Electromagnetic waves within a model for charged solitons. *J. Phys. A: Math. Gen.*, 2007, v. 40, 525–531. arXiv: hep-th/0708.3173v1.
9. Diaz-Alonso J., Rubiera-Garcia D. Generalized gauge field theories with non-topological soliton solutions. 2007, arXiv: hep-th/0708.0636v1.
10. Blas H., Carrion H.L. Solitons, kinks and extended hadron model based on the generalized sine-Gordon theory. *JHEP*, 2007, 0701, 027. arXiv: hep-th/0610107v2, 2006.
11. Cui H.Y. Direction adaptation nature of Coulomb's force and gravitational force in 4-Dimensional spacetime. 2001, arXiv: physics/0102073.
12. Laidlaw A. On the Electromagnetic basis for gravity. *Apeiron*, 2004, v. 11, 3.
13. Selleri F. Remarks on the transformations of space and time. *Apeiron*, 1997, v. 9(4), 116–120.
14. Selleri F. Non-invariant one-way speed of light. *Found. Phys.*, 1996, v. 26, 641.
15. Puccini G., Selleri F. Doppler effect and aberration from the point of view of absolute motion. *Nuovo Cim. B*, 2002, v. 117, 283.
16. Orefice A., Giovanelli R., Ditto D. Complete Hamiltonian Description of wave-like features in Classical and Quantum Physics. *Found. Phys.*, 2009, v. 39, 256.
17. Orefice A., Giovanelli R., Ditto D. Helmholtz wave trajectories in Classical and Quantum Physics. 2011, ArXiv: 1105.4973.
18. Donev S., Tashkova M. On the structure of the nonlinear vacuum solutions in extended Electrodynamics. 2002, arXiv: hep-th/0204217.
19. Donev S. Screw photon-like (3+1)-solitons in extended Electrodynamics. 2001, arXiv: hep-th/0104088.
20. Donev S., Tashkova M. From Maxwell stresses to nonlinear field equations. 2006, arXiv: physics/0604021v6.
21. Kim Y.S. Internal space-time symmetries of massive and massless particles and their unification. *Nucl.Phys.Proc.Suppl.*, 2001, v. 102, 369–376. arXiv: hep-th/0104051.
22. Messiah A. Quantum Mechanics. Vol 2. 1965, Ch XX, 922-925, North Holland Publishing Company.
23. Bohm D. The Special Theory of Relativity. 1965, 23–25, W.A. Benjamin New York.
24. Hafele J., Keating R. Around-the-world atomic clocks: predicted relativistic time gains. *Science*, 1972, v. 177, 166.
25. Kundig W. Measurement of the transverse Doppler effect in an accelerated system. *Phys Rev.*, 1963, v. 129, 2371.
26. Ives H., Stillwell G. An experimental study of the rate of a moving atomic clock. *Journal of the Optical Society of America*, 1938, v. 28, 215–226 and 1941, v. 31, 369.
27. Tangherlini F.R. On energy momentum tensor of gravitational field. *Supl. Nuov. Cim.*, 1961, v. 20, 351–367, (2^{nd} Trimestre 1961).
28. Rizzi G., Ruggiero M.L., Serafini A. Synchronization gauges and the principles of Special Relativity. *Found. Phys.*, 2005, v. 34, 1885.
29. Selleri F. Superluminal signals and causality. *Annales de la Fondation Louis de Broglie*, 2003, v. 28, 3–4.
30. Goy F. Derivation of three-dimensional inertial transformations. 1997, arXiv: gr-qc/9707004.
31. Goy F., Selleri F. Time on a rotating platform. 1997, arXiv: gr-qc/9702055v2.
32. Hardy L. Quantum Mechanics, local realistic theories, and Lorentz-invariant realistic theories. *Phys. Rev. Lett.*, 1992, v. 68, 2981–1284.
33. Percival I. Quantum transfer functions, weak nonlocality and relativity. *Physical Letters A*, 1998, v. 244(6), 495–501. arXiv: quant-ph/9803044.
34. Percival I. Quantum measurement breaks Lorentz symmetry. 1999, arXiv: quant-ph/9906005.
35. Selleri F. Weak relativity - The Physics of space and time without paradoxes. 2009, C. Roy Keys Inc.
36. Clauser J., Horne M. Detector inefficiencies in the Einstein-Podolsky-Rosen experiment. *Phys. Rev. D*, 1987, v. 35(12), 3831–3835.
37. Hensen B. et al. Experimental loophole-free violation of a Bell inequality using entangled electron spins separated by 1.3 km. *Nature*, 2015, v. 526, 682–686. arXiv: 1508.05949.
38. Peebles P.J.E., Wilkinson D.T. Comment on the anisotropy of the primeval fireball. *Phys. Rev.*, 1968, v. 174, 2168.
39. Smoot G. Detection of anisotropy in the cosmic blackbody radiation. *Physical Review Letters*, 1977, v. 39(14), 898.
40. Blake C., Wall J. A velocity dipole in the distribution of radio galaxies. *Nature*, 2002, v. 416, 180–182.
41. Aspect A., Grangier P., Roger B. Experimental realization of EPR-Bohm gedankenexperiment: A new violation of Bell's inequalities. *Phys. Rev. Lett.*, 1982, v. 49, 1804–1807.
42. Scarani V., Tittel W., Zbinden H., Gisin N. The speed of quantum information and the preferred frame: Analysis of experimental data. *Phys. Lett. A*, 2000, v. 276, 1–7. arXiv: quant-ph/0007008.
43. Ou Z.Y., Pereira S.F., Kimble H.J., Peng K.C. Realization of the Einstein-Podolsky-Rosen paradox for continuous variables. *Phys. Rev. Lett.*, 1992, v. 68, 3663.
44. Konopinski E.J. Electromagnetic Fields and relativistic particles. 1981, Mcgraw Hill.
45. Redhead M. Incompleteness, nonlocality and realism. 1987, Oxford University Press.
46. Einstein A., Podolsky B., Rosen N. Can Quantum-mechanical description of physical reality be considered complete? *Phys. Rev.*, 1935, v. 47, 777.
47. Bell J.S. On the Einstein Podolsky Rosen Paradox. *Physics*, 1965, v. 1, 195–200.
48. Norsen T. J.S. Bell's Concept of local causality. 2007, arXiv: 0707.0401v3.
49. Bell J.S. Speakable and unspeakable in Quantum Mechanics: Collected papers on quantum philosophy. 2004, Cambridge University Press.

Appendix 1

Consider a constant momentum density $\vec{\rho}_{pi}$ in a region of transverse crossectional area A and length l_i. The total momentum is $\mathbf{p}_i = Al_i\rho_{pi}\hat{\mathbf{k}}$. Let this be normally incident on

a mirror that is moving with velocity $\mathbf{v} = -v\hat{\mathbf{k}}$. Let the reflection begin at $t = 0$. It then ends at $\Delta t = l_{\rm i}/(c+v)$, after which there is a reflected wave with momentum density $\vec{\rho}_{pr}$ that occupies a region of length $l_{\rm r} = (c-v)\Delta t$ and crossectional area A, so the momentum of the reflected light flash is $\mathbf{p}_{\rm r} = -Al_{\rm r}\rho_{pr}\hat{\mathbf{k}}$.

During the reflection, the rates of change of momentum for the incident and reflected waves are $\dot{\mathbf{p}}_i = -(c+v)A\vec{\rho}_{\rm pi}$ and $\dot{\mathbf{p}}_{\rm r} = (c-v)A\vec{\rho}_{\rm pr}$ respectively, where a dot over a variable indicates the time differential. The total rate of change of momentum is:

$$\dot{\mathbf{p}} = \dot{\mathbf{p}}_{\rm i} + \dot{\mathbf{p}}_{\rm r} = -A((c+v)\rho_{pi} + (c-v)\rho_{pr})\hat{\mathbf{k}}\,,$$

where $\rho_{pi} = |\vec{\rho_{pi}}|$ and $\rho_{pr} = |\vec{\rho_{pr}}|$. As far as scalar momentum is concerned, for the incident wave $\dot{p}_{\rm i} = c\dot{m}_{\rm i} = -A(c+v)\rho_{pi}$, for the reflected wave $\dot{p}_{\rm r} = c\dot{m}_{\rm r} = A(c-v)\rho_{\rm pr}$ and the total is:

$$\dot{p} = c\dot{m} = c\dot{m}_{\rm r} + c\dot{m}_{\rm i} = A((c-v)\rho_{pr} - (c+v)\rho_{pi})\,.$$

The work done by the mirror on the incident and reflected waves is: $\int \dot{\mathbf{p}}_{\rm i}\cdot d\mathbf{s}_{\rm i} = -\int_0^{\Delta t} A(c+v)\rho_{\rm pi}\ cdt$ and $\int \dot{\mathbf{p}}_{\rm r}\cdot d\mathbf{s}_{\rm r} = \int_0^{\Delta t} A(c-v)\rho_{pr}\ cdt$ respectively, where $d\mathbf{s}_{\rm i}$ and $d\mathbf{s}_{\rm r}$ are the incremental movements of the incident and reflected waves, in the directions $\hat{\mathbf{k}}$ and $-\hat{\mathbf{k}}$ respectively. The total work done is just $W = \int_0^{\Delta t} c\,\dot{m}c\,dt = (m_{\rm r} - m_{\rm i})c^2$.

The energy change of the light flash is of course equal and opposite to the work done by the radiation pressure force on the mirror, so $(m_{\rm r} - m_{\rm i})c^2 = -(-\dot{\mathbf{p}})(-v)\Delta t$, and it is easily shown that $p_{\rm r}/p_{\rm i} = (c+v)/(c-v)$, from which we may infer the momentum shift factor for light emitted by a source moving towards an observer as $\sqrt{(c+v)/(c-v)}$, in agreement with the usual relativistic doppler shift.

Appendix 2

With respect to the system of light flashes in Subsect. 2.2, let us impose the condition in some inertial frame that $\mathbf{P}_0 = \sum_i \mathbf{p}_{i0} = 0$. The momentum of the i^{th} light flash, referred to this frame, is then:

$$\mathbf{p}_{i0} = p_{i0}\left(\cos\theta_{i0}\,\hat{\mathbf{i}} + \sin\theta_{i0}\cos\phi_{i0}\,\hat{\mathbf{j}} + \sin\theta_{i0}\sin\phi_{i0}\,\hat{\mathbf{k}}\right)\,,$$

where θ_{i0} is the angle with the x-axis and $\sum_i p_{i0}\cos\theta_{i0} = \sum_i p_{i0}\sin\theta_{i0}\cos\phi_{i0} = \sum_i p_{i0}\sin\theta_{i0}\sin\phi_{i0} = 0$.

Let an observer move relative to this frame with velocity $\mathbf{v} = -\beta c\hat{\mathbf{i}}$. Since $p_i/p_{i0} = f_i/f_{i0}$, the standard relativistic doppler shift and aberration formulae (with the observer moving towards the source at speed v) give, respectively:

$$p_i = p_{i0}\gamma\left(1 + \frac{v}{c}\cos\theta_{i0}\right) \text{ and } \cos\theta_i = \frac{\cos\theta_{i0} + \dfrac{v}{c}}{1 + \dfrac{v}{c}\cos\theta_{i0}}\,.$$

Note that the same result also holds for non-monochromatic light flashes. The scalar momentum of the i^{th} flash in the observer frame is:

$$p_i = p_{i0}\gamma(1 + \beta\cos\theta_{i0})\,.$$

Summing over i, the total energy, $m_e c^2 = \gamma c\sum_i p_{i0} = \gamma m_0 c^2$, where m_e and m_0 are as defined in subsection 2.2 and Section 3 respectively. The (vector) momentum of the i^{th} flash is:

$$\mathbf{p}_i = p_{i0}(\gamma(\beta + \cos\theta_{i0})\,\hat{\mathbf{i}} + \sin\theta_{i0}\cos\phi_{i0}\,\hat{\mathbf{j}} + \sin\theta_{i0}\sin\phi_{i0}\,\hat{\mathbf{k}})\,.$$

Summing over i, the total momentum is $\mathbf{P} = \gamma\beta\sum_i p_{i0}\,\hat{\mathbf{i}}$. Differentiating each of the two previous equations with respect to β, we get $d\mathbf{p}_i/d\beta = \gamma^2 p_i\,\hat{\mathbf{i}}$ and $d\mathbf{P}/d\beta = \gamma^2 m_e c\,\hat{\mathbf{i}}$, so that:

$$\frac{d\mathbf{p}_i}{d\beta} = \frac{d\mathbf{P}}{d\beta}\frac{p_i}{\sum_j p_j} = \frac{d\mathbf{P}}{d\beta}\frac{p_i}{m_e c}\,.$$

Finally, since the above expressions for $\mathbf{p}_i$ and $\mathbf{P}$ are functions of β alone, the incremental changes can be written as $d\mathbf{p}_i = (d\mathbf{p}_i/d\beta)\,d\beta$ and $d\mathbf{P} = (d\mathbf{P}/d\beta)\,d\beta$, upon which:

$$d\mathbf{p}_i = \frac{p_i}{m_e c}d\mathbf{P}\,.$$

Therefore (8) holds for a collinear incremental boost. For transverse boosts, consider as initial condition a system with a centre of inertia that is moving in the y-direction at speed V, so $m_e = \gamma(V)m_0$. We may repeat the above analysis for an observer moving at speed v_x in the x-direction with $\beta = v_x/c$ and $\sum_i p_{i0}\sin\theta_{i0}\cos\phi_{i0} \neq 0$. Evaluating the resulting expression for $d\mathbf{P}/d\beta$ at $v_x = 0$, then yields the same result, $d\mathbf{p}_i = p_i\,d\mathbf{P}/m_e c$, for an incremental transverse boost. In Special Relativity, the general boost decomposes into a collinear boost, a transverse boost and a rotation (a Thomas precession). As the latter has no impact on linear momenta, (8) is generally valid for incremental boosts of systems of luminal wave momenta.

Occurrence and Properties of Low Spin Identical Bands in Normal-Deformed Even-Even Nuclei

A. M. Khalaf, M. D. Okasha[1] and K. M. Abdelbased
Physics Department, Faculty of Science, Al-Azhar University, Cairo, Egypt

[1]Physics Department, Faculty of Science (Girls branch), Al-Azhar University, Cairo, Egypt. E-mail: mady200315@yahoo.com

The identical bands (IB's) phenomenon in normally deformed rare-earth nuclei has been studied theoretically at low spins. Six neighboring even-even isotopes ($N = 92$) and the isotopes ^{166,168,170}Hf are proposed that may represent favorable cases for observation of this phenomenon. A first step has been done by extracting the smoothed excitation energies of the yrast rotational bands in these nuclei using the variable moment of inertia (VMI) model. The optimized parameters of the model have been deduced by using a computer simulated search programm in order to obtain a minimum root mean square deviation between the calculated theoretical excitation energies and the experimental ones. Most of the identical parameters are extracted. It is observed that the nuclei having N_pN_n/Δ values exhibit identical excitation energies and energy ratio R(4/2), R(6/4) in their ground-state rotational bands, N_p and N_n are the valence proton and neutron number counted as particles or holes from the nearest spherical shell or spherical subshell closure and Δ is the average pairing gap. The nuclear kinematic and dynamic moments of inertia for the ground state rotational bands have been calculated, a smooth gradual increase in both moments of inertia as function of rotational frequency was seen. The study indicates that each pair of conjugate nuclei have moments of inertia nearly identical.

1 Introduction

One of the most remarkable properties so far discovered of rotational bands in superdeformed (SD) nuclei is the extremely close coincidence in the energies of the deexciting γ-ray transitions or rotational frequencies between certain pairs of rotational bands in adjacent even and odd nuclei with different mass number [1–5]. In a considerable number of nuclei in the Dy region as well as in the Hg region one has found different in transition energies E_γ of only 1-3 KeV, i.e there exist sequence of bands in neighboring nuclei, which are virtually identical $\Delta E_\gamma/E_\gamma \sim 10^{-3}$. This means that the rotational frequencies of the two bands are very similar because the rotational frequency (dE/dI) is approximately half the transition energy, and also implies that the dynamical moments of inertia are almost equal. Several groups have tried to understand the phenomenon of SD identical bands (IB's) or twin bands [5–10] assuming the occurrence of such IB's to be a specific property of the SD states of nuclei.

Shortly afterwards, low spin IB's were found in the ground state rotational bands of normally deformed (ND) nuclei [11–14], which showed that the occurrence of IB's is not restricted to the phenomenon of superdeformation and high-spin states. Since then, a vast amount of IB's have been observed both in SD and ND nuclei, and there have been a lot of theoretical works presented based on various nuclear models [15–18]. All explantation to IB's in SD nuclei differing by one or two particle numbers factor to the odd-even difference in the moments of inertia, namely the pair force, is substantially weakened for high-spin SD states. However, these outlines would fail to explain IB's at low spin, where the blocking of the pairing contributions of the odd nucleon is predicted to reduce the nuclear superfluidity, there by increasing the moment of inertia of the odd-A nucleus. Because of the known spins, configurations and excitations energies of the ND bands, the systematic analysis of IB's in ND nuclei would be useful in investigation of the origin of IB's.

It is the purpose of this paper to point out that existence of low-spin IB's in the well deformed rare-earth region is a manifestation of a more general property of nuclear excitation mechanism in this region, i.e, almost linear dependence of the moment of inertia on a simple function of the valence proton and neutron number. The properties of rotational bands in our selected normal deformed nuclei have been systematically analyzed by using the variables moment of inertia (VIM) model [19, 20].

2 Description of VMI model

The excitation energy of the rotational level with angular moment I for an axially symmetric deformed nucleus is given by

$$E(I) = \frac{\hbar^2}{2J} I(I+1), \tag{1}$$

with J being the rigid moment of inertia. This rigid rotor formula violated at high angular momenta. Bohr and Mottelson [21] introduced a correction term

$$\Delta E(I) = -B\,[I\,(I+1)]^2 \tag{2}$$

which is attributed to rotation-vibration interaction where J and B are the model parameters.

In the variable moment of inertia (VMI) model [19] the level energy is given by

$$E\left(I,J,J_0,c\right)=\frac{\hbar^2}{2J}I\left(I+1\right)+\frac{c}{2}\left(J-J_{00}\right)^2 \tag{3}$$

where J_0 is the ground-state moment of inertia. The second term represents the harmonic term with c in the stiffness parameter. The moment of inertia J is a function of the spin $I(J(I))$.

The equiblirium condition

$$\frac{\partial E}{\partial J}=0 \tag{4}$$

determines the values of the variable moment of inertia J_I, one obtains

$$J_I^3-J_0J_I^2=\frac{1}{2c}I\left(I+1\right). \tag{5}$$

This equation has one real root for any finite positive value of J_0 and c can be solved algebraically to yield

$$\begin{aligned}J(J_0,c,I)&=\frac{J_0}{3}\\&+\left\{\frac{1}{2}\frac{I(I+1)}{2C}+\frac{J_0^3}{27}+\left[\frac{1}{4}\frac{I^2(I+1)^2}{4c^2}+\frac{J_0^3}{27}\frac{I(I+1)}{2c}\right]^{\frac{1}{2}}\right\}^{\frac{1}{3}}\\&+\left\{\frac{1}{2}\frac{I(I+1)}{2c}+\frac{J_0^3}{27}-\left[\frac{1}{4}\frac{(I+1)^2}{4c^2}+\frac{J_0^3}{27}\frac{I(I+1)}{2c}\right]^{\frac{1}{2}}\right\}^{\frac{1}{3}}.\end{aligned} \tag{6}$$

A softness parameter σ was introduced, which measures the relative initial variation of J with respect to I. This quantity is obtained from the equation (3)

$$\sigma=\frac{1}{J}\frac{dJ}{dI}\mid_{I=0}=\frac{1}{2cJ_0^3}. \tag{7}$$

To find the rotational frequency $\hbar\omega$, the kinematic $J^{(1)}$ and dynamic $J^{(2)}$ moments of inertia for VMI model, let $\hat{I}=[I(I+1)]^{\frac{1}{2}}$. Equations (3,5) can be written in the form

$$E=\frac{\hbar^2}{2J}\hat{I}^2+\frac{c}{2}\left(J-J_0\right)^2, \tag{8}$$

$$J^3-J_0J^2-\frac{\hat{I}^2}{2c}=0. \tag{9}$$

Differentiating these two equations with respect to $\hat{I}$ and using the chain rule, we get

$$\frac{dE}{d\hat{I}}=\frac{\hat{I}}{J}+\left[c\left(J-J_0\right)-\frac{\hat{I}^2}{2J^2}\right]\frac{dJ}{d\hat{I}}, \tag{10}$$

$$\begin{aligned}\frac{d^2E}{d\hat{I}^2}=&\frac{1}{J}-\frac{2\hat{I}}{J^2}\frac{dJ}{d\hat{I}}+\left(c+\frac{\hat{I}^2}{J^3}\right)\left(\frac{dJ}{d\hat{I}}^2\right)\\&+\left[c\left(J-J_0\right)-\frac{\hat{J}^2}{2J^2}\right]\frac{d^2J}{d\hat{I}^2},\end{aligned} \tag{11}$$

$$\frac{dJ}{d\hat{I}}=\frac{\hat{I}}{cJ(3J-2J_0)}, \tag{12}$$

$$\frac{d^2J}{d\hat{I}^2}=\frac{1-2c(3J-J_0)}{cJ(3J-2J_0)}\left(\frac{dJ}{d\hat{I}}\right)^2. \tag{13}$$

Using the above differentiations, we can extract $\hbar\omega$, $J^{(1)}$ and $J^{(2)}$ from their definitions:

$$\hbar\omega=\frac{dE}{d\hat{I}}, \tag{14}$$

$$J^{(1)}=\hbar^2\hat{I}\left(\frac{dE}{d\hat{I}^2}\right)^{-1}\simeq\frac{2I-1}{E_\gamma(I\rightarrow I-2)}, \tag{15}$$

$$J^{(2)}=\hbar^2\left(\frac{d^2E}{d\hat{I}^2}\right)^{-1}\simeq\frac{4}{E_\gamma(I+2\rightarrow I)-E_\gamma(I\rightarrow I-2)}. \tag{16}$$

The $J^{(1)}$ moment of inertia is a direct measure of the transition energies while $J^{(2)}$ is obtained from differences in transitions energies (relative change in transition energies).

3 Identical bands parameters

In the concept of F-spin [22], the N_π proton bosons and N_ν neutron bosons are assigned intrinsic quantum number called F-spin $F=\frac{1}{2}$, with projection $F_0=+\frac{1}{2}$ for proton bosons and $F_0=-\frac{1}{2}$ for neutrons bosons.

Therefore, a given nucleus is then characterized by two quantum numbers $F=\sum_i F_i=\frac{1}{2}(N_\pi+N_\nu)=\frac{1}{4}(N_p+N_n)$ and it's projection $F_0=\frac{1}{2}(N_\pi-N_\nu)=\frac{1}{4}(N_p-N_n)$. Squaring and subtracting, yield $4(F^2-F_0^2)=4N_\pi N_\nu=N_pN_n$.

That is any pairs of conjugate nuclei with the same F-spin and $\pm F_0$ values in any F-spin multiplet have identical N_pN_n values [23]. The product N_pN_n was used in classification the changes occur in nuclear structure of transitional region [13, 24].

It was assumed that [14], the moment of inertia J has a simple dependence on the product of valence proton and neutron numbers (N_pN_n) written in the form

$$J\propto SF\cdot SP \tag{17}$$

where SF and SP are called the structure factor and saturation parameter given by

$$SF=N_pN_n(N_p+N_n), \tag{18}$$

$$SP=\left[1+\frac{SF}{(SF)_{\max}}\right]^{-1}. \tag{19}$$

Computing by taking

$$N_p = \min\left[(\mathrm{Z}-50),(82-\mathrm{Z})\right], \tag{20}$$

$$N_n = \min\left[(\mathrm{N}-82),(126-\mathrm{N})\right], \tag{21}$$

it was found that the low spin dynamical moment of inertia defined as

$$J^{(2)}(I=2) = \frac{4}{E_\gamma(4^+ \to 2^+) - E_\gamma(2^+ \to 0^+)} \tag{22}$$

shows an approximate dependence on SF

$$J^{(2)}(I=2) \propto (SF)^{\frac{1}{2}}. \tag{23}$$

Since the nuclei having identical N_pN_n and $|N_p - N_n|$ values are found to have identical moment of inertia, the structure factor SF is related not only to the absolute value of ground state moment of inertia but also to its angular momentum dependence.

Also it was shown [11, 25, 26] that the development of collectivity and deformation in medium and heavy nuclei is very smoothly parameterized by the p-factor defined as

$$P = \frac{N_pN_n}{N_p + N_n}. \tag{24}$$

The p-factor can be viewed as the ratio of the number of valence p-n residual interaction to the number of valence like-nucleon-pairing interaction, or, if the p-n and pairing interactions are orbit independent, then p is proportional to the ratio of the integrated p-n interaction strength.

Observables such as $E(4_1^+)/E(2_1^+)$ or $B(E_2, 0_1^+ \to 2_1^+)$ that are associated with the mean field vary smoothly with p-factor.

The square of deformation parameter β^2 is invariant under rotations of the coordinate system fixed in the space. In the SU(3) limit of the interacting boson model (IBM) [27], the matrix elements of β^2 in a state with angular momenta I are given by

$$\langle\beta^2\rangle_I = \frac{1}{6(2N-1)}\left[I(I+1) + 8N^2 + 22N - 15\right] \tag{25}$$

where N is the total number of the valence bosons For the expectations value of β^2 in the ground state $I = 0$, yielding

$$\langle\beta^2\rangle_{I=0} = \frac{1}{6(2N-1)}\left[8N^2 + 22N - 15\right] \tag{26}$$

which is increasing function of N.

In order to determine β from equation (26) to a given rotational region or grouped of isotopes, one should normalize it, then

$$\beta_0 = \alpha\left[\frac{8N^2 + 22N - 15}{6(2N-1)}\right]^{\frac{1}{2}} \tag{27}$$

where α is the normalization constant ($\alpha = 0.101$ for rare earth nuclei.)

Table 1: The simulated adopted best VMI parameters used in the calculations for the identical bands in normal deformed even-even ^{158}Dy, ^{160}Er, ^{162}Yb and $^{166-170}$Hf nuclei. σ denoting the softness parameter of the VMI model. We also list the total percent root mean square deviation.

Nucleus	J_0 ($\hbar^2$ MeV^{-1})	c (10^{-1}MeV^3)	$\sigma = 1/2cJ_0^3$ (10^{-1})	% rmsd
^{158}Dy	28.8866	2.37364	8.7372	0.57
^{170}Hf	29.9116	1.93836	9.6386	0.87
^{160}Er	22.7538	2.65536	15.9839	0.86
^{168}Hf	22.8761	2.48160	16.8303	0.70
^{162}Yb	16.8587	2.83884	36.7584	0.60
^{166}Hf	17.6941	2.76559	32.6359	0.82

4 Results and discussion

A fitting procedure has been applied to all measured values of excitation energies $E(I)$ in a given band. The parameters J_0, c and σ of the VMI model results from the fitting procedure for our selected three pairs IB's are listed in Table 1. The percentage root mean square (rms) deviation of the calculated from the experimental level energies is also given in the Table and is within a fraction of 1%. To illustrate the quantitative agreement obtained from the excitation energies, we present in Table 2 the theoretical values of energies, transition energies, rotational frequencies kinematic $J^{(1)}$ and dynamic $J^{(2)}$ moments of inertia and the variable moment of inertia J_{VMI} as a function of spin for our three pairs of IB's which each pair has identical $N_p\,N_n$ product. The calculated kinematic $J^{(1)}$ and dynamic $J^{(2)}$ moments of inertia are plotted against rotational frequency $\hbar\omega$ in Figure 1.

The similarities are striking, although the frequency range covered in each two IB's is smaller than that observed in the

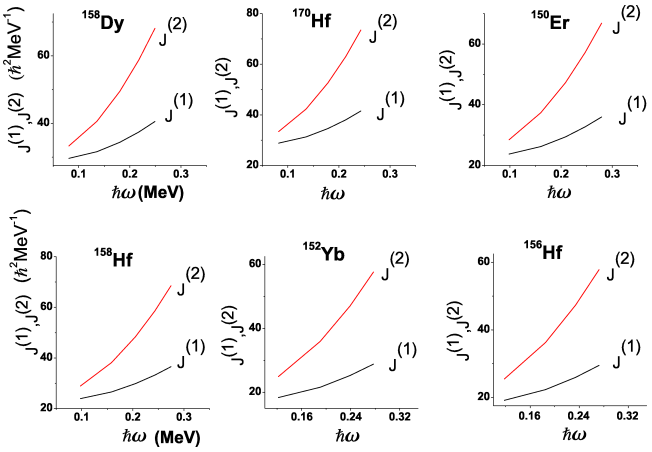

Fig. 1: Plot of the calculated kinematic $J^{(1)}$ and dynamic $J^{(2)}$ moments of inertia versus the rotational frequency $\hbar\omega$ for the low lying states in the conjugate pairs (^{158}Dy, ^{170}Hf), (^{160}Er, ^{168}Hf) and (^{162}Yb, ^{166}Hf).

Table 2: Theoretical calculations to outline the properties of our selected even rare-earth nuclei in framework of VMI model for each nucleus we list the energy E(I), the gamma ray transition energy $E_\gamma(I \to I-2)$, the rotational frequency $\hbar\omega$, the dynamic moment of inertia $J^{(2)}$, the kinematic moment of inertia $J^{(1)}$ and the variable moment of inertia J_{VMI}

$E_{exp}(I)$ (keV)	I^π ($\hbar$)	$E_{cal}(I)$ (keV)	$E_{\gamma(I\to I-2)}$ keV	$\hbar\omega$ (MeV)	$J^{(2)}$ ($\hbar^2$ MeV^{-1})	$J^{(1)}$ ($\hbar^2$ MeV^{-1})	J_{VMI} ($\hbar^2$ MeV^{-1})
			$^{158}Dy_{92}$				
99	2^+	101.379	101.379	0.0807	33.2515	29.5919	30
317	4^+	323.053	221.674	0.1354	40.5724	31.5779	33
638	6^+	643.316	320.263	0.1803	49.4620	34.3467	36
1044	8^+	1044.449	401.133	0.2175	58.8001	37.3940	39
1520	10^+	1513.609	469.160	0.2492	68.1419	40.4979	42
2050	12^+	2041.470	527.861			43.5720	45
			$^{170}Hf_{92}$				
100.8	2^+	104.135	104.135	0.0820	33.3828	28.8087	30
321.99	4^+	328.092	223.957	0.1356	42.2275	31.2560	33
642.9	6^+	646.774	318.682	0.1783	52.5513	34.5171	36
1043.3	8^+	1041.572	394.798	0.2132	63.1123	37.9941	40
1505.5	10^+	1499.749	458.177	0.2426	73.5077	41.4686	43
2016.4	12^+	2012.342	512.593			44.8699	47
			$^{160}Er_{68}$				
126	2^+	126.476	126.476	0.0983	28.4620	23.7199	25
390	4^+	393.490	267.014	0.1603	37.3148	26.2158	28
765	6^+	767.700	374.210	0.2082	47.2533	29.3452	31
1229	8^+	1226.560	458.860	0.2469	57.1845	32.6897	34
1761	10^+	1755.369	528.809	0.2793	66.8337	35.9297	37
2340	12^+	2344.028	588.659			39.0718	41
			$^{168}Hf_{96}$				
124	2^+	125.554	125.544	0.0974	28.8591	23.8941	25
386	4^+	389.712	264.158	0.1583	38.0709	26.4992	28
757	6^+	758.937	369.225	0.2052	48.3412	29.7921	31
1214	8^+	1210.907	451.970	0.2430	58.5677	33.1880	35
1736	10^+	1731.174	520.267	0.2747	68.4802	36.5194	38
2306	12^+	2309.582	578.678			39.7457	41
			$^{162}Yb_{92}$				
166	2^+	163.728	163.728	0.1220	24.9036	18.3230	20
487	4^+	488.075	324.347	0.1900	35.9266	21.5818	23
923	6^+	923.760	435.685	0.2390	47.0494	25.2475	27
1445	8^+	1444.462	520.702	0.2777	57.6036	28.8072	30
2023	10^+	2034.604	590.142			32.1936	34
			$^{166}Hf_{94}$				
159	2^+	157.173	157.173	0.1179	25.4281	19.0872	20
470	4^+	471.652	314.479	0.1848	36.2236	22.2590	24
897	6^+	896.556	424.904	0.2336	47.2768	25.8882	28
1406	8^+	1406.068	509.512	0.2720	57.8285	29.4399	31
1970	10^+	1984.750	578.682			32.8332	34

SD nuclei. The $J^{(2)}$ is significantly larger than $J^{(1)}$ over a large rotational frequency range.For our three IB pairs, the IB parameters are listed in Table 3.

5 Conclusion

The problem of identical bands(IB's) in normal deformed nuclei is treated. We investigated three pairs of conjugate normal deformed nuclei in rare-earth region (^{158}Dy,^{170}Hf), (^{160}Er, ^{168}Hf) and (^{162}Yb, ^{166}Hf) with the same F spin and projections $\pm F_0$ values have identical product of valence proton and neutron numbers N_pN_n values. Also the values of dynamical moment of inertia $J^{(2)}$ for each IB pair are approximately the same. We extracted all the IB symmetry parameters like p-factor, saturation factor SF, structure factor SP etc. which all depending on the valence proton and neutron numbers. By using the VMI model, we find agreement between experimental excitation energies and theoretical ones.

The optimized model free parameters for each nucleus have been deduced by using a computer simulation search programm to fit the calculated theoretical excitation energies with the experimental energies.

Submitted on October 17, 2016 / Accepted on October 24, 2016

Table 3: The calculated correlation factors for selected three pairs of even-even rare-earth nuclei having nearly identical bands.

	^{158}Dy	^{170}Hf	^{160}Er	^{168}Hf	^{162}Yb	^{166}Hf
(N_π, N_ν)	(8,5)	(5,8)	(7,5)	(5,7)	(6,5)	(5,6)
N_pN_n	160	160	140	140	120	120
F	6.5	6.5	6	6	5.5	5.5
F_0	1.5	-1.5	1	-1	0.5	-0.5
P	6.1538	6.1538	5.8333	5.8333	5.4545	5.4545
SF	4160	4160	3360	3360	2640	2640
SP	0.6176	0.6176	0.666	0.666	0.7179	0.7179
$J^{(2)}_{SF}$	32.2643	32.2645	28.9966	28.9966	25.7027	25.7027
$E^{(2)}_{SF}$	103.0160	103.0160	127.5437	127.5437	162.3283	162.3283
R(4/2)	3.2060	3.1943	3.0993	3.1096	2.9230	2.9671
R(6/2)	6.4468	6.3771	6.0866	6.1040	5.5430	5.6586
β_0	0.3322	0.3322	0.3218	0.3218	0.3110	0.3110
Δ	0.9546	0.9203	0.9486	0.9258	0.9428	0.9313
N_pN_n/Δ	167.6094	173.8563	147.5859	151.2205	127.2804	128.8521

References

1. Byrski T., Beck F.A., Curien D., Schuck C., Fallon P., Alderson A., Ali I., Bentley M.A., Bruce A.M., Forsyth P.D., Howe D., Roberts J.W., Sharpey-Schafer J.F., Smith G., and Twin P.J. Observation of identical superdeformed bands in N=86 nuclei. *Phys. Rev. Lett.* 1990, v. 64, 1650.
2. Janssens R.V.F. and Khoo T.L. Superdeformed Nuclei. *An. Rev. Nucl. Part. Sci.*, 1991, v. 41, 321.
3. Baktash C., Nazarewics W. and Wayss R. On the question of spin fitting and quantized alignment in rotational bands. *Nucl. Phys. A*, 1993, v. 555, 375.
4. Stephens F.S. Spin alignment in superdeformed Hg nuclei. *Phys. Rev. Lett.*, 1990, v. 64, 2623, and v. 65, 301.
5. Nazarewics W., Twin P.J., Fallon P. and Garrett J.D. Natural-parity states in superdeformed bands and pseudo SU(3) symmetry at extreme conditions. *Phys. Rev. Lett.*, 1990, v. 64, 1654.
6. Ragnarason I. Transition energies in superdeformed bands: Dependence on orbital and deformation. *Nucl. Phys. A*, 1990, v. 520, 76.
7. Chen B.Q. Observation of identical bands in superdeformed nuclei with the cranked Hartree-Fock method. *Phys. Rev. C*, 1992, v. 46, R1582.
8. Khalaf A., Sirag M. and Taha M. Spin assignment and behavior of superdeformed bands in A∼ 150 mass region. *Turkish Tournal of Physics*, 2013, v. 37, 49.
9. Khalaf A. and Okasha M.D. Properties of Nuclear Superdeformed Rotational Bands in A∼190 Mass. *Progress in Physics*, 2014, v. 10,246.
10. Khalaf A., Abdelmaged K. and Sirag M. Description of the yrast superdeformed bands in even-even nuclei in A∼190 region using the nuclear softness model. *Turkish Journal of Physics*, 2015, v. 39, 178.
11. Ahmad I., Carpenter M.P., Chasman R.R., Janssens R.V.F. and Khoo T.L. Rotational bands with identical transition energies in actinide nuclei. *Phys. Rev. C*, 1992, v. 44, 1204.
12. Baktash C., Garrett J.D. , Winchell D.F. and Smith A. Low-spin indentical bands in neighboring odd-A and even-even nuclei: A challenge to mean-field theories. *Phys. Rev. Lett.*, 1992, v. 69, 1500.
13. Casten R.F., Zamfir N.V., von Brentano P., and Chou W.-T. Identical bands in widely dispersed nuclei. *Phys. Rev. C*, 1992, v. 45, R1413.
14. Saha M. and Sen S. Low-spin identical bands in the NpNn scheme. *Phys. Rev. C*, 1992, v. 46, R1587.
15. Baktash C., Hass B. and Nazarewics W. Identical Bands in Deformed and Superdeformed Nuclei, *Annual Review of Nuclear and Particle Science*, 1992, v. 45, 485.
16. Zeng J.Y., Liu S.X., Lei Y.A. and Yu L. Microscopic mechanism of normally deformed identical bands at low spin in the rare-earth nuclei. *Phys. Rev. C*, 2001, v. 63, 024305.
17. Baktash C., Winchell D.F., Garrett J.D., Smith A. Low-spin identical bands in neighboring odd-A and even-even nuclei. *Nucl. Phys. A*, 1993, v. 557, 145.
18. Saha M. and Sen S. Simple phenomenology for the ground-state bands of even-even nuclei. *Phys. Rev. C*, 1994, v. 50, 2794.
19. Mariscotti M.A.J., Schaf G., Goldhaber G. and Buck B. Phenomenological Analysis of Ground-State Bands in Even-Even Nuclei. *Phys. Rev.*, 1969, v. 198, 1864.
20. Scharf G., Dover C.B. and Goodmann A.L. The Variable Moment of Inertia (VMI) Model and Theories of Nuclear Collective Motion. *Ann. Rev. Sci.*, 1976, v. 26, 239.
21. Bohr A. and Mottelson B. Nuclear structure. Vol. 2, Nuclear deformations. Benjamin (London), 1975.
22. Otsuka T., Arima A., Iachello F., Talmi I. Shell model description of interacting bosons. *Phys. Lett. B*, 1978, v. 76, 139.
23. Mittal H.M. and Devi V. Search for low-spin identical bands in light Xe-Gd nuclei. *Int. J. Nucl. Energy Sci. Techn.*, 2011, v. 6, 224.
24. Casten R.F. A simple approach to nuclear transition regions. *Phys. Lett. B*, 1985, v. 152, 145.
25. Zhang J.-Y., Casten R.F., Chou W.-T., Brenner D.S., Zamfir N.V. and von Brentano P. Identical bands and the varieties of rotational behavior. *Phys. Rev. Lett.*, 1992, v. 69, 1160.
26. Foy B.D., Casten R.F., Zamfir N.V. and Brenner D.S. Correlation between ε/Δ and the P factor. *Phys. Rev. C*, 1994, v. 49, 1224.
27. Iachello F. and Arima A. The Interacting Boson Model. Cambridge Univ. Press, Cambridge, 1987.

Progress in Physics is an American scientific journal on advanced studies in physics, registered with the Library of Congress (DC, USA): ISSN 1555-5534 (print version) and ISSN 1555-5615 (online version). The journal is peer reviewed and listed in the abstracting and indexing coverage of: Mathematical Reviews of the AMS (USA), DOAJ of Lund University (Sweden), Scientific Commons of the University of St.Gallen (Switzerland), Open-J-Gate (India), Referential Journal of VINITI (Russia), etc. Progress in Physics is an open-access journal published and distributed in accordance with the Budapest Open Initiative: this means that the electronic copies of both full-size version of the journal and the individual papers published therein will always be acessed for reading, download, and copying for any user free of charge. The journal is issued quarterly (four volumes per year).

Electronic version of this journal: http://www.ptep-online.com

Postal address:
Department of Mathematics and Science, University of New Mexico,
705 Gurley Avenue, Gallup, NM 87301, USA